SAPIENZA
University of Rome
Department of Medical-Surgical Sciences and Biotechnologies

Biochemical and biophysical characterization of Glutamate decarboxylase of bacterial origin

Fabio Giovannercole

XXXI cycle

PhD PROGRAMME IN LIFE SCIENCES

Tutor
Prof. Daniela De Biase

Coordinator
Prof. Marco Tripodi

INDEX

Abbreviations used

ADAR	arginine-dependent AR
AFI	acid fitness island
AR	acid resistance
ATP	adenosine triphosphate
ATR	acid tolerance response
AUC	analytical ultracentrifugation
BCG	bromocresol green
*Bm*GadB	*Brucella microti* GadB
CCM	central carbon metabolism
DEAE	diethylaminoethyl
DTT	dithiothreitol
*Ec*GadB	*Escherichia coli* GadB
EDTA	ethylenediaminetetraacetic acid
FRET	fluorescence resonance energy transfer
GABA	γ-aminobutyrate
Gad	glutamate decarboxylase
GDAR	glutamate-dependent AR
GIT	gastro-intestinal tract
HEPES	2-[4-(2-hydroxyethyl)piperazin-1-yl]ethanesulfonic acid
HEPPS	3-[4-(2-Hydroxyethyl)-1-piperazinyl]propanesulfonic acid
IMAC	immobilized metal affinity chromatography
iNOS	inducible nitric oxide synthase
IPTG	isopropril-β-D-1-thiogalactopyranoside
LAB	lactic acid bacteria
*Mt*GadB	*Mycobacterium tuberculosis* GadB
NO	nitric oxide
ON	overnight
PLP	pyridoxal 5'-phosphate
PMP	pyridoxamine 5'-phosphate
PTM	proton moving force
RNI	reactive nitrogen intermediates

ROI	reactive oxygen intermediates
RT	room temperature
SAXS	small-angle X-ray scattering
SCFAs	short chain fatty acids
SDS	sodium dodecyl sulfate
SDS-PAGE	SDS-polyacrylamide gel electrophoresis
SEC	size-exclusion chromatography
SKIE	solvent kinetic isotope effect
TCA cycle	tricarboxylic acid cycle
TCS	two-component system
Tris	2-Amino-2-(hydroxymethyl)propane-1,3-diol

SUMMARY

Bacteria are constantly exposed to harsh conditions during their life cycle. Thus, the development of molecular strategies to overcome stressful environments is required for their survival. The acid stress is considered one of the most severe life-threatening conditions for neutralophiles, *i.e.* microorganisms that live and replicate best at neutral pH. An acidic stress is frequently encountered in natural habitats and/or within the host during the infectious process. Therefore, if not properly counteracted, it can lead to death. In food-borne neutralophilic bacteria, the acid stress in mostly encountered during their transit through the host gastro-intestinal tract where the environmental pH fluctuates between 1.5-2.5 in the stomach and 4.5-5.0 in the distal intestine.

In the last decades, several acid resistance molecular mechanisms have been identified; amongst them, the glutamate-dependent acid resistance mechanism is regarded the most potent. In *Escherichia coli* it relies on pyridoxal 5'-phosphate (PLP)-dependent glutamate decarboxylase GadA/B, which catalyze the proton-consuming decarboxylation of glutamate (*L*-Glu) to γ-aminobutyric acid (GABA), which is then exported by GadC, a Glu/GABA antiporter. The reaction consumes 1 H^+/cycle.

The pH-dependent biochemical properties of GadB from *E. coli* (*Ec*GadB) have been studied in depth since the first publication of the purification protocol (De Biase *et al.*, 1996), but several unanswered questions remain.

As part of the research work leading to my PhD degree, I investigated *Ec*GadB properties at different biochemical and biophysical levels, with regard to: *i*) the influence of PLP and of exposure to neutral-alkaline pH values on the quaternary structure of *Ec*GadB; *ii*) the role of aspartate 86 in the pH-dependent control of *Ec*GadB enzymatic activity. Moreover, I carried out a preliminary biochemical characterization of GadB from *Mycobacterium tuberculosis* to shed light on the hypothetical involvement of a Gad enzyme on either acid resistance within

phagosome/phagolysosome in macrophages or as a key enzyme of the GABA-shunt, which provides succinate from α-ketoglutarate, thus refilling the otherwise incomplete TCA cycle.

Finally, I focused on the antimicrobial activity of analogues of dicarboxylic acids, the results of which are under final assessment for deposit as an Italian patent.

CHAPTER I
General Introduction

Part of the content of this chapter was published as book chapters:

1) Pennacchietti, E., Giovannercole, F. and De Biase, D. (2016) 'Acid survival mechanisms in neutralophilic bacteria', in Bruijn, F. J. De (ed.) *Stress and Environmental Regulation of Gene Expression and Adaptation in Bacteria, I&II*. WILEY, pp. 911–926.

2) Giovannercole, F., Pennacchietti, E. and De Biase, D. (2017) 'Glutamate decarboxylase in bacteria', in D'Mello, J. P. F. (ed.) *The handbook of microbial metabolism of amino acids*. CABI, p. 15. doi: 10.1079/9781780647234.0015.

1.1. The glutamate-dependent acid resistance system in *Escherichia coli*

1.1.1. The acid stress challenge: how bacteria protect themselves from the entry of harmful protons

The evolution of bacteria is very much the result of their genome plasticity, leading to the fast adaptation to different niches and stressful conditions which would otherwise be life-threatening (Bennet, 2004).

Amongst the myriad of environmental stresses, the acid stress, *i.e.* the significant drop of external pH (pH_o) to values well below the physiological conditions, is by far one of the most challenging for neutralophilic bacteria, which, by definition, are those microorganisms typically growing in the 5-9 pH range. One such example is *Escherichia coli*, a microorganism that survives and replicates by maintaining the intracellular pH (pH_i) between 7.0 and 7.8 (Slonczewski *et al.*, 2009) when exposed to a pH_o ranging from 5 to 8. This is because an uncontrollable increase in intracellular protons, entering the cell either as H^+ or in the form of undissociated organic acids, has deleterious effects on the microbe physiology by slowing down or even halting biochemical processes and enzymatic reactions, as well as by altering the electrochemical gradient across the bacterial membrane, thus impairing the proton moving force (PMF) responsible for the generation of ATP (Foster, 2004; Krulwich *et al.*,, 2011; Lund *et al*., 2014). Overall, the uncontrolled drop of pH_i causes cell growth arrest and, if not efficiently counteracted, it can be even life-threatening.

Several different niches can be the source of the acid stress. The mammalian gastro-intestinal tract (GIT) is by far one of the most striking examples of environment, which shaped the evolution of commensal and pathogenic microorganisms. This is because, in order to colonize the intestine, food-borne beneficial and pathogenic bacteria transit through the GIT where the pH_o ranges from the extreme acidity of the stomach (pH 1.5-2.0) to the mild acidity of the distal gut (pH 5.5-6.0) (Evans *et al.*, 1988). The acidity of the former mostly derives from the dissociation of hydrochloric acid (HCl) and makes the stomach an effective bactericidal environment of the GIT (Martinsen *et al*., 2005); on the contrary, the

accumulation of short-chain fatty acids (SCFAs) accounts for the mild acidity in the latter. Indeed, the high amount of carbohydrates derived from food intake, along with the mostly anaerobic environment of the intestine, favors the fermentative processes of commensal bacteria, which lead to the accumulation of SCFAs in the form of formic, acetic, propionic and butyric acids. These organic acids enter the microbial cell in the undissociated form and then they dissociate delivering H^+ ions in the cytoplasm, which acidify the cell (Hirshfield *et al*., 2003; Flint *et al.*, 2008). It is important to recall here that the intestine is the most colonized surface of the human body, with up to 10^{12} cells per gram in the colon (Dethlefsen *et al.*, 2006).

In line with this, the microbial fermentation in the oral cavity, another important colonized niche of the human body, mainly causes the production of lactic acid that significantly drops the pH_o, thus causing the proliferation of specific bacterial strains responsible for the dental caries (Struzycka, 2014).

Still, during an infectious process, the pH of the phagolysosome in activated macrophages falls significantly to 4.5-5.0 in the attempt to kill phagocytosed bacteria, thus determining an acidic environment, which supports the immune system to clear the infection (Vandal *et al*., 2009a).

Apart from the human body, neutralophilic bacteria deal with the acid stress in several other instances. In industry, for example, lactic acid bacteria (LAB), comprising the genera *Lactobacillus, Lactococcus, Streptococcus* and many others, are exploited as main source of lactic acid, propionic acid and ethanol derived from microbial fermentation of vegetables, fish and dairy products. Indeed, fermented food are typical of many traditional cooking (Giovannercole *et al*., 2017b). The accumulation of organic acids inevitably causes a drop in pH_o. As such, this trait has linked LAB throughout human history with food fermentation aimed at preserving food from spoilage (Gobbetti *et al*., 2010). Last but not least, bacteria that live in soil are also exposed to an acidic environment: this is due to the NH_4^+/H^+ exchange in

plant roots for nitrogen assimilation (Hinsinger *et al.*, 2003) as well as to the acid mine drainage (Johnson and Hallberg, 2005).

Altogether, these examples provide an indication on how often an acidic environment can be encountered during the life cycle of neutralophilic bacteria, which therefore have to arm themselves. As such, the evolution of molecular strategies aimed at conferring tolerance/resistance to the acid stress is an essential prerequisite for survival in both commensal and pathogenic microorganisms (Foster, 1999). Interestingly, the evolutionary pressure prompted different pathogens to exploit different survival strategies to acid stress. For example, some of them did not evolve specific acid resistance (AR) mechanisms and they simply rely on a high infection dose (ID_{50} = $1x10^9$ cells) to guarantee the survival of a few cells able to reach and colonize the gut. *Vibrio cholerae* falls into this category.

On the other hand, many bacteria, including pathogens, such as the enterobacteria *Escherichia coli*, *Shigella flexneri* and *Salmonella enterica* serovar Typhimurium, have evolved molecular systems for survival in acidic environments, including the GIT. This explains why these microorganisms have a low the infection dose (ID_{50} = $1x10^2$ cells).

The survival to the acid stress is accomplished through two main strategies: *i*) the acid tolerance response (**ATR**), *i.e.* adaptive systems typical of exponential and stationary phase of growth that require a pre-exposure to an environment with moderate acidity (pH = 4.5-5.0); *ii*) the acid resistance (**AR**), typical of stationary phase (but also detected in exponential phase), which guarantees survival even at extreme acidity (pH $\leq$ 2.5) and does not require pre-adaptation to a mildly acidic pH (Foster, 2001; Lund *et al*,, 2014).

At the molecular level, several different mechanisms are involved in the ATR and AR responses and are all depicted in Fig. 1.1. They include: *i*) the active pumping out of intracellular protons via the F_1/F_o ATPase; *ii*) the consumption of intracellular protons through decarboxylation of cytoplasmic amino acids up taken from the external environment; *iii*) the release of ammonia (NH_3) by deaminases, deiminases and ureases enzymes; *iv*) the protection and repair of biological damaged-macromolecules by chaperons (including

periplasmic ones) and proteases, respectively; *v*) the modification of the permeability of the plasma membrane via modification in its lipid composition to reduce the uncontrolled influx of extracellular protons (Lund *et al*., 2014; Pennacchietti *et al*., 2016).

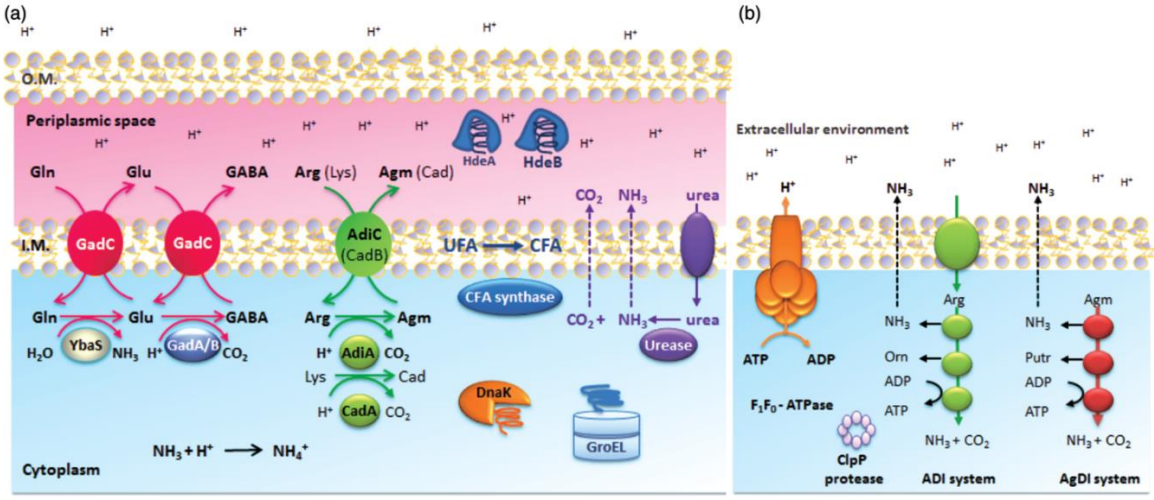

Figure 1.1. *Schematic representation of the most common molecular strategies to cope with the acid stress.* These molecular systems are typically present in bacteria: the Gram-negative context is provided as example in **(a)** whereas those present only in Gram-positive are shown in **(b).** Image from Pennacchietti *et al*., 2016**.**

In the last decades, the mechanisms of acid resistance have been deeply documented and studied in *E. coli* (Foster, 2004; Krulwich *et al*., 2011; Lund *et al*., 2014). Basically, the scientific community distinguishes between oxidative and fermentative AR systems. The first class is represented by **AR1**, a glucose-repressed system that is triggered when cells previously grown in rich medium at pH 5.5 are exposed to an extreme acid stress (pH $\leq$ 2.5). Although very little is known about AR1, recently it has been proposed an intriguing connection of the system with glutamate and nitrogen metabolism, in which the biochemical

components of the AR2 (see below) consume the intracellular glutamate (Aquino *et al.*, 2017).

Unlike AR1 (oxidative system, glucose repressed), the other known AR systems are maximally induced under fermentative conditions and are typically detected in the stationary phase of growth (though not exclusively); each of them relies on the PLP-dependent decarboxylation of a specific amino acid, with concomitant incorporation of an intracellular proton, that is then exported by a membrane antiporter exchanging the decarboxylated product for a new molecule of amino acid. These systems are all depicted in Fig. 1.1 and include: **AR2**, a glutamate-dependent acid resistance mechanism, which relies on the decarboxylation of glutamate by Glutamate decarboxylase (GadA/B, UniProt code*: P69908/P69910; *when not otherwise stated the UniProt code is referred to *E. coli* K12 MG1655) with production of γ-aminobutyric acid (GABA) that is exported via GadC (UniProt code: P63235), the Glu/GABA antiporter; **AR3**, an arginine-dependent acid resistance mechanism in which the amino acid arginine is converted to agmatine by arginine decarboxylase (AdiA, UniProt code: P28629) and then exported via AdiC (UniProt code: P60061), the arginine/agmatine antiporter; in **AR4** lysine decarboxylase (CadA, UniProt code: P0A9H3) yields cadaverine while CadB (UniProt code: P0AAE8) provides to the lysine/cadaverine exchange; **AR5**, whose components are the ornithine-dependent decarboxylase SpeF (UniProt code: P24169) and the ornithine/putrescine antiporter PotE (UniProt code: P0AAF1) (Foster, 2004; Kanjee and Houry, 2013; Lund *et al*., 2014; De Biase and Lund, 2015). More recently a new system that exploits the biochemical component of the AR2 system has been found to contribute significantly to the acid resistance in *E. coli*. This system is dependent on glutamine, the most abundant amino acid available in the free form, and utilizes GadC to import glutamine which is then deaminated by an acid glutaminase YbaS/GlsA (UniProt code: P77454) and the glutamate derived from the hydrolysis of glutamine is then converted to GABA by GadA/B (Lu *et al.*, 2013; Lund *et al*., 2014; Teixeira *et al.*, 2014; Freddi *et al.*, 2017; Pennacchietti *et al*., 2018).

The activity of AR2 and AR3 systems was originally shown to provide the highest protection against extreme acidity (pH ≤ 2.5) in *E. coli* cells, provided that glutamate or arginine are present in the medium (Lin *et al.*, 1995, 1996; Castanie-Cornet *et al.*, 1999). More recent reports suggest that this is likely to be true for many other bacteria as far as the AR2 system (Feehily and Karatzas, 2013; Damiano *et al.*, 2015) and the AR2_Q system, *i.e.* the one dependent on glutamine (Lu *et al.*, 2013; Freddi *et al.*, 2017; Pennacchietti *et al.*, 2018), are concerned.

What makes these AR systems so efficient in allowing the bacteria to withstand the acidity is the effective consumption of intracellular protons occurring during the catalytic cycle of the reaction (1 H^+/amino acid decarboxylation). Indeed, as shown later in this General Introduction and in the following Chapters, each decarboxylation is followed by the incorporation of a proton to compensate for the negative charge left on the amino acid substrate (as the consequence of the amino acid Cα-COO^- bond breakage). Moreover, following the incorporation of the proton into the amine product of the reaction, the export of the amine via the relevant membrane antiporter leads to effective export of protons. In addition to this, CO_2 at acidic pH leaves the solution as gas, thereby not contributing to changes in pH. Thus, the beneficial effect of these systems consists of the net consumption of H^+ and pumping out positive charges (Lund *et al.*, 2014). Overall, the presence of these molecular systems and the overlap in the pH-range of their activity is regarded as the evolutionary success for the survival to a wide acidic pH range.

1.1.2. Physiological insights into the AR2 system

Amongst the AR systems, the AR2 system is the most deeply studied and investigated because of its extreme potency in coping with extreme acid stress (pH ≤ 2.5) in several food-borne pathogens and orally acquired bacteria such as *E. coli*, *S. flexneri*, *Listeria monocytogenes*, *Brucella microti*, *L. lactis* and many others (Lin *et al.*, 1995, 1996; Sanders *et*

al., 1998; De Biase *et al.*, 1999; Cotter *et al.*, 2001; De Biase and Pennacchietti, 2012; Occhialini *et al.*, 2012; Damiano *et al.*, 2015).

The system is typically induced in either rich medium in stationary phase cell cultures independently from the pH of the medium, or in minimal medium when cells in exponential phase are grown at pH 5.0-5.5 (Ma *et al.*, 2003a; 2003b). The experimentally-supported model proposed for the mechanism of action of the AR2 suggests that when the cell is exposed to an extreme pH value (pH $\leq$ 2.5), the uncontrolled entry of protons causes a significant intracellular fall in pH (pH $\leq$ 5.0), that is close to the pH-optimum of enzymatic activity of GadA/B (Gale, 1946; Shukuya and Schwert, 1960; Fonda, 1972; Pennacchietti *et al.*, 2009).

Recent studies, using proteoliposomes reconstituted with GadC, have shown that when glutamate (Glu) is present in the medium, it is imported via GadC in the form of Glu^0 while GABA is exported as $GABA^{+1}$. Thus, the $Glu^0/GABA^{+1}$ exchange contributes to the net export of positive charges. For the sake of clarity, the reported charge on the molecules refers to the global charge of the species under consideration that is transported in/out of the cell by GadC. For example, as shown in Fig 1.2, at pH 3.1 Glu exists as Glu^0 because it is protonated on its γ-carboxyl group (γ-COOH; pK_a 4.1) and on its α-amino group (Cα-NH_3^+; pK_a 9.6) while its α-carboxyl group is deprotonated (Cα-COO^-; pK_a 2.1). Thus, the net electric charge is 0 (zero) and reported as Glu^0.

According to the transport activity carried by GadC, this antiporter recognises and distinguishes Glu and GABA based on their net charges, which result in an electrogenic (or electroneutral) transport (Fig. 1.2) (Ma *et al*., 2013; Tsai *et al*., 2013). This model was called "logic-gate" and was supported by experiments carried out with glutamine (Gln) which, though lacking the γ-carboxyl group, is selectively recognized and imported by GadC in the form Gln^0 (*i.e.* the species with a negative charge on α-carboxyl group and a positive charge on the α-amino group). Overall, the $Glu^0/GABA^{+1}$ exchange not only relieves the drop of pH_i, but also restores the electrochemical gradient across the bacterial membrane that is necessary

to generate ATP (Shepherd *et al.*, 2010; Tsai *et al.*, 2013). Moreover, a third level of protection is obtained through the buffering capacity of the γ-carboxyl groups in Glu and GABA, whose pK_a are close to pH_i during the acid stress, *i.e.* 4.1 and 4.0 for Glu and GABA, respectively (Lund *et al*., 2014).

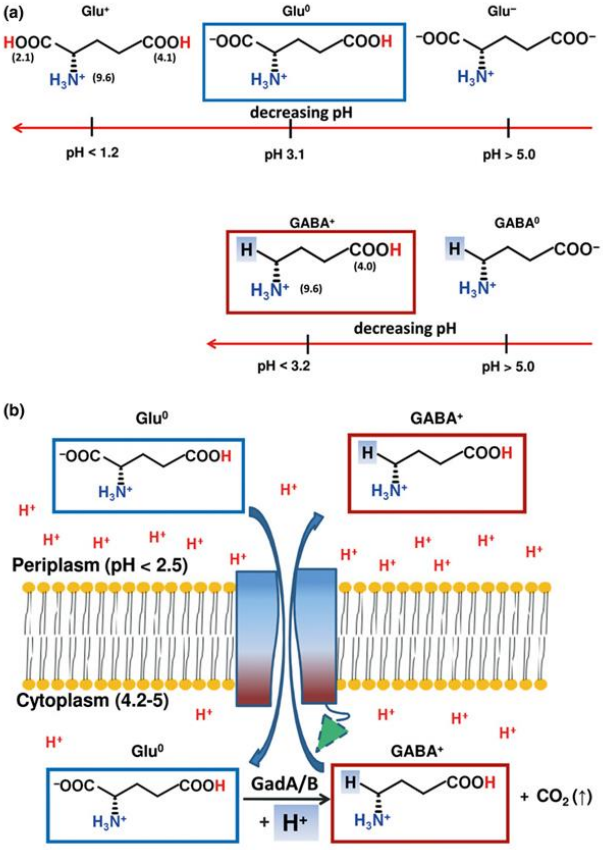

Figure 1.2. *Logic-gate mechanism of GadC.* **(a)** Possible protonation state of Glu and GABA occurring a different pHs. The indicated pH is when the species above the values is >95% abundant. **(b)** Proposed mechanism for Glu^0 and $GABA^{+1}$ selection by GadC. Image from Lund *et al*., 2014.

The finding that GadC can also transport Gln has important implications in linking the AR2 and AR2_Q systems, especially for those bacteria that rely on glutamine to deal with the acid stress, because glutamine can be not only exploited by the AR2 system but also by the cellular metabolism as an important supply of glutamate (Lu *et al.*, 2013; Ma *et al*., 2013; Freddi *et al.*, 2017).

Finally, a possible contribution may derive from chloride channels via H^+_{out}/Cl^-_{in} antiport that relieves the excessive hyperpolarization of the bacterial membrane (Accardi and Miller, 2004; Foster, 2004).

1.1.3. Genetic regulation of the AR2 system

In the *E. coli* genome, *gadB* and *gadC* constitute and operon, *gadBC*, which guarantees the synchronous expression of the decarboxylase and its cognate antiporter, respectively; however, *gadC* can also be expressed by its own promoter (Fig. 1.3) (De Biase *et al.*, 1999). The gene coding for GadA is instead 2.1 Mb distant from the operon *gadBC* and it is located at the 3' end of a 14 kb-long genome region, called acid fitness island (AFI), coding for 14 genes, all of which are involved in the AR response, though at various levels. H-NS (the histone-like nucleoid-structuring protein, UniProt code: P0ACF8) and RpoS (the stationary phase σ factor of the RNA polymerase, UniProt code: P13445) act as global regulators of the expression of AFI genes (De Biase *et al.*, 1999; Hommais *et al.*, 2004; Weber *et al.*, 2005).

The following operon organization in AFI is observed (Fig. 1.3): *slp-yhiF, hdeAB-yhiD, gadE-mtdEF, gadXW and gadAX* (Tramonti *et al.*, 2002b; Tucker *et al.*, 2003; Tramonti *et al*., 2008). Notably, *gadA* can be either independently or co-transcribed with *gadX* (Tramonti *et al.*, 2002b).

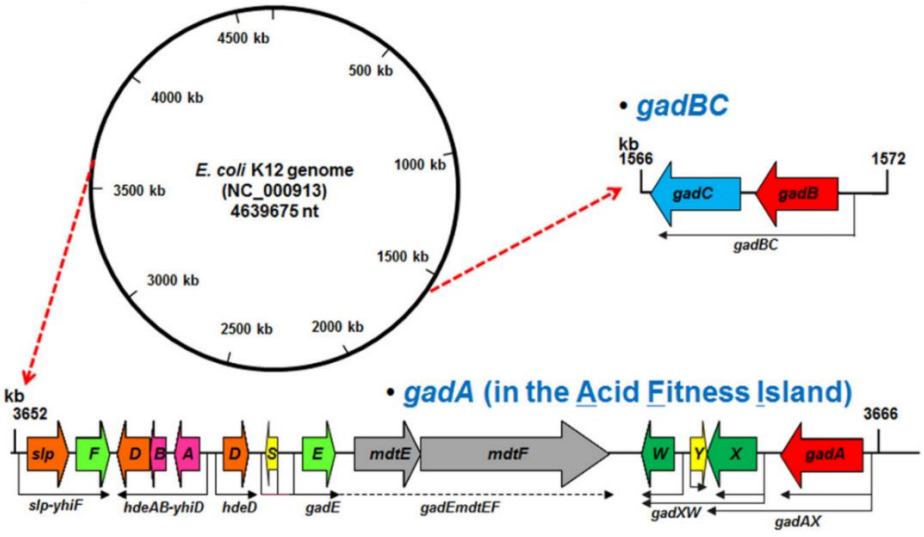

Figure 1.3. *Genomic organization of the GDAR and AFI genes*. Representation of the *E. coli* genome map with the location of the loci encoding GadA/B (red), GadC (blue), additional membrane proteins (orange), multidrug exporters (grey), acid stress periplasmic chaperons (magenta), LuxR-like transcriptional regulators (light green), AraC-like transcriptional regulators (green) and a small regulatory RNAs (yellow). The bent arrows show the transcripts' start and length of the operons. Image from De Biase and Pennacchietti, 2012.

Depending on the growth conditions, all the AFI-genes contribute to the AR response at various levels:

i) transcriptional regulation is carried out by GadX (UniProt code: P37639), GadW (UniProt code: P63201) and YdeO (UniProt code: P76135, belonging to AraC-like family of transcriptional regulators), by YhiF (UniProt code: P37195) and GadE (UniProt code: P63204, belonging to the LuxR family of transcriptional regulators), and by GadY and ArrS. The latter two are small RNAs that affect the stability of *gadE* and *gadX* mRNAs (Tramonti *et al.*, 2002b, 2006, 2008; Ma *et al.*, 2003a; Tucker *et al.*, 2003; Opdyke *et al*., 2004; Aiso *et al*., 2011). Notably, the transcriptional regulators GadE, GadW, GadX and GadY were all shown

to positively regulate the expression of the operon *gadBC* (Tramonti *et al.*, 2002b; Hommais *et al.*, 2004; Tramonti *et al.*, 2006; Tramonti *et al*., 2008).

ii) Protection of acid-denatured proteins via the periplasmic chaperones HdeA (UniProt code: P0AES9) and HdeB (UniProt code: P0AET2) (Hong *et al.*, 2005; Kern *et al.*, 2007);

iii) protection from acidic metabolites such as lactate, succinate and formate by membrane proteins coded by *slp, yhiD* and *hdeD* (Mates *et al*., 2007);

iv) multidrug export through *mdtE* and *mdtF* induced by GadX in stationary phase (Kobayashi *et al.*, 2006; Nishino *et al*., 2008).

Usually, the proximity of *gadB* and *gadC* in the genome of food-borne, orally acquired, enterobacteria passing through the GIT is regarded as a mark of the involvement of the glutamate decarboxylase-dependent system to cope with the acid stress in this compartment (De Biase and Pennacchietti, 2012).

Due to the essential activity of the AR2 system in *E. coli*, it is not surprising that it shows a high complexity in its regulation and in the mechanisms of detection and response to the acid stress (Fig. 1.4). At the top of the AR2 regulation is the two-component system (TCS) EvgAS, in which the low pH is primarily sensed in exponential growing cells by the sensor-kinase EvgS (UniProto code: P30855) that phosphorylates and activates the transcriptional factor EvgA (UniProt code: P0ACZ4). Amongst the numerous target of EvgA, there are *ydeP*, whose function in the AR is still debated, and the *safA-ydeO* operon (Eguchi *et al.*, 2011). SafA (UniProt code: P76136) mediates a cross-talk between several TCSs while YdeO activates GadE, a key regulator of the AR2 (Ma *et al.*, 2003a). SafA also activates the PhoPQ (UniProt code: P23836/P23837) system that increases the level of RpoS, a stationary-phase alternative σ factor that regulates the activity of several genes, amongst which those involved in the acid resistance response, such as GadE. Interestingly, RpoS levels are also found

increased when exponential growing cells are shifted to pH 5 and, though still poorly understood, this might be due to EvgAS. GadE, by acting as an central regulator of AR2, positively regulates the expression of *gadBC*, *gadA*, and *hdeAB* (Masuda and Church, 2003; Ma *et al*., 2004; Itou *et al*., 2009).

Besides the molecular EvgAS/YdeO/PhoPQ circuit, two other networks are responsible for the activation of GadE in acid conditions: the TrmE circuit (UniProt code: P25522), typical of stationary phase cells grown in LB medium at pH 5.2 supplemented with *D*-glucose (Gong *et al*., 2004), and the GadX/GadW circuit, which operates in stationary phase cells in LB medium at pH 5.5. GadX and GadW can, in fact, activate *gadA* and the operon *gadBC* directly or indirectly. In the latter case GadE is involved (Tramonti *et al.*, 2002b, 2006, 2008; Sayed *et al*., 2007). The GadX/GadW circuit is mostly controlled by GadY, a small regulatory RNA, that post-transcriptionally ensures the stabilization of the *gadX* transcript (Opdyke *et al*., 2004; Tramonti *et al*., 2008). On the other hand, GadX was shown to regulate its own mRNA by positively affecting the expression of *gadY* (Tramonti *et al*., 2008). Interestingly, the expression conditions of *gadX* and *gadY* overlap those of *gadBC* and *gadA*; furthermore, GadX and GadW were suggested to oppose the silencing of *slp-yhiF*, *hdeAB* and *gadE-mtdEF* operons mediated by H-NS (Tramonti *et al*., 2008).

A further level of complexity is given by the RcsB protein (UniProt code: P0DMC7), a transcriptional regulator that is responsible for the GadE-dependent or -independent expression of the AR2 genes. Moreover, RcsB is reported to affect the levels of H-NS and RpoS; in the latter case by inducing the expression of a small regulatory RNA, RprA, that enhances the translation of RpoS mRNA (Lund *et al*., 2014; De Biase and Lund, 2015).

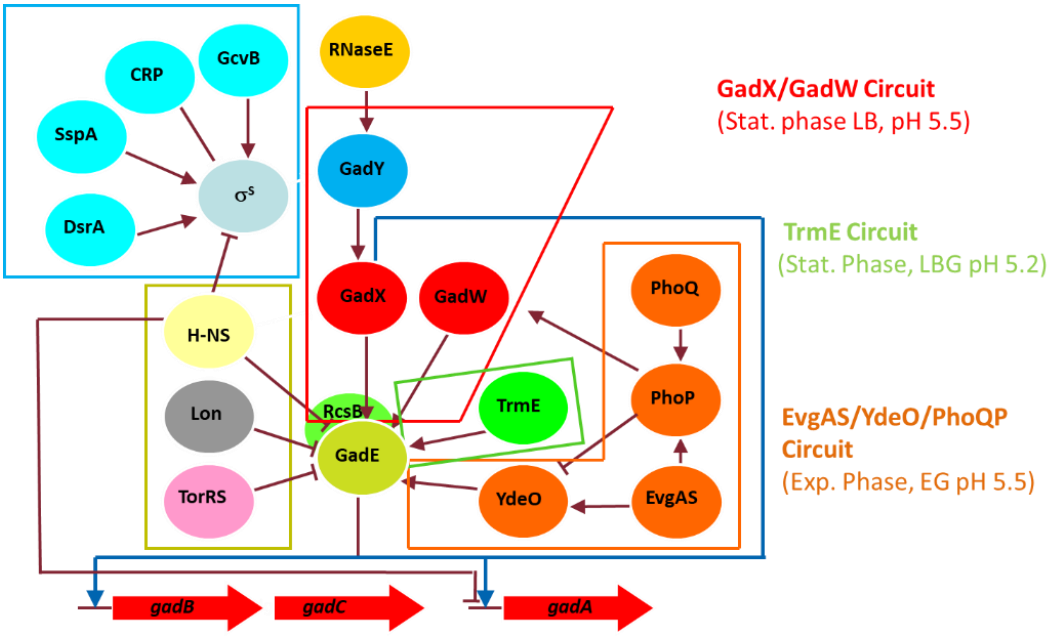

Figure 1.4. *Circuits that control the activation of the gad genes in* E. coli. The role of GadE as a central regulator is highlighted. The different environmental conditions and the key players that activate the *gad* genes are shown in panels of the same colors.

1.1.4. Biochemical and structural features of the AR2 system in *E. coli*

1.1.4.1. GadA and GadB

At the heart of the AR2 system is the PLP-dependent irreversible decarboxylation of glutamate to GABA catalysed by the enzyme glutamate decarboxylase (Gad; E.C. 4.1.1.15). In response to the acid stress, *E. coli* synthetizes two Gad isoforms, GadA and GadB, both 466 amino acids long, which share 99% of the amino acidic sequence identity, differing only for 5 residues: 4 of them are localized at the N-terminus while the fifth in position 153. These residues are in GadA and GadB, respectively: Gln3Lys, Leu6Val, Phe9Leu, Ala22Ser and

Asn153Asp. None of them is involved in catalysis, nor in the pH-dependent regulation of enzymatic activity. Therefore GadA and GadB are biochemically indistinguishable (De Biase *et al.*, 1996).

The first biochemical studies on Gad clarified that the enzyme is specific for glutamate and shows a pH-dependent enzymatic activity below pH 5, with a maximum at pH 4.5, whereas it is completely inactive above pH 5.5 (Shukuya and Schwert, 1960; Fonda, 1972).

The pH-dependent biochemical and spectroscopic properties of GadB from *E. coli* (hereafter *Ec*GadB) have been intensively investigated since it was successfully overexpressed and purified in large quantities (De Biase *et al.*, 1996). At the biochemical level, *Ec*GadB exhibits a pH-dependent spectroscopic absorption of PLP (Fig. 1.5): at pH 4.6, where the enzyme is catalytically active, PLP displays an absorption peak at 420 nm (the enzyme is therefore yellow), which corresponds to the *ketoenamine*, the tautomeric form of the internal aldimine typical of an hydrated active site; whereas when *Ec*GadB is enzymatically inactive (above pH 5.5), the cofactor displays an absorption peak at 340 nm (colourless), which was proposed to correspond to an *aldamine*, where a sulfhydryl group at the active site of the enzyme adds to the carbon of the internal aldimine (O'Leary and Brummund, 1974).

Crystallographic (see below) and rapid kinetic studies carried out on *Ec*GadB strongly suggest that the pH-dependent spectroscopic transition is a cooperative process (Fig. 1.5, inset), which involves the loss/gain of >6 protons that indirectly affect the accessibility of the active site. In line with this, the crystal structures show that GadB active site at acidic pH is open and more hydrated (Capitani *et al.*, 2003a), which supports the spectrophotometric observation that PLP is present as *ketoenamine* (Fig. 1.6A). This is the species responsible for the absorption at 420 nm. On the contrary, the 340 nm-absorbing species is a *substituted aldamine* (Fig. 1.6C), which is not generated with a sulfhydryl group, as suggested by O'Leary and Brummund, 1974. Rather the formation of the covalent bond involves the side-chain imidazole ring of a histidine residue, His465, with the PLP-Lys276 Schiff-base; this

causes a sp^2 to sp^3 change in the hybridization state of C4' (Gut *et al.*, 2006; Pennacchietti *et al.*, 2009).

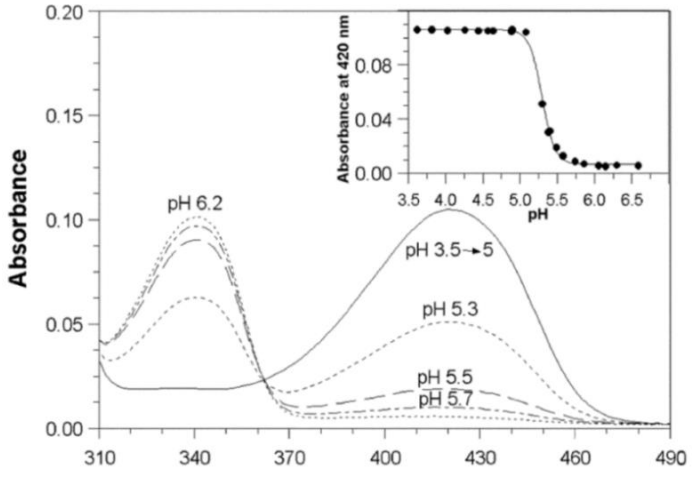

Figure 1.5. *Absorption spectra of* Ec*GadB*. The absorbing peaks at 340 and 420 nm are appreciable in the spectral region between 300 – 500 nm. The spectrum acquired at pH 5.3 is the closest to the p*K* of the spectroscopic midpoint transition. Inset panel: titration curve obtained by plotting the 420 nm absorbance values as a function of pH changes. Image adapted from Tramonti *et al.*, 2002a.

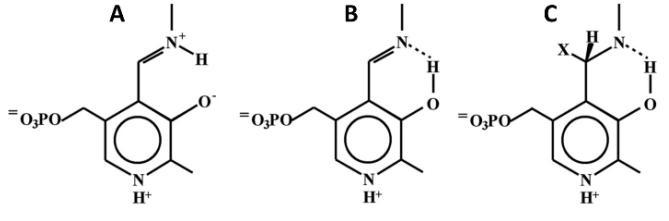

Figure 1.6. *Chemical structures of* ***(A)*** *ketoenamine,* ***(B)*** *enolimine and* ***(C)*** *substituted aldamine.* "X" is the side chain imidazole ring of *Ec*GadB His465. Image adapted from Pennacchietti *et al*., 2009.

Importantly, the pH-dependent spectroscopic transition is strongly influenced by the binding of halides which, according to the following scale of strength $I^- > Br^- > Cl^-$, promote and stabilize the enzymatic active form (O'Leary and Brummund, 1974). Amongst these halides, Cl^- is biologically relevant since it is abundant in the gastric juice; therefore, its positive influence on *Ec*GadB constitutes a successful biochemical evolution (Gut *et al.*, 2006).

The high resolution structure of *Ec*GadB was solved by X-ray crystallography at pH 4.6 and 7.6 (Fig. 1.7), *i.e.* in the active and inactive form respectively, and represented a key point for the understanding of the pH-dependent biochemical features of the enzyme at atomic scale (Capitani *et al.*, 2003a). Based on the crystal structure, *Ec*GadB is an homohexamer of 318 kDa, which can be described as trimer of dimers organized on two spatial levels, in which the dimer represents the minimal unit for the enzymatic activity, with residues at the active site contributed by both subunits of the active dimer. This is typical in the fold of PLP-dependent enzymes.

Each monomer presents three different domains: *i*) an N-terminal domain (residues 1-57); *ii*) the central PLP-binding domain (residues 58-346); *iii*) a C-terminal domain (residues 347-466). The latter is involved in the closure of the active site at pH > 5.5, thus playing an important regulatory role of the activity. The stability of the oligomeric assembly is given by each monomer's N-terminal domain, which departs perpendicularly as a hook from one subunit to reach the opposite layer, thus establishing important contacts with the counterpart in the functional dimer and with a subunit from a neighbouring dimer.

*Ec*GadB structure is highly influenced by pH, with three major structural changes occurring in the first 15 residues of the N-terminal domain, in a small β-hairpin structure (residues 300-313) and in the last 15 amino acids of the C-terminal domain, respectively.

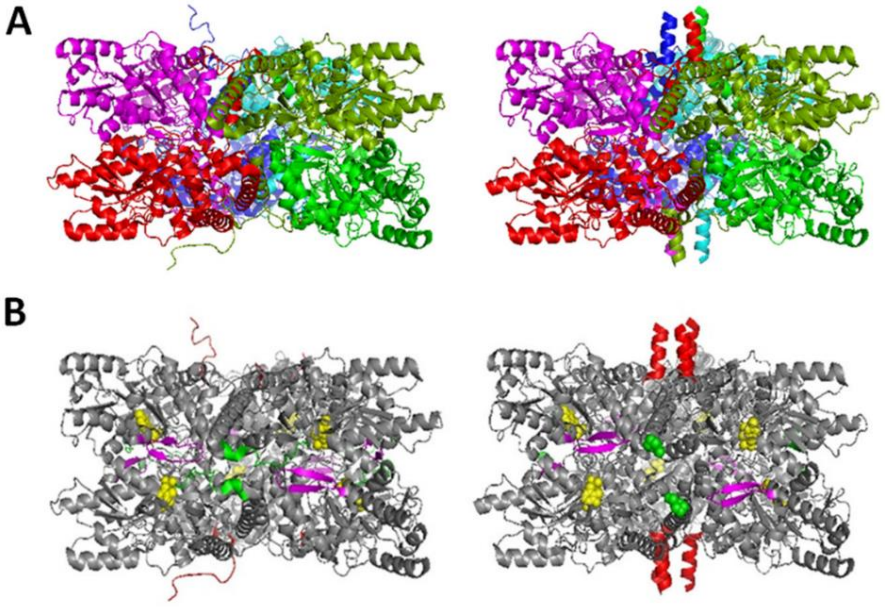

Figure 1.7. *Side views of the* Ec*GadB hexamer at neutral (left) and acidic (right) pH.* **(A)** The two-layered GadB hexamer is shown in colors. Each dimer contributes to both layers. **(B)** Major conformational changes in *Ec*GadB. The hexamer is in gray; the 1–14 N-terminal region, which at acidic pH forms the two triple helix bundles, are in red; the 452–466 C-terminal tail is in green; the 300–313 β-hairpin is in magenta. PLP is shown in filled space (yellow). From De Biase and Pennacchietti, 2012.

The comparison of the atomic structures solved at pH 4.6 and 7.6 provided insights into these structural changes. At neutral pH (Fig. 1.7 right), the N-terminal domain is completely disordered, whereas it becomes structurally ordered at acidic pH (Fig. 1.7 left). This is due to side chains of several acidic amino acids in the N-terminal domain which, at neutral pH, are negatively charged, thus repelling each other and preventing the formation of an ordered structure. On the other hand, when *Ec*GadB is exposed to low pH, the protonation of these side chains abolishes the reciprocal repulsions and allows the formation of α-helices that give rise to two triple helical bundles, each departing perpendicularly from the opposite layers of

the hexamer (Capitani *et al.*, 2003a). The formation of these triple helical bundles is biologically significant since it allows *Ec*GadB to get closer to the membrane compartment, where the antiporter GadC is also located. This was suggested to be key in best coupling the decarboxylase activity to the Glu/GABA exchange and to effectively remove protons as soon as they enter in the cell, *i.e.* reducing the cell damage by extensive cytosolic acidification below a threshold level (Capitani *et al.*, 2003a). Moreover, the formation of the triple helical bundles provides the binding site for the halides, allowing them to act a positive allosteric modulators of the pH-dependent enzymatic activity, as demonstrated by studies carried out on a mutant enzyme depleted of the first 14 amino acids (*Ec*GadBΔ1-14) which was found to be not affected by the presence of Cl^- ions and to display a cooperativity in the conformational change which is halved ($n = 2.5$) respect to that reported for wild type enzyme ($n > 6$) (Gut *et al.*, 2006; Pennacchietti *et al.*, 2009).

The second pH-dependent change occurs at the C-terminal domain and represents the biochemical mechanism of inactivation of the enzyme when pH increases to no more harmful levels (pH > 5.7). In fact, compared to pH 4.6, in the structure resolved at pH 7.6 the C-terminal domain is structurally ordered and points toward the active site, in which the side-chain of the penultimate residue, His465, establishes a covalent bond with the C4' of PLP (Fig. 1.8); this not only determines the formation of the *substituted aldamine*, a chemically inactive form of PLP, but also closes up the active site, thereby making it not accessible to the entry of glutamate, the substrate. In support of this hypothesis, the *Ec*GadB alanine mutant for H465 (*Ec*GadB_H465A) and the enzyme deleted of the last two residues, *i.e.* His465 and Thr466 (*Ec*GadBΔHT), clearly show that the enzyme is still catalytically able to decarboxylate glutamate and produce GABA at pH > 6.0. However, neither mutants display alterations in the membrane localization, suggesting that the events accompanying the folding/unfolding of the triple helical bundles are completely independent from the opening/closure of the active site (Pennacchietti *et al.*, 2009). However, the unfolding of the

α-helices affects the rate at which the C-terminal end regains access into the active site (Gut *et al.*, 2006).

A third large pH-dependent structural change is evident in the active structure resolved at pH 4.6, in which the displacement of the C-terminal domain from the active site, allows a small sequence (300-313) folded as a β-hairpin, coming from the other subunit of the dimer, to partially occupy the open active site following the displacement of the C-terminal tail, with which it interacts at neutral pH (inactive form) (Capitani *et al.*, 2003a).

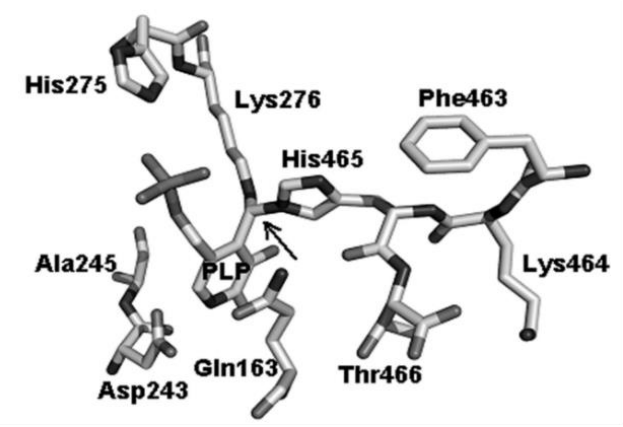

Figure 1.8. *Structure of substituted aldamine at atomic scale.* The arrow indicates the formation of the covalent bond between the imidazole ring of *Ec*GadB H465 and the C4' of PLP. Image from Pennacchietti *et al.*, 2009.

1.1.4.2. GadC

The Glu/GABA antiporter GadC belongs to the superfamily of amino acid-polyamine-organocation (APC) membrane transporters that comprises also the AdiC antiporter of the AR3 system. The structure of GadC (Fig. 1.9) was solved at pH 8.0 and revealed interesting structural features of the inactive (inward-open) conformation (Ma *et al.*, 2012). GadC is composed of 12 transmembrane (TMs) α-helices arranged in two inverted repeats: TM1-TM5

and TM6-TM10. Two short α-helices connected by a discontinuous stretch in the middle form TM1 and TM6.

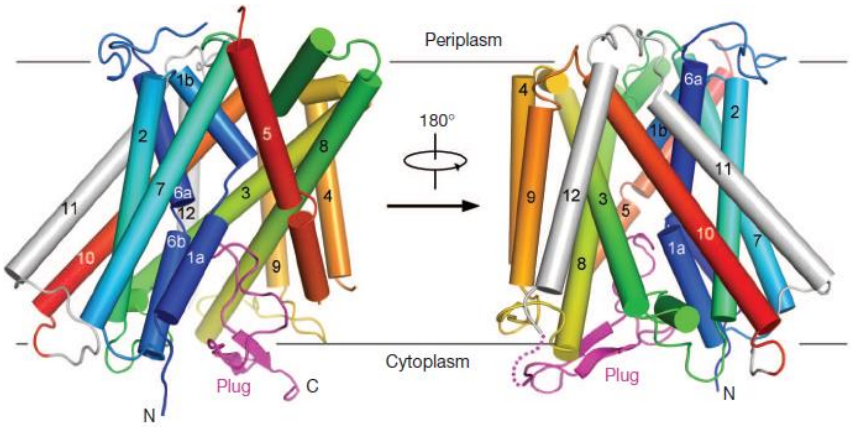

Figure 1.9. *Overall structure of GadC.* TM1-TM10 are rainbow-colored, with TM1 in blue and TM10 in red. TM11 and TM12 are in gray. The C-terminal fragment (C-plug) is in magenta. Image from Ma *et al.*, 2012.

Experiments carried out with reconstituted proteoliposomes demonstrated that, alike GadA/B, GadC exhibits a pH-dependent activity profile, being active only at pH ≤ 5.5, thus overlapping completely the activity profile of GadA/B (Gut *et al.*, 2006; Ma *et al.*, 2012). Interestingly, another important feature that the proteins have in common, is the pH-dependent regulation of the activity mediated by the C-terminal tail of GadC (C-plug, residues 477-511) at pH > 5.5. This C-plug is structurally ordered and points toward the putative substrate binding path, thus blocking it. The C-plug is rich of positively charged residues (His and Arg) that are thought to contribute to the its structural stabilization by establishing hydrogen bonds with other residues of the protein cytosolic side. Indeed, a C-plug deletion mutant exhibits a shift in the midpoint of the activity profile by 0.5 pH unit toward alkaline

pH. Therefore, likewise GadA/B, the pK_a of these residues (His in particular) may significantly contribute to the pH-dependent regulation of the protein (Ma *et al.*, 2012).

The crystal structure of GadC also provides insights into the Glu/GABA exchange path. In the closed conformation, in addition to the C-plug oriented towards the cytoplasm side, the L7 loop lies at the periplasmic side. The substrate path is sandwiched between the C-plug and the L7 loop and surrounded by the TM1-2-6-8-10; therefore, to allow the binding of the substrates, both the C-plug and the T7 loop have to be displaced.

As mentioned above, GadC mainly imports Glu^0 and exports $GABA^{+1}$, resulting in the removal from the cytoplasm of 0.8-0.9 H^+ *per* cycle, thus contributing to the negative polarization of the membrane. Therefore, in the outward-opened conformation, GadC does not accept the +1 valence, whereas in the inward-opened conformation it discharges Glu^0 and uptakes $GABA^{+1}$ (Ma *et al*., 2013; Tsai *et al*., 2013).

1.1.5. Bacterial Gads signature

GadA and GadB, together with the other cytoplasmic amino acid dependent decarboxylases previously discussed, require PLP to catalyze their reactions. PLP is the biological active form of vitamin B_6 and plays a key role as a coenzyme in over 160 distinct enzymes, about 4% of all the biochemical reactions so far known (Percudani and Peracchi, 2003, 2009). Thanks to their catalytic versatility and their broad distribution in biochemical reactions in living cells, such as the metabolisms of amino acid, nucleotides, sugars, cofactors and neurotransmitters, PLP-dependent enzymes have always been regarded also as potential drug targets for the treatment of diseases (Percudani and Peracchi, 2003, 2009).

All the PLP-dependent enzymes that use amino acids as substrates show common biochemical features: PLP is anchored to the polypeptide chain via a covalent bond between the C4' of its aldehyde group and the ε-amino group of a lysine residue (Schiff-base) forming the *internal aldimine*. Following the entrance of the amino acid substrate in the active site, the reaction occurring between the α-amino group and the internal aldamine brings to the

formation of the *external aldimine* through a process called transaldimination involving geminal diamine intermediates. As a result, PLP becomes covalently bound to the α-amino group of the substrate and a new Schiff-base is generated (external aldimine). The reaction proceeds with the bond breakage at Cα, a process kinetically favored when the bond is perpendicularly positioned with respect to the pyridine ring of PLP, thus allowing the delocalization of the negative charge across the π-orbitals of the ring (Fig. 1.10).

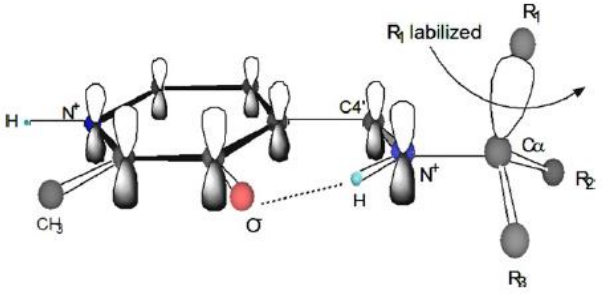

Figure 1.10. *Schematic representation of the π-orbital system in PLP participating in the electron delocalization.* The specificity of the reaction is given by the rotation of the bond between Cα and the amine nitrogen. Image from Toney, 2005.

In detail, the negative charge of the carbanion intermediate is stabilized by the nitrogen of pyridine ring positively charged as well as by the π-orbital system. This peculiar chemical feature allows PLP to act as an electron sink that stabilizes the intermediates of reaction. As such, PLP is extremely versatile and able to catalyze spontaneously a myriad of different biochemical reactions, though slowly (Dunathan, 1966; Toney, 2005). In fact, the role of the polypeptide chain is to provide the ideal chemical environment to favor and speed up one specific reaction. However, secondary biochemical reactions are reported to occur in several PLP-dependent enzymes as the result of their catalytic promiscuity due to their evolution from common progenitors (Grishin *et al*., 1995).

The last species common in all the PLP-dependent reactions is the quinonoid intermediate that originates either from Cα-proton abstraction or CO_2 release. From this point the reaction can proceed in different ways (Fig. 1.11): *i*) protonation on Cα (in decarboxylases) or on C4' (in decarboxylative transamination); *ii*) elimination of the R-group with concomitant protonation on Cα (aldol cleavage) or addition of a new R-group on Cα (α-synthesis); *iii*) reprotonation on Cα which brings to racemization; *iv*) reprotonation on C4' which brings to transamination, *v*) reprotonation on Cγ and then on Cα for γ-synthesis; *vi*) loss of halogen (X) from Cβ and adding of R on Cβ followed by protonation on Cα for β-synthesis (Jansonius, 1998).

The PLP-dependent decarboxylation of an amino acid is catalyzed by α-decarboxylases, which play a significant role in numerous physiological processes inside the cell, such as the synthesis of neurotransmitters and polyamines or in the regulation of pH_i.

Glutamate decarboxylases belongs to the group II of decarboxylases, based on the sequence similarity (Sandmeier *et al*., 1994), and to the aspartate aminotransferase family (Fold type I) because of the significant structural conservation (Momany *et al*., 1995b).

At the biochemical level, the reaction of transaldimination brings to the external aldamine which, in all α-decarboxylases, presents the chemical bond between the Cα and the α-carboxyl group perpendicular to the pyridine ring of PLP. Therefore, as explained above, the heterolytic cleavage of this bond is favored, determining the release of CO_2 and the formation of the quinonoid intermediate. From this point, a proton is provided to the Cα. This leaves the Schiff base unaffected and therefore the entry of a water molecule brings to the release of the amine product and restoration of the Schiff-base between the C4' of PLP and the ε-amino group of the lysine residue at the active site (Fig. 1.11, Decarboxylation).

Racemization (alanine racemase)

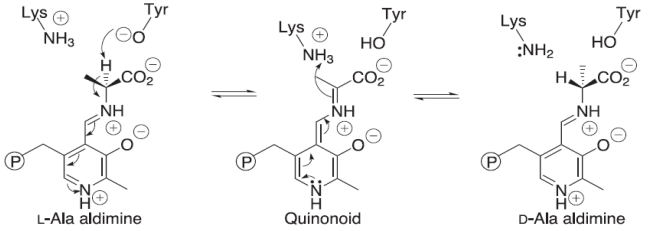

Decarboxylation (prokaryotic ornithine decarboxylase)

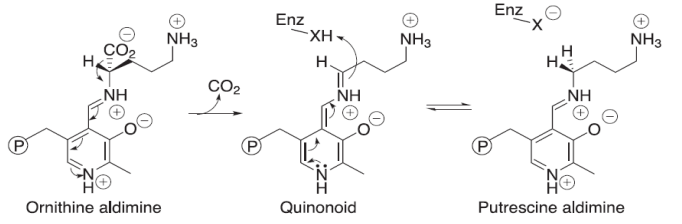

α–Elimination and replacement (serine hydroxymethyltransferase)

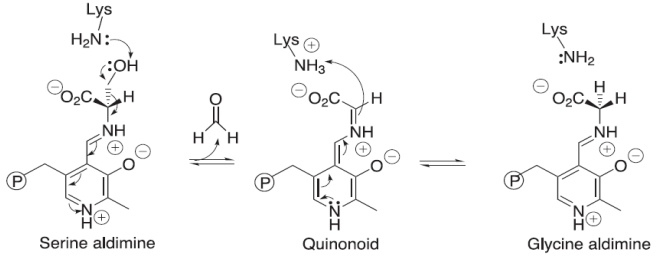

Transamination (tyrosine aminotransferase first half-reaction)

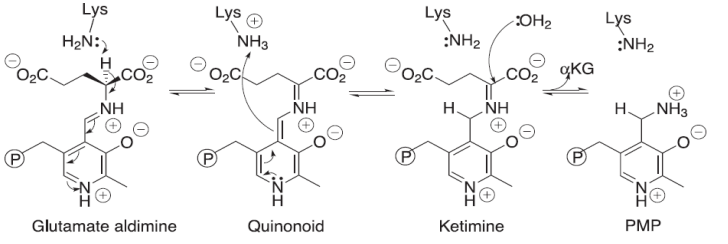

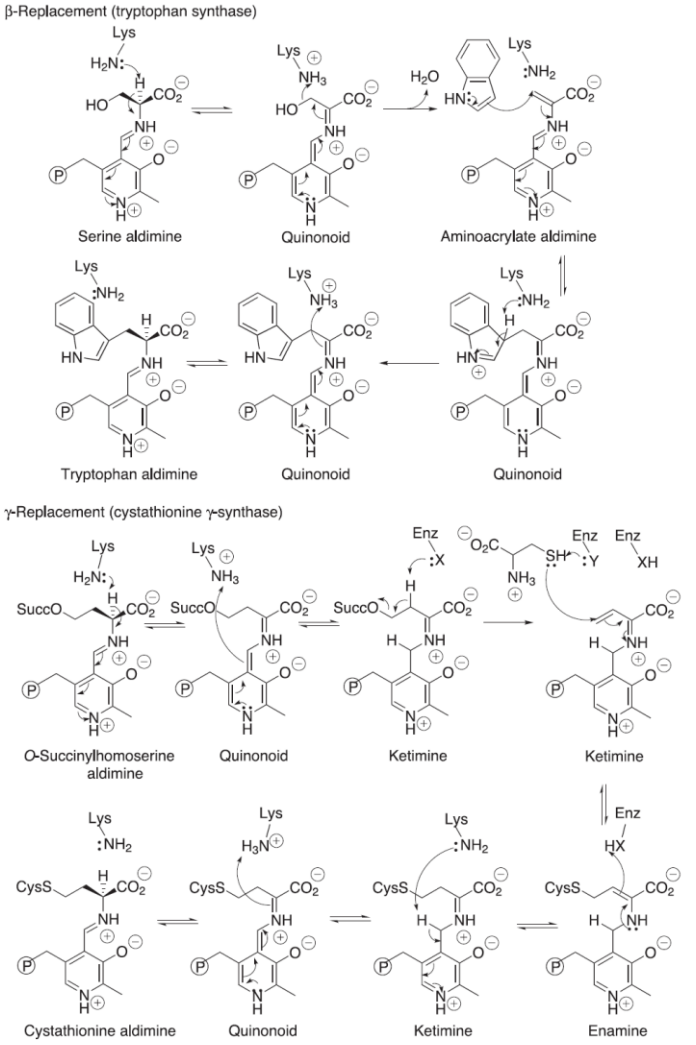

Figure 1.11. *Catalytic versatility of PLP-dependent enzymes*. All the possible reactions on the Cα or side chain of amino acids are exemplified. The quinonoid intermediate is formed in all the reactions. Further details are provided in the text. Image from Eliot and Kirsch, 2004**.**

Rarely, the amino acid-dependent decarboxylation proceeds with a side reaction leading to of abortive decarboxylation-transamination occurring every 10^4-10^5 catalytic events (Sukhareva, 1986). When this occurs, the quinonoid intermediate, instead of being protonated on Cα, gains a proton on C4'. The reaction goes to completion with the release of the amino acid-derived ketoacid and PMP (pyridoxamine-5'-phosphate) which irreversibly inactivates the enzyme. As previously reported, this is due to the common ancestral origin of these enzymes, but it might have been evolutionally conserved as an intrinsic control of the enzymatic activity within the cell.

The alignment of the group II decarboxylases displays a high conservation of 8 residues in the active site. In *Ec*GadB these are, respectively: Lys276, whose ε-amino group forms the Schiff-base with C4' of PLP; Asp243, which, by forming a salt bridge between its side chain and the pyridine's nitrogen of PLP, enhances the electron sink feature of the pyridine ring; Ala245, which establishes a hydrophobic contact with its side chain and the pyridine ring; the hydrophobic contact between His241 and Ser269 stabilizes the interaction between two β-filaments and a long α-helix in the central domain; Thr212, which could be involved in a intramolecular proton transfer with the PLP hydroxyl group; Gly120 and Gly210, playing probably a structural role (De Biase and Pennacchietti, 2012).

Likewise, the alignment of 20 bacterial Gad highlights the conservation of 84 residues, about 18% of the *Ec*GadB sequence, most of them occupying critical positions in regions where the major pH-dependent structural changes take place. 21 of these residues are regarded as GAD-signature, *i.e.* residues characteristic of all bacterial Gads because always present in them (Table 1.1).

Table 1.1. *Amino acid residues composing the bacterial Gad-signature*. Adapted from De Biase and Pennacchietti, 2012.

Residue[a]	Role
Thr62 (side chain OH)	Binding of substrate γ-carboxylate
Phe63 (amide N)	Binding of substrate γ-carboxylate
Phe63 (side chain)	Prevents Arg422 binding to substrate α-carboxylate
Asp86* (β-carboxylate)	Binding of substrate γ-carboxylate
Glu89* (side chain)	Significant change in orientation upon pH-shift
Gly120[b]	Structural role
Ser126 (amide N)	Hydrogen bond with PLP phosphate oxygen
Ser127 (side chain OH)	Hydrogen bond with PLP phosphate oxygen
Gln163 (alkyl chain)	PLP stacking
Gly210	Probable structural role
Thr212 (side chain OH)	Interacting with PLP OH (intramolecular proton transfer?)
His241 (side chain π N)	Hydrogen bond with Ser269
Asp243 (β-carboxylate)	Interacting with the pyridine N of PLP
Ala245 (side chain)	Hydrophobic contact with the pyridine ring of PLP
Ser269 (side chain OH)	Hydrogen bond with His241
His275 (side chain τ N)	Hydrogen bond with PLP phosphate oxygen
Lys276 (ε-amino group)	Forming the Schiff-base with the C4' of PLP
Tyr305* (side chain OH)	Interacts with residues 461–463 of the C-terminus (reprotonation?)
Leu306*	Interacts with residues 461–463 of the C-terminus
Gly307*	In the β-turn of β-hairpin 300–313
His465 (side chain τ N)	Covalent bond with PLP-Lys276 Schiff base

a, numbers refer to *Ec*GadB;
b, residues in plain text are strictly conserved in the decarboxylases of the PFAM PF00281;
*, refers to residues from the other subunit in the functional dimer.

These residues include: Asp86* (*from the neighbouring subunit in the functional dimer), whose side-chain points into the active site in the open conformation and contacts the γ-carboxylate of glutamate (the role of this residue is deeply investigated in Chapter III of this thesis); Glu89, which is either near or distant from Asp86* in the active and inactive conformations, respectively (Capitani *et al.*, 2003a); Gln163, whose alkyl-chain is involved in a stacking interaction with the pyridine ring of PLP (notably, in the other PLP-dependent decarboxylases glutamine is replaced by phenylalanine, tryptophan, tyrosine or histidine); Thr162 and Phe63, which interacts with glutamate (in particular, Phe63 is important to preclude the interaction between the α-carboxyl group of glutamate with the side-chain of Arg422 as observed in aminotransferases); His275, which precedes the PLP-bond residue

Lys276, whose side-chain τ nitrogen makes a hydrogen bond with the PLP phosphate oxygen, necessary to correctly position the PLP in the active site (Tramonti *et al.*, 1998; Capitani *et al.*, 2003a); Tyr305* and Leu306* of the β-hairpin, which interact with residues 461-463 of the C-terminus in the inactive form; Tyr305* may also be probably involved in the protonation of the glutamate-Cα occurring during the reaction as already observed for Tyr332 in *L*-DOPA decarboxylase (UniProt code: P80041) (Bertoldi *et al.*, 2002); His465, responsible for the pH-dependent control of the enzymatic activity by closing the active site and promoting the formation of the substituted aldamine at neutral pH (Gut *et al.*, 2006; Pennacchietti *et al.*, 2009); Cys64, 130 and 165 in the active site, of which the latter two are spatially organized to potentially form a disulfide bridge, though not observed in the crystallographic structures (Capitani *et al.*, 2003a; De Biase and Pennacchietti, 2012).

1.2. Biochemical aspects of *L*-glutamate in bacteria

1.2.1. Centrality of *L*-glutamate in bacterial metabolism and physiology

L-Glutamate is one of the 20 proteinogenic amino acids, *i.e.* required as a building block to make proteins in all living systems, and one of the eleven amino acids that are not essential in humans since it can be synthetized *de novo* without being introduced through diet. Far beyond protein synthesis, *L*-glutamate is a key metabolite in a wide array of biochemical processes of the primary metabolism that include the carbon and nitrogen metabolism, synthesis of amino acids, polyamines, nucleosides and cofactors, most of them strictly required for the survival of the cell. As also described in great detail in previous paragraphs, glutamate serves also as a central metabolite in defence mechanisms to harsh environmental conditions, such as in the acid resistance systems exploited by several food-borne pathogens transiting through the host GIT (De Biase and Pennacchietti, 2012; Lund *et al.*, 2014), or in the form of glutathione to maintain the redox homeostasis (Giovannercole *et al.*, 2017b).

Therefore, it is not surprising that in *E. coli* it constitutes the most abundant intracellular metabolite (40% of the metabolome), with a concentration estimated to be 120 mM that

largely exceeds the concentration of all the other amino acids; moreover, it is the main intracellular counter-ion of K^+ (McLaggan *et al.*, 1994; Bennett *et al.*, 2009).

Fig. 1.12 reports all the biochemical transformations in which *L*-glutamate has been found to be a key player in bacteria.

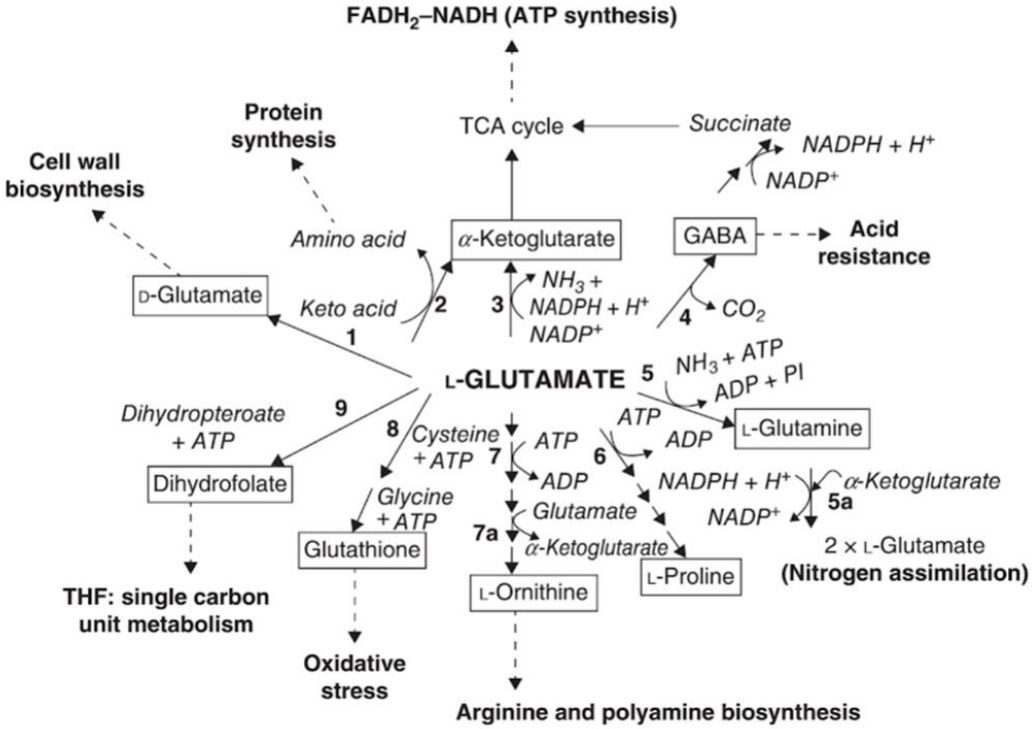

Figure 1.12. *Centrality of* L-*glutamate in microbial metabolism.* The bold numbers shown abutting the reaction arrows refer to the most well-known enzymatic transformations of *L*-glutamate: racemization **(1)**; transaminations **(2)** with *L*-glutamate as amino donor; oxidative deamination **(3)**; decarboxylation **(4)**; and ATP-dependent ligations **(5–9)**. Reactions **(1–3)** can be reversible. The metabolites in the boxes will then enter into metabolic pathways (dashes and arrows) affecting many biological processes (in bold). Abbreviations: FADH2, reduced form of flavin adenine nucleotide; GABA, γ -aminobutyrate; TCA cycle, tricarboxylic acid (or Krebs) cycle. Image from Giovannercole *et al*., 2017b.

These transformations include:

1. ***Racemization*** of *L*-glutamate to *D*-glutamate which serves as an essential component of peptidoglycan of the bacterial cell wall. The transformation is catalyzed by glutamate racemase (UniProt code: P22634), encoded by *murI* gene in *E. coli*.

2. ***Transamination*** via specific PLP-dependent amino acids transaminases that catalyze the transfer of the amine from glutamate to the *α*-ketoacid precursors of alanine, valine, leucine, isoleucine, phenylalanine, tyrosine, serine and aspartate, with concomitant conversion of glutamate to α-ketoglutarate (Umbarger, 1978).

3. ***Oxidative deamination*** by *L*-glutamate dehydrogenase (GDH, UniProt code: P00370-), in which *L*-glutamate is involved in an oxidation-reduction reaction that results in the production of *α*-ketoglutarate, ammonia (NH_3) and NAD(P)H. Ammonia takes part in the urea cycle, while *α*-ketoglutarate can either directly enter the TCA cycle (Fig. 1.12, 5a) or act as substrate in transamination reactions, as described in 2, but in the reverse direction. As the reaction is a chemical equilibrium, *α*-ketoglutarate can also be converted to *L*-glutamate, which serves a nitrogen acceptor in the low-assimilation pathway mostly observed in bacteria and plants. Therefore, depending on environment and stress, GDH links catabolic and anabolic metabolisms and it plays a key role in nitrogen assimilation.

4. ***Decarboxylation*** into γ-aminobutyric acid (GABA) by glutamate decarboxylase (Gad), a pH-regulated transformation occurring as main mechanism of acid resistance in neutralophilic bacteria as well as starting reaction of the GABA-shunt pathway. The biochemical characterization of Gad is the object of Chapter II, III and IV of this thesis.
   Notably, in the last decades this transformation has been deeply exploited in industry to produce GABA in large quantities given the positive effects of GABA on human health, as well as its importance in the green chemistry as a building block for biocompatible and biodegradable polymers for industrial applications (Giovannercole *et al*., 2017b).

5. ***Synthesis of* L-*glutamine*** in a ATP-dependent manner by glutamine synthetase (GS, UniProt code: P0A9C5), in which free ammonia (NH_3) is condensed to *L*-glutamate to yield *L*-glutamine, a key molecule for the nitrogen assimilation (Fig. 1.12, 5a). GS, together with glutamate synthase (GOGAT, UniProt code: P09831/P09832), plays a central role in the high affinity nitrogen flow, by incorporating free ammonia into glutamate and glutamine, which serve as bioorganic nitrogen donor and acceptor, respectively.

6. ***Proline biosynthesis*** in which *L*-glutamate intervenes in the first reaction (out of four) to be activated as γ-glutamyl phosphate by the enzyme γ-glutamyl kinase (UniProt code: P0A7B5). All the carbons and the α-amino group in proline derive from glutamate.

7. ***Ornithine biosynthesis*** in which *L*-glutamate is converted in the polyamine *L*-ornithine via *N*-acetylated intermediates by N-acetylglutamate synthase (UniProt code: P0A6C5) (Cunin *et al.*, 1986).

8. ***Biosynthesis of glutathione,*** a tripeptide of cysteine, glycine and glutamate with antioxidant properties, catalysed by the consecutive action of two ATP-dependent enzymes: glutamate-cysteine ligase (UniProt code: P0A6W9, related to GS enzyme) and glutathione synthetase (UniProt code: P04425). Glutathione is used to maintain the redox homeostasis within the cell and to protect from the oxidative damage.

9. ***Biosynthesis of dihydrofolate*** catalyzed by dihydrofolate synthetase (UniProt code: P08192) in an ATP-dependent manner. Dihydrofolate is a folate (vitamin B_9) derivative that it is necessary to synthetize purine and pyrimidines for DNA and RNA. *In vivo* folate exists as a pool of polyglutamylated derivatives that are thought to prevent the diffusion of folate out of the cell and allow its enzymatic recognition.

Together with dihydrofolate, several other enzymatic cofactors contain polyglutamyl moieties, such as methanofuran, involved in the reduction of carbon dioxide to methane by methanogens, and F_{420}, a cofactor widely distributed in archaea (Walker and van der Donk, 2016).

Apart from the primary metabolism, many glutamate-specific adenylation domains in nonribosomal peptide synthetases (NRPS) have been observed by bioinformatic analysis. Moreover, glutamate serves as a starting unit in the biosynthesis of polyketides, a class of secondary metabolites, such as the antibiotic macrolactam vicenistatin and incednine or the tetramic acid antibiotic streptolydigin (Walker and van der Donk, 2016).

Many biosynthetic pathways use glutamate as a protective group and/or scaffold to prevent unproductive off-reactions. Glutamylation has been found to prevent intramolecular cyclization, as in the case of putrescine catabolism in *E. coli* and *Pseudomonas aeruginosa* occurring in the assimilation of nitrogen, or during the synthesis of Butirosin in *Bacillus circulans*, an aminoglycoside antibiotic. Other examples include the N-oxidation and N-N bond formation of several amines. Interestingly, in all of these pathways, glutamate is recognized by homologous of GS, which activate the γ-carboxyl group in ATP-dependent manner (Walker and van der Donk, 2016 and reference therein).

Last but not least, several pathways have been observed to use $tRNA^{Glu}$ as a substrate, in reactions unrelated to protein biosynthesis. In fact, different microorganisms synthetize several $tRNA^{Glu}$ macromolecules, which serve for distinct biosynthetic purposes; remarkable is the case of the synthesis of $tRNA^{Gln}$ that derives from the ATP-dependent transamidation reaction which converts a $tRNA^{Glu}$ in $tRNA^{Gln}$ by using glutamine as a nitrogen donor (Walker and van der Donk, 2016).

That of glutamate represents a key metabolism also in pathogenic bacteria such as *M. tuberculosis* with respect to the fact that in this microbe there is a group of proteins named PE/PPE, unique families of proteins that account for about 10% of the mycobacterial genome and are highly represented also in other pathogenic bacteria. The name originates from the characteristic proline-glutamate (PE) and proline-proline-glutamate (PPE) signature motifs often found at the N-terminus (Cole *et al.*, 1998).

The members of the PE protein family present a highly conserved N-terminal domain of ~110 amino acids with predicted globular structure, followed by a C-terminal segment varying in length and sequence identity. The amino acid contents of the members of this family vary significantly, with few members having only the N-terminal domain, and the remaining presenting a C-terminal segment from 100 to 1400 residues. The few members of the PPE family present a ~180 amino acid-long N-terminal domain with a C-terminal fragment varying in sequence and length (Cole *et al.*, 1998).

Although their physiological function is still poorly investigated, PE/PPE proteins are recognized important immunologically, but also in mycobacterial virulence (Cole *et al.*, 1998; Fishbein *et al.*, 2015; Phelan *et al.*, 2016; Singh *et al.*, 2016). Expression profiling experiments of *M. tuberculosis* linked the gene expression variations of the PE/PPE coding genes to adaptation of the pathogen to the changing of the microenvironment upon infections within the host. Other studies reported the overexpression of some PE/PPE proteins under harsh environmental conditions that mimic those of the phagosomal environment; on this regard, significant examples of their contribution to mycobacterial pathogenesis have been observed, together with a pH-dependent regulation of their gene expression (Fisher *et al*,, 2002; Rohde *et al*., 2007; Abramovitch *et al.*, 2011; Mukhopadhyay *et al*., 2012).

1.3. Aims of this thesis

The contents of this thesis focus on four different but related topics, each in-depth studied in a specific chapter, which has been structured and developed as an independent scientific article. The connecting core of everything is the GadB enzyme of AR2 system, which has been investigated at different levels, spanning from biochemistry to biophysics to microbial physiology; from the molecular aspects that underlie the biochemical and structural features of Gad also as a characteristic PLP-dependent enzyme, to its broader involvement in microbial metabolism as key player of glutamate metabolism in bacteria, both in a physiological and potentially infective contest.

Chapter II sheds new lights on the influence of PLP and exposure to an alkaline pH (an environmental condition potentially encountered) on the oligomeric assembly of GadB.

In chapter III the pH-dependent regulation of GadB enzymatic activity is investigated by side-directed mutagenesis, providing exciting findings in our understanding of the decarboxylation mechanism.

Chapter IV reports a preliminary biochemical characterization of GadB from *M. tuberculosis*, with the final goal to understand if this enzyme provides protection from acidity encountered within macrophages or as a source of GABA in the cell.

Chapter V is only showing the contribution that I have given to the development of a patent (deposit pending) on the possible use of analogues and derivatives of glutamate with phosphinic groups as potential antibiotics.

.

CHAPTER II

On the effect of alkaline pH and cofactor availability in the conformational and oligomeric state of *Escherichia coli* glutamate decarboxylase

This chapter was published (in adapted form) as:

Giovannercole, F., Mérigoux, C., Zamparelli, C., Verzili, D., Grassini, G., Buckle, M., Vachette, P., De Biase, D. (2017) 'On the effect of alkaline pH and cofactor availability in the conformational and oligomeric state of *Escherichia coli* glutamate decarboxylase', *Protein Engineering, Design and Selection*, 30(3), pp. 1–10. doi: 10.1093/protein/gzw076.

2.1. Introduction

The enzyme glutamate decarboxylase (Gad; EC 4.1.1.15) plays a major role in protecting *E. coli* from acid stress (De Biase *et al.*, 1999). This role is also played in other bacteria which, like *E. coli*, typically encounter acid stress during their life cycle (for reviews: (De Biase and Pennacchietti, 2012; Lund *et al*., 2014; Pennacchietti *et al*., 2016)). Thus, the established physiological role of *E. coli* Gad (*Ec*Gad) resides in its ability to consume one proton (H^+)/catalytic cycle as part of the pyridoxal 5′-phosphate (PLP)-dependent α-decarboxylation of *L*-glutamate that yields carbon dioxide and γ-aminobutyrate, and, in so doing, protects the cell from harmful acidification of the cytosol. It is therefore not unexpected that acidic pH (the origin of which can be inorganic or organic) typically induces an increase in the expression of *gadA* and *gadB*, the genes coding for the two isoforms of Gad in *E. coli*, namely GadA and GadB (Castanie-Cornet *et al.*, 1999; De Biase *et al.*, 1999; De Biase and Lund, 2015). Because of the above, most of the biochemical and structural work on bacterial Gad was carried out in a pH range where the enzyme performs its beneficial activity to the bacterial cell, *i.e.* pH ≤ 6.0. Crystal and solution studies, combined with site-directed mutagenesis studies, have clarified the molecular basis and the sequence of events that lead either to the activation of this enzyme at acidic pH or to its auto-inhibition at pH ≥ 6.0 (Capitani *et al.*, 2003a; Gut *et al.*, 2006; Pennacchietti *et al.*, 2009). These studies also showed that the 318-kDa homohexameric structure of *E. coli* GadB (and GadA; Dutyshev *et al.*, 2005) is a trimer of dimers, arranged as two three subunit layers with each dimer providing a monomer to each layer (Fig. 1.7). The entangled and compact oligomeric assembly of GadB is rather different from that of the other pH-inducible bacterial decarboxylases for which the crystal structures have been solved, *i.e.* dodecameric ornithine decarboxylase (Momany *et al.*, 1995a) and decameric arginine and lysine decarboxylases (Andréll *et al.*, 2009; Kanjee *et al.*, 2011a), in which the dimers are less tightly associated. Unlike these pH-inducible decarboxylases (Kanjee *et al.*, 2011b), the hexameric assembly in GadB is not affected by a change in pH in the range 4.6–7.6, at least in its *holo*form, *i.e.* with PLP bound (Capitani *et*

al., 2003a; Gut *et al.*, 2006). Overall, the crystallographic data show that the *holo* enzyme (*holo*Gad) is hexameric in the pH range 4.6–7.6 in line with previous analytical ultracentrifugation (AUC) (Strausbauch and Fischer, 1970) and electron microscopy (Tikhonenko *et al*., 1968; To, 1971) studies. The only evidence for dissociation of the hexamer into dimers comes from studies carried out either in diluted solutions at 4°C or on the apoenzyme at pH ≥ 6.0 (Sukhareva, 1986 and references therein).

Based on the above, it is less straightforward to provide an explanation for the induced/increased expression of *gadA* and *gadB* genes (and of the corresponding protein products) under conditions, which are not directly linked to acid stress and which comprise starvation as well as osmotic stress at neutral pH (Castanie-Cornet *et al*., 1999; De Biase *et al.*, 1999), cold stress (White-Ziegler *et al.*, 2008), respiratory stress (Shepherd *et al.*, 2010) and anaerobiosis under alkaline conditions (Blankenhorn *et al*., 1999). To explain some of the above findings it has been suggested that the GadA/GadB activity helps to relieve acid stress only if the protein is already present in the cell prior to an exposure to an acidic environment (Castanie-Cornet *et al.*, 1999; De Biase *et al.*, 1999). Also, GadA/GadB activity should protect against acidification caused by anaerobic fermentation occurring in alkaline-grown cells (Blankenhorn *et al*., 1999). However, GadA/B increased expression occurs also under respiratory stress, during which intracellular and extracellular pH were shown to be slightly alkaline and never become acidic (Shepherd *et al.*, 2010).

Thus, it appears that Gad, though active at acidic pH, can be expressed and present in the cell under conditions in which the intracellular and extracellular pH are above neutral.

2.1.1. Aims

Although the structural and biochemical properties of *Ec*GadB have been deeply investigated, very poor is known on the role played by the PLP upon folding, oligomeric assembly and enzymatic stability. The few studies carried out in the last decades indicate that the binding of PLP in every subunit of the enzyme (*holo*enzyme) is strictly necessary to stabilize the oligomeric assembly in the homohexamer, whereas the loss of PLP from the active sites (*apo*enzyme) is responsible for the dissociation from hexamer to dimer (Fig. 2.1). Moreover, the same outcome can be also obtained when the enzyme is greatly diluted. However, due to the reversible nature of this dissociation, at least three equivalents of PLP are sufficient to restore the hexameric assembly, though a full complement is required for a complete recovery of the enzymatic activity (Shukuya and Schwert, 1960; Tikhonenko *et al*., 1968; Strausbauch and Fischer, 1970; To, 1971; Sukhareva, 1986).

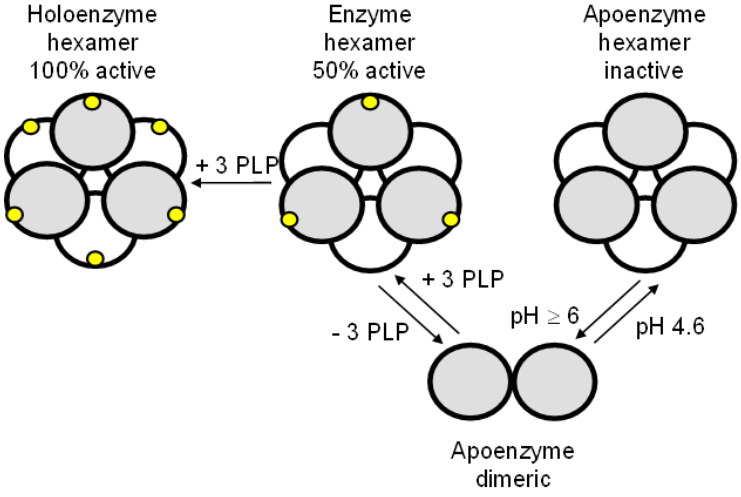

Figure 2.1. *Interconversion between the hexameric and dimeric form of* Ec*GadB.* Image adapted from Sukhareva, 1986.

Interestingly, recent studies on the biochemical and biophysical mechanisms occurring during the *holo* ↔ *apo* transition carried out on other PLP-dependent enzymes, such as the human Gad counterpart (Gad65, UniProt code: Q05329) and human Dopa decarboxylase (DDC, UniProt code: P20711), highlighted the key role of PLP in determining a stable quaternary structure that it is necessary for the cell physiology (Giardina *et al.*, 2011; Kass *et al.*, 2014).

The above findings prompted us to investigate the role of the coenzyme and pH in the structural stability of *Ec*GadB. As part of a project aimed at investigating the structure and function of *E. coli* GadB in conditions far from those in which it plays its well-established physiological role (*i.e.* relieving the cell from acid stress), we undertook an in solution study of this enzyme in the range 7.5–8.6, never investigated in previous studies. We found that the compact and entangled hexameric structure of GadB undergoes dissociation into dimers and this dissociation is not only affected by the presence of PLP, but also by an increase in pH.

2.2. Material and methods

2.2.1. Materials

Materials for bacterial growth were from Difco (BD, USA). Streptomycin sulfate was from USA Biochemical Corp. (Cleveland, OH, USA). HiPrep DEAE FF 16/10 (20 ml) and PD-10 Desalting (8.3 ml) columns were from GE Healthcare Life Sciences. Analytical grade sodium acetate was from VWR International. Vitamin B_6, potassium dihydrogen phosphate, dipotassium hydrogen phosphate, *L*-glutamic acid and kanamycin were from Fluka. Unstained Protein Molecular Weight Marker for SDS-PAGE was from Thermo Scientific. Trypsinultra was purchased from New England Biolabs. PLP and all other chemicals were from Sigma-Aldrich.

2.2.2. Expression and purification of *E. coli* GadB

Overexpression and purification of recombinant wild type *E. coli* GadB in the *holo*form (*i.e.* with the full complement of PLP; *holo*GadB) were carried out essentially as previously described (De Biase *et al.*, 1996). Protein purity was assessed by 12% SDS-PAGE and by measuring the PLP content that was determined by treating GadB with 0.1 N NaOH and then measuring the absorbance of the cofactor free in solution at 388 nm (ε_{388} = 6550 M^{-1} cm^{-1}; Peterson and Sober, 1954). Enzyme concentration and activity were measured as previously described (De Biase *et al.*, 1996).

2.2.3. Preparation of *apo*GadB and reconstitution with PLP

The *apo*form of *E. coli* GadB (*apo*GadB) was prepared by taking advantage of the abortive transamination occurring in the presence of the substrate 2-methyl glutamic acid (Yang and Metzler, 1979; Grant *et al*., 1987). Briefly, 500 µl of GadB (10 mg/ml), was diluted 1:3 with 1 ml of buffer 0.2 M Pyridine/HCl, pH 4.6, containing 0.1 mM DTT and incubated with 26 mg of *D,L*-2-methylglutamic acid (to obtain a final concentration of 0.1 M) for 40 min at RT. During the incubation, the solution was mixed by gently pipetting to allow the full

solubilization of the substrate and ~100 µl of 1.0 M potassium phosphate buffer, pH 7.5, was added to keep the pH at 4.6. The reaction was allowed to reach completion overnight at 4°C. The following day, the mixture was loaded onto a PD-10 desalting column (GE Healthcare) both to exchange the buffer to pH 4.6, 7.5, 8.0 or 8.6 and to fully separate the *apo*GadB from pyridoxamine 5'-phosphate, the product of the abortive transamination which is not retained in the enzyme active site. In all, 0.5 ml aliquots were collected in 1.5 ml eppendorf tubes. Based on the absorption spectra, only the purest fractions of *apo*GadB were pooled and the final concentration of *apo*GadB was measured spectrophotometrically using the molar absorption coefficient ε_{280} = 86 000 M^{-1} cm^{-1} (Yang and Metzler, 1979).

Reconstitution with PLP to yield *holo*$_{rec}$GadB was carried out at a 1.1:1 PLP:GadB monomer ratio and by incubating at RT for ~2.0 h, in the buffer at the required pH (4.6, 7.5, 8.0 or 8.6 depending on the experiment), *Holo*GadB (3 mg) was also passed on PD-10 desalting columns and a similar elution procedure was applied in order to have the downstream analyses performed on samples, at the relevant pH, that underwent similar treatment as the apo samples above.

2.2.4. Analytical ultracentrifugation (AUC)

AUC is the most versatile, accurate and rigorous technique for calculating the thermodynamic and hydrodynamic properties and the molecular weight of macromolecules in solution, as it allows to determine experimentally all the terms of the sedimentation equation. The technique is widely employed in the assessment of sample purity, in the determination of molecular weight, in the calculation of the equilibrium constants in chemical equilibria, in the detection of conformational changes and in the study of interactions between macromolecules.

Molecules with different molecular weights (or different shapes or sizes) have a sedimentation coefficient, *s* (an index of the sedimentation rate), different under a centrifugal field, equal to:

$$\frac{s}{D} = \frac{M(1 - \tilde{\upsilon}p)}{RT}$$

Where:

- *s* is the sedimentation coefficient;
- *D* is the diffusion constant;
- *M* is the molar mass
- ῡ is the partial specific volume;
- *p* is the solvent density;
- *R* is the gas constant
- *T* is the absolute temperature.

s is expressed in seconds but since in most of biological macromolecules it is between 1 and 100 10^{-13} seconds, the Svedberg unit (S), defined as 10^{-13} seconds, is preferred. The Svedberg unit offers a measure of particle's size based on its sedimentation rate, describing how fast a specified particle of given size and shape reaches the bottom of a solution.

The hexamer ↔ dimer equilibrium in *holo*GadB and *apo*GadB with/without PLP at pH > 7 was instigated by applying specific angular velocity which pushes the molecular components of the sample to distribute across the sample cell according to their molecular weights with the heaviest species most concentrated at the bottom of the cell, whereas the lightest ones near the meniscus. Then, the molecular weights are derived by the following equation:

$$M = \frac{2\,RT}{(1-\tilde{\upsilon}p)\,\omega^2} \frac{d\,(ln\,c)}{dr^2}$$

Where:

- *M* is the molecular weight (g/mol);
- ω is the angular velocity (radians/sec);
- c is the solute concentration (g/L) at distance (r) from the rotor.

Data obtained from AUC are records of the concentration distributions, which are measured by refractometric methods, such as the Schlieren optical system. Light passing through the sample cell where concentration is changing will be deviated radially. The Schlieren optical system converts this deviation of light into a vertical displacement of an image at the camera and this is proportional to the concentration gradient.

Experimental procedure: sedimentation velocity experiments were carried out on a Beckman Coulter Proteomelab XL- I analytical ultracentrifuge equipped with absorbance optics. The experiments were performed in collaboration with Prof. Carlotta Zamparelli and Dr. Daniela Verzili at Department of Biochemistry, at "Sapienza, University of Rome". Experiments were conducted at 25 000 rpm and 20°C. Radial absorbance scans were obtained in a continuous scan mode at 280 nm at a spacing of 0.003 cm. Sedimentation coefficients were calculated using the program Sedfit (provided by P. Schuck, National Institutes of Health) and were reduced to water and 20°C ($s_{20,w}$) according to standard procedures. Both *holo*GadB and *apo*GadB (0.5 ml each; with an absorbance at 280 nm of 1.0 AU in a 1.2 cm optical path cell, corresponding to ~0.5 mg/ml) were analyzed in the following buffers: 50 mM EPPS, 150 mM NaCl, at pH 7.5, 8.0 and 8.6, respectively.

2.2.5. Spectroscopic measurements and data analysis

GadB UV-Visible spectra were recorded at controlled temperature on a Hewlett–Packard Agilent model 8452 diode array spectrophotometer. Fluorescence emission spectra were recorded with a FluoroMax-3 spectrofluorometer (Horiba Jobin–Yvon) equipped with a thermostatically controlled cell compartment at 20°C using 3 nm bandwidth on both slits and at a scan speed of 100 nm/min. The spectra were corrected by subtracting the corresponding buffer's emission spectrum (blank). When necessary, spectra were normalized to the same optical density at 280 nm (starting from values ± 10% with respect to that used for normalization) using GraphPad Prism 4.0 (GraphPad Software, San Diego, CA).

2.2.6. Small-angle X-ray scattering (SAXS)

Small-angle scattering (SAS) is an elastic scattering technique based on the deflection of collimated radiation away from the straight trajectory after it interacts with structures that are much larger than the wavelength of the radiation. SAXS and SANS (small-angle neutron scattering) are the two main SAS derivative techniques: the former uses X-rays (wavelength between 0.5-2.0 Å), while the latter uses thermal neutrons (wavelength between 1-10 Å). These techniques allow the investigation of biological macromolecules with a resolution between 10-100 Å, which makes them able only to detect consistent structural changes of biological macromolecules in solution.

SAXS, like X-ray crystallography and NMR, is mostly exploited for the study of tertiary and quaternary structures but, unlike X-ray crystallography and NMR, it is extremely faster, not-destructive, requires only little amount of sample, and the experiment is completely carried out in solution, though sample needs to be as much pure as possible.

Briefly, the sample is hit by a monochromatic beam of photons with wavelength of the order of X-rays which mainly impacts the electrons of the sample, causing the emission of a second wave beam (scattering) that is then impressed on a detector located downstream. For diluted solutions, the scattering intensity (I) is isotropic and depends only on the angle 2θ, the angle between the scattering wave and the incident wave. For a monodisperse system containing molecules oriented randomly and ideally non-interacting with each other, the correct scattering intensity of background noise is proportional to that of a single molecule mediated for all possible orientations. Since the sample is in solution, the scattering intensity of the solvent is recorded separately and then subtracted from that of the sample. The resulting scattering profile is a function of the transfer moment, *s*, calculated according to the equation:

$$q = \frac{4\pi \sin(\theta)}{\lambda} = 2\pi s$$

where λ is the wavelength of the hitting beam and *s* is the modulus of the scattering vector given by:

$$s = \frac{2\sin(\theta)}{\lambda}$$

It is then possible to derive the mass, the radius of gyration (R_g), which measures the quadratic mean of distances to the center of mass weighted by the contrast of electron density, and the forward scattering I(0) from the Guinier law (Guinier and Fournet, 1955):

$$\mathrm{I}(s) = \mathrm{I}(0)\exp\left(-\frac{1}{3}Rg^2s^2\right)$$

The law is usually used in its log form, in which the linear regression yields two parameters: I(0) (y-intercept) and R_g from the slope. The molecular weight of the molecule is calculated by dividing the scattering forward by the concentration of the molecule, then it is expressed as cm^{-1} by using the diffusion of water for the normalization. It is also possible to calculate the hydrated volume of the molecule, V*p*, from the Porod law (Porod, 1982):

$$\mathrm{V}p = \frac{2\pi^2 I(0)}{Q}$$

$$\mathrm{Q} = \int_0^\infty s^2\, I(\mathrm{s})\, ds$$

where Q is the Porod invariant. Once obtained *Vp*, it is possible to calculate an estimate of the molecular weight of the molecule without introducing the concentration. Moreover, through the indirect Fourier transform (Glatter, 1977), it is possible to obtain the D_{max}, *i.e.* the maximum distance between the molecules in solution.

After the experimental phase follows the computational part, in which the application of certain bioinformatics algorithms allows to derive a structural model of the macromolecules and to be able to refine it by taking advantage of additional information from other structural

resolution techniques. The determination of the structure can be done by applying distinct computational methods based on the available data: if nothing is known of the structure of the molecule under examination, it is possible to proceed with the *ab-initio* methods that allow the creation of a series of models that are in agreement with experimental data. DAMMIN is the most used program for this approach.

If instead pre-existing structural data derived from other structural investigation techniques (NMR, X-ray crystallography, electron microscopy, etc.) are available, it is possible to take advantage of the modeling of rigid bodies in which the information of the high-resolution structure domains or subunits of complexes is exploited to obtain their spatial orientation that best matches the SAXS data. SASREF and BUNCH are generally the most popular programs. This method requires the structural data of all the domains or subunits of a complex, therefore, when not available, it is possible proceed with a hybrid approach that involves the implementation of the *ab-initio* methods with the modeling of rigid bodies. The BUNCH and CORAL programs have been updated for this type of operation.

To validate a computational model, having the structure of the molecule of interest, it is possible to proceed with the bioinformatic execution of its scattering profile to be compared with the experimental one. It is necessary to take into consideration the following parameters: the excluded volume, *i.e.* the volume occupied by the molecule in the solution, and the scattering of the hydration surface of the molecule. The most efficient method to this aim, is the use of spherical harmonics implemented in CRYSOL, which uses spherical harmonics to describe the molecular surface and represents hydrating water as a uniform layer of 3 Å (*i.e.* a water molecule) thickness. These models have been often used to identify biologically active conformations of crystallographic structures and to help distinguish between dimers and/or higher-order structures.

SAXS is therefore widely used in model validation and molecular replacement in crystallography, in providing information on the overall structure and shape of macromolecules and for refining NMR data and imposing structural constraints. SAXS can be

used as a complementary technique to validate high-resolution models, solve the phase problem in crystallography and to redefine the structures (Mertens and Svergun, 2010; Blanchet and Svergun, 2013; Petoukhov and Svergun, 2013).

Experimental procedure: X-ray scattering data of GadB in *holo* and a*po* form were collected at the SWING beamline of the SOLEIL Synchrotron (Gif-sur-Yvette, France), in collaboration with Dr. Patrice Vachette and his équipe. The data were recorded using a CCD-based detector (AVIEX) with a sample-detector distance of 1775 mm, covering the momentum transfer range 0.007 Å−1 < q < 0.3 $Å^{-1}$ ($q = 4\pi \sin\theta/\lambda$, where 2θ is the scattering angle, and $\lambda = 1.0$ Å the wavelength of the X-rays). Measurements were performed using the size exclusion HPLC instrument (Agilent) together with a Bio SEC-3 column (300 Å porosity, 4.6 × 300 mm, Agilent) on-line with the small-angle X-ray scattering (SAXS) measuring cell, a 1.5 mm diameter quartz capillary contained in an evacuated vessel (David and Pérez, 2009). Each sample of GadB was studied at 15°C. The *holo*GadB was studied in HEPES 50 mM buffer, pH 6.9, NaCl 150 mM and 2 mM DTT, while the *apo*GadB was in Tris 20 mM buffer, pH 8.0, NaCl 150 mM and 2 mM DTT. In this experiment, 30 µl of *holo*GadB and *apo*GadB at 19 and 15 mg/ml, respectively, was loaded onto the column equilibrated with the corresponding elution buffer. Scattering of the elution buffer before the column's void volume was recorded and used as buffer scattering to be subtracted from that of the protein species. 1.5 s successive frames were recorded separated by a 0.5 s interval since the elution flow of 0.2 ml min^{-1} ensured that no protein was irradiated for >0.4 s. Primary data reduction was performed using the SWING in-house software Foxtrot, yielding scattering intensities. The buffer-subtracted data sets were analyzed using the HPLC-SAXS module from the US-SOMO software (Brookes *et al.*, 2013, 2016). Each data set recorded during a chromatographic run is an ensemble of N $I_t(q)$ SAXS patterns (frames) of M *q*-values each collected at successive times *t*. The program first performs a transposition of this 2D intensity matrix $I(q,t)$ to produce elution profiles $I_q(t)$ for each *q*-value. The $I_q(t)$ is subsequently deconvolved into a set of Gaussians or asymmetric, modified Gaussians. Each

Gaussian represents the contribution to the scattering of an eluting species. The 280 nm absorbance profile from the UV detector of the HPLC instrument is also fed into the program and similarly deconvolved using the same set of Gaussians. The final output of the program is the reconstructed scattering curves of each species *i*, $I_i(q)$. The values of the GadB absorbance at 280 nm is ε_{280} = 86 000 M^{-1} cm^{-1} (referred to the monomeric species). The reconstructed scattering patterns were subsequently processed using the program package PRIMUS (Konarev *et al.*, 2003). The forward scattering I(0) and the radius of gyration (R_g) were evaluated using the Guinier approximation (Guinier, 1939). The distance distribution function p(r) was determined using the indirect Fourier transform method as implemented in the program GNOM (Svergun, 1992). Notably, these parameters provide information on mass and/or shape of the protein species. An alternative estimate of the molecular mass was obtained using the SAXSMoW program available at the URL http://www.if.sc.usp.br/~saxs/ that is based on the determination of the Porod volume, which is independent of the sample concentration (Fischer *et al.*, 2010). Scattering patterns were calculated from atomic coordinates using Crysol (Svergun *et al.*, 1995). The crystal structure of *holo*GadB (pdb file: 1PMO) lacks coordinates for a few N-ter residues that were added manually. The completed hexamer file was also used to provide coordinates for a tetramer (chains A to D) and a dimer of GadB (chains A and B). The N terminus of each chain within the hexamer reaches out to contact another chain on the other side of the molecule (*e.g.* A with F). In an isolated dimer, these extremities appear implausibly extended in the solvent and are most likely highly flexible. They were accordingly manually folded to adopt a more likely average conformation.

2.2.7. Limited proteolysis

Limited proteolysis was exploited to detect where critical structural changes, triggered by the loss of the cofactor, occur in *E. coli* Gad. Shortly, 100 µg of each protein form (*i.e. holo-*, *apo-* and $holo_{rec}$-GadB) was incubated at a concentration of 1 µg/µl and at 25°C with bovine

pancreatic trypsin (New England Biolabs) in buffer 50 mM Tris-HCl, pH 8.0, containing 10 mM $CaCl_2$. The trypsin:GadB (w/w) ratio was set to 1:100. At time intervals, 5 µl aliquots (corresponding to 5 µg of GadB) were withdrawn and the reaction halted by adding SDS-PAGE sample buffer containing 10 mM EDTA.

2.2.8. Proteomic methods

Following limited proteolysis with trypsin and SDS-PAGE, GadB protein bands were excised and digested in-gel using trypsin (New England Biolabs) at 37°C, at pH 8.0 for 18 h. The tryptic peptides were separated using Ultimate/Famos LC system (LC packings). The peptides were trapped onto a 300 µm × 5 mm C18 precolumn (Dionex) in 0.1% formic acid (FA) 2% acetonitrile (ACN) at flow rate of 30 µl min^{-1}. After 3 min loading the precolumn was switched in line with C18 column (150 mm × 50 µm, 5 µm, VYDAC) and the peptides were eluted with ACN gradient using 5% ACN in 0.1% FA as buffer A and 95% ACN in 0.1% FA as buffer B. First 3 min: gradient 100% buffer A; from 3 to 25 min: decrease of buffer A to 55%; from 25 to 35 min: decrease of buffer A to 15%. Buffer A was kept at the same level for 45 min and was brought back to 100% by 46 min. The total run time was 80 min. The mass spectra were recorded with QSTAR XL hybrid quadrupole TOF instrument (Applied Biosystems, Foster City, CA, USA) QSTAR XL hybrid quadrupole TOF instrument (Applied Biosystems) in positive mode using nano-ESI ion source. Information-dependent acquisition method was used and 1s TOF MS scans were recorded for mass range m/z 400–2000 followed by 4 s MS/MS scans of the most intense ions with charge +2 or +3. The instrument was calibrated on known trypsin autolysis peptides.

Data processing was performed using Analyst QS v1.1 software (Applied Biosystems). The tryptic peptides of GadB were identified with MASCOT MS/MS ions search (www.matrixscience.com). Parent ion and fragment mass tolerances were 0.1 and 0.2 Da, respectively. Carbamidomethylation of Cys was selected as fixed modification and oxidation of Met as variable modification.

HPLC-MS/MS and data processing were carried out by our collaborator Dr. Janne Weisell (School of Pharmacy, Biocenter Kuopio, University of Eastern Finland, Kuopio, FI; at the time this work was carried out).

2.2.9. Molecular modeling

All molecular modeling studies were performed on an Intel Xeon(R)CPU E5462 2.80 GHz × 4 running Ubuntu 14.04 LTS. The *Ec*GadB structures were downloaded from the PDB (http://www.rcsb.org/): *holo*GadB, pdb code 1PMO (Capitani *et al.*, 2003a); *apo*GadB, pdb code 3FZ7 (Malashkevich *et al*., 2009). Superimposition and RMSD computations were carried out using Chimera (Pettersen *et al.*, 2004). The pictures reported in the manuscript were created with Pymol (The PyMOL Molecular Graphics System, Version 1.8.2.3 Schrödinger, LLC).

2.3. Results

Intrigued by a number of studies (Blankenhorn *et al*., 1999; Castanie-Cornet *et al.*, 1999; De Biase *et al.*, 1999; White-Ziegler *et al.*, 2008; Shepherd *et al.*, 2010) showing that *Ec*Gad is expressed in the bacterial cell under stress conditions in which the intracellular and extracellular pH are typically above neutral, it was decided to investigate the effect of alkaline pH and PLP availability on the conformational and oligomeric state of *Ec*GadB. This was carried out by analysing purified, recombinant GadB with a number of spectroscopic and biophysical techniques as well as by limited proteolysis. To this aim, *holo*GadB (*i.e.* the enzyme with a full complement of PLP) was compared with *apo*GadB (*i.e*. the enzyme where at least 95% of the PLP content was removed) as well as with *holo*$_{rec}$GadB (*i.e.* the enzyme reconstituted with the full complement of PLP) at three pH values, *i.e.* 7.5, 8.0 and 8.6, never investigated in previous studies. For comparative purposes most of the experiments were also carried out at pH 4.6.

2.3.1. Tryptophan fluorescence emission as a probe of *Ec*GadB conformational and oligomeric changes

As shown in Fig. 2.2, when *holo*GadB (blue) is compared with *apo*GadB (red, dashed line) at pH 7.5 (Fig. 2.2, upper panel) and 8.6 (Fig. 2.2, central panel), the emission spectra recorded by exciting at 295 nm (specifically exciting Trp side chains) show an increase of the emission ranging from 60% to over 100% of the starting value following PLP removal. The *holo*GadB fluorescence emission spectra also indicate that fluorescence increases with pH only above pH 7.0. Indeed, GadB fluorescence at pH 4.6 is comparable with that at pH 7.5, though the emission maximum is slightly red-shifted as pH increases. *Ec*GadB contains 11 Trp residues and at present it is not possible to assign the observed noticeable increase in fluorescence that accompanies PLP removal to any specific Trp residue (one or more). However, this observation suggests that Trp fluorescence can be employed to finely monitor

conformational changes that occur upon PLP binding and, at least in part, report on the dissociation of the hexamer into dimers (see SAXS and AUC sections).

The reconstitution of *apo*GadB with PLP (with a 10% excess with respect to the full complement) is complete as confirmed not only by the fact that the reconstituted enzyme (*holo*$_{rec}$GadB) regains the original UV-Visible spectrum (Fig. 2.2, inset), regardless of the pH, but also by the almost complete restoration of the fluorescence emission spectra of *holo*GadB. Complete reconstitution of *apo*GadB with PLP at acidic pH was reported in the past (De Biase, *et al*., 1991 and references therein), but never at pH > 6.0. The present findings imply that *apo*GadB has a rather accessible active site, with the C-terminal tail (*i.e.* residues 452–466) likely to be in a flexible conformation. The data recorded at pH 7.5 and 8.6 are practically identical (Fig. 2.2); similar results were obtained at pH 8.0 (data not shown).

In order to prove that the observed restoration of the UV-Visible and fluorescence spectra upon reconstitution with PLP coincides with a restoration of the enzyme activity, assays were carried out at pH 4.6 (*i.e.* the pH at which the enzyme displays its maximal activity) on all the three forms of GadB incubated and analysed at the three chosen pH values as well as at pH 4.6 as control. Data in Table 2.1 show that the restoration of the UV-Visible and fluorescence spectra in *holo*$_{rec}$GadB with respect to *holo*GadB are accompanied by substantial recovery of the enzyme activity (*i.e.* > 90%). Notably, the *holo*$_{rec}$GadB analyzed at pH 8.6 has a fluorescence spectrum that shows only partial (80%) restoration of the fluorescence of the *holo*GadB at the same pH (Fig. 2.2, central panel). This might provide an explanation for the finding that only 90% of the activity is recovered at this pH (Table 2.1). Very likely, as pH increases, PLP rebinding to the enzyme becomes more difficult, though the recovery of the activity still remains significant.

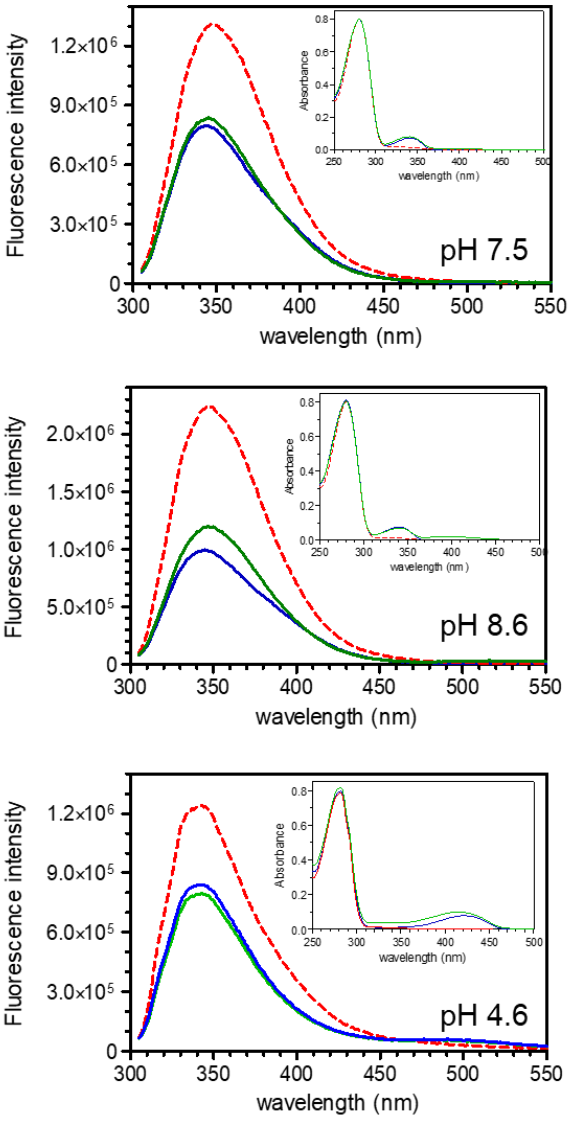

Figure 2.2. *UV-Visible and fluorescence emission spectra of* Ec*GadB.* Trp fluorescence emission spectra of the samples (0.85 μM) are shown in the main panels: *holo*GadB (blue), *apo*GadB (red, dashed) and *holo*$_{rec}$GadB (green). The upper panel refers to the spectra recorded at pH 7.5, the central panel refers to the spectra recorded at pH 8.6, while the lower panel refers to the spectra recorded at pH 4.6. The absorption spectra of the relevant samples at a concentration of 9.3 μM are shown in the insets: the 340 nm peak (at pH 7.5 and 8.6) and the 420 nm peak (at pH 4.6) corresponding to the substituted aldamine and the ketoenamine, respectively, both disappearing following removal of the cofactor (as in *apo*GadB), are restored upon reconstitution of the *apo*form with 1.1-fold excess of PLP, to yield *holo*$_{rec}$GadB. Some residual PLP free in solution is generating a minor band centered at 388 nm.

Table 2.1. *GadB activity (in %) at the indicated pH in samples analyzed by different spectroscopic and biophysical techniques (Fig. 2.2).*

pH	GadB		
	*holo*GadB	*apo*GadB	$holo_{rec}$GadB
4.6	100[a]	2.8	100
7.5	100[a]	2.4	98
8.0	100[a]	1	96
8.6	100[a]	2.6	90

[a] The starting activity of *holo*GadB was 163 ± 13 U/mg and was set as 100%.

2.3.2. Size exclusion chromatography-Small-angle X-ray scattering (SEC-SAXS) and analytical ultracentrifugation analysis on *holo*- and *apo*GadB

Until very recently (see Discussion), very few data were available on *Ec*GadB in solution using SAXS, whereas many crystal structures were reported in the pH range 4.6–7.6 (never above) (Capitani *et al.*, 2003a; Dadinova *et al.*, 2016). In addition to this, the crystal structure of an *apo*GadB was deposited in the PDB databank in 2009 from an old data set (dated 1996) collected at pH 7.6 (PDB code: 3FZ7). The latter structure does not show any substantial difference with that of *holo*GadB (deposited in 2003 with the PDB code: 1PMO (Capitani *et al.*, 2003a)). Indeed, when each chain of 1PMO is compared with its counterpart in 3FZ7, computed RMSDs are all lower than 0.4 Å. Because the crystal structure of the PLP-free GadB (3FZ7) did not provide information on the structural changes occurring upon PLP removal, and given the possibility that during that specific crystallization set up only the species better crystallizing, but not representative of the species in solution, was selected, it was decided to investigate further the nature of the species that in solution displays strong fluorescence emission (Fig. 2.2). This is possible through SAXS (Small-angle X-ray

scattering) which like X-ray crystallography and NMR, is mostly exploited for the study of tertiary and quaternary structures (see paragraph 2.2.6. in Materials and Methods).
Thus, first *holo*GadB in HEPES buffer at pH 6.9 was injected onto a size exclusion chromatography (SEC) column equilibrated in the same buffer and a SAXS analysis was carried out on-line on the material directly eluting from the column, as described in detail in Materials and Methods. Two components were detected: a major one (Component 1) centered at frame 67 and a second one (Component 2) that appears as a tail extending on the right side of the main peak. The profile is well described as the combination of two modified gaussian curves as shown in Fig. 2.3A. Frames 60–74 were averaged since they contained no contribution from Component 2 (Fig. 2.3A, hatched area). The SAXS profile is shown in Fig. 2.3C (blue). The results from Guinier (Guinier, 1939) and p(r) analyses are given in Table 2.2. In particular, the value of the molecular mass is very close to that of a hexamer of GadB. The second component is present at a very low concentration and the corresponding frames always contain a significant contribution from the hexamer. The reconstructed scattering profile was not constant across the chromatographic peak, so that no convincing characterization of this species could be performed.

Subsequently, *apo*GadB in Tris buffer at pH 8.0 was loaded on the size-exclusion column and SAXS analysis carried out on-line. In *apo*GadB two fairly well resolved components were detected and the profile could be nicely described by a combination of two modified gaussian curves (Fig. 2.3B). Frames from 61 to 71 (light gray hatching, for Component 1) that did not contain any detectable contribution from Component 2, were averaged. Unexpectedly, the molecular mass of the corresponding species was practically identical to that of a tetramer of GadB chain (Fig. 2.3C). The scattering pattern Component 2, reconstructed using the above decomposition, was averaged over frames 95–110 (orange hatching). These are shown in Fig. 2.3C. As expected from the literature data for the *apo* sample, the derived molecular mass was found close to that of the dimer.

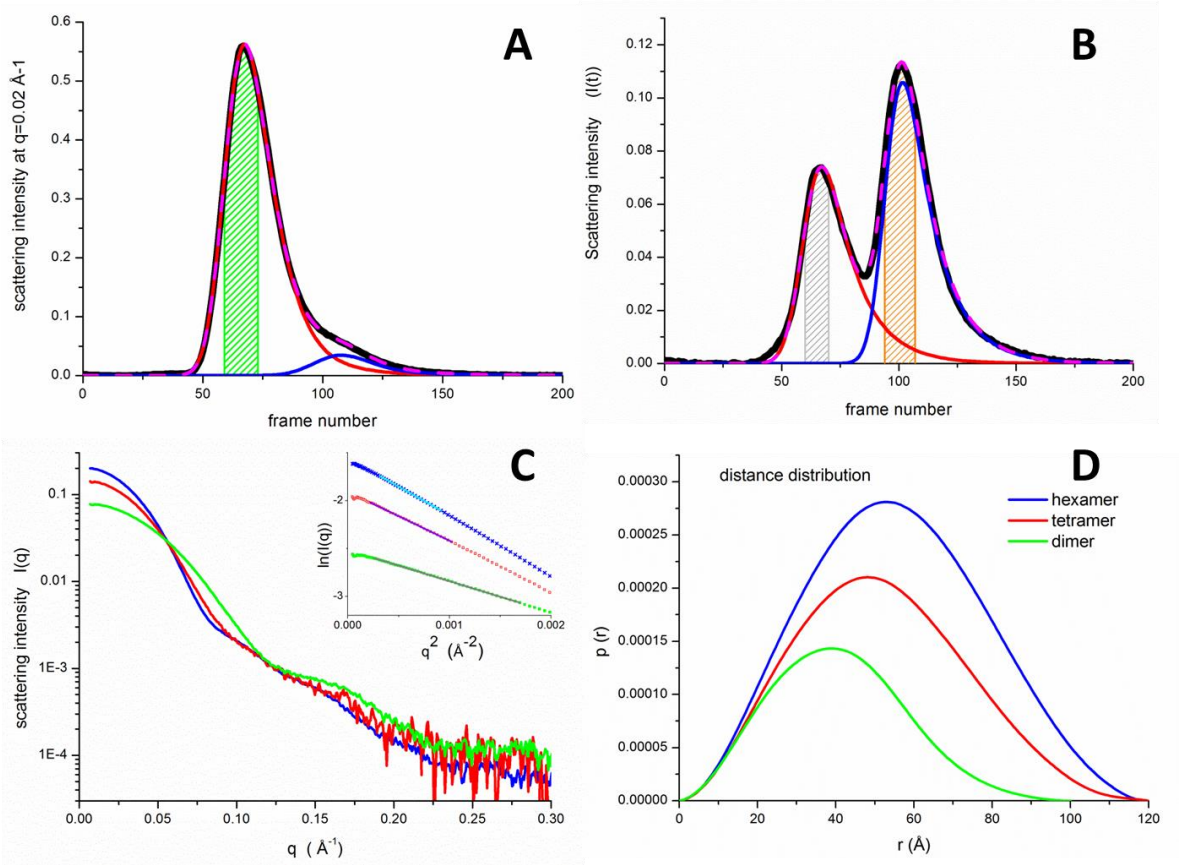

Figure 2.3. *SEC elution profiles and SAXS patterns of* Ec*GadB protein in the* holo *and* apo *forms*. The SAXS intensity at q = 0.02 $Å^{-1}$ (black line) as a function of frame number, of **(A)** *holo*GadB and **(B)** *apo*GadB. Each profile was deconvoluted into two peaks (fitting sum shown as a dashed line) using modified Gaussians. SAXS patterns (dashed line) were reconstructed using these decompositions. In *holo*GadB **(A)**, frame from 60 to 74 are averaged (hatching) **(B)**; in *apo*GadB, frames from 61 to 71 for the first peak (light gray hatching) were averaged while the reconstructed intensities for peak 2 (after correction for the contribution of the tetramer) were averaged from 95 to 110 (orange hatching). The three resulting average scattering patterns **(C)** and distance distribution functions p(r) **(D)** are shown using the following color code: *holo*GadB (blue); *apo*GadB tetramer (red); *apo*GadB dimer (green). The inset in panel C shows the three corresponding Guinier plots.

Table 2.2. *Data collection and scattering derived parameters of* Ec*GadB.*

	***Holo* form**	***Apo* form**	
	Main peak Hexamer	**First peak Tetramer**	**Second peak Dimer**
Data collection parameters			
Instrument	Beamline SWING (synchrotron SOLEIL)		
Detector	CCD-based AVIEX		
Beam geometry	0.8 x 0.15 mm		
Wavelength [Å]	1.0		
q-range [$Å^{-1}$]	$0.007 < q < 0.30$		
Exposure time [s]	1.5		
Temperature [K]	288		
Structural parameters			
I(0) Guinier [cm^{-1}]	0.211	0.149	0.081
R_g Guinier [Å]	42.2±0.5	39.3±0.04	31.3±0.11
I(0) p(r) [cm^{-1}]	0.213	0.150	0.081
R_g p(r) [Å]	42.2±0.2	39.4±0.02	31.2±0.10
D_{Max} [Å]	120	120	100
Molecular mass determination			
$MM_{sequence}$ [kDa]	316.0	210.7	105.3
Partial specific volume [$cm^3.g^{-1}$]	0.733	0.733	0.733
$MM_{I(0)/c}$ [kDa]	303/305	214/215	116
$MM_{SAXS\ MoW}$ [kDa]	290	216	110

Scattering patterns of the various oligomeric forms were calculated using the atomic coordinates of the hexamer (1PMO) after addition of a few N-terminal missing residues (see Material and Methods for details) and the program Crysol. They are presented in the three panels of Fig. 2.4 superimposed with the corresponding experimental data.

The hexamer curve is very close to the experimental data, suggesting that the hexamer conformation in solution is practically identical to the crystal structure although some minor

differences cannot be ruled out. In the case of the tetramer, a clear difference between both curves appears around q = 0.09 $Å^{-1}$. Since both the hexamer and the tetramer appear to elute quasi simultaneously from the SEC column, we considered the possibility that the sample could contain a mixture of tetramer and hexamer. However, no significant improvement in the fit could be obtained. Although the presence of a minor, residual amount of hexamer cannot be ruled out, it may be concluded that the hypothetical tetramer in solution exhibits a different conformation from that derived from the crystallographic hexamer.

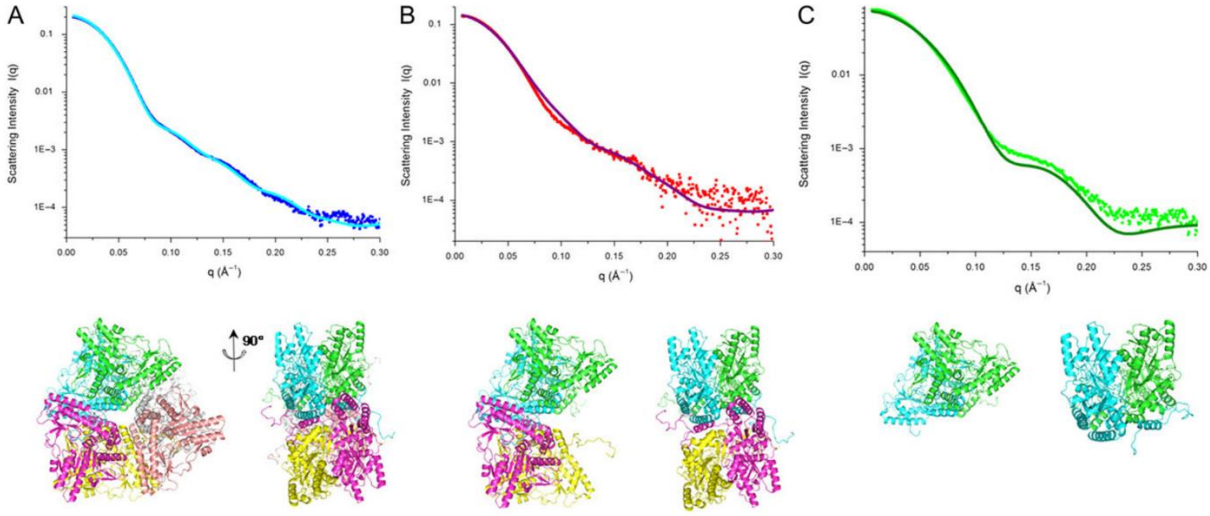

Figure 2.4. *Experimental and calculated SAXS patterns.* Comparison of experimental SAXS patterns (symbols) for **(A)** GadB hexamer, **(B)** tetramer and **(C)** dimer, with scattering patterns of completed crystal models calculated with Crysol (solid line). Top row: scattering curves. Bottom row: Top and side view (following the indicated rotation along the vertical axis) of the corresponding models.

Finally, although similar, the two dimer curves exhibit significant differences, with a larger value of the radius of gyration from the experimental data (31.2 Å vs 29.4 Å) as compared

with the calculated curve. This strongly suggests that following hexamer dissociation the dimeric *apo*GadB and, to smaller extent, the tetrameric *apo*GadB adopt a less compact arrangement than that observed within the hexamer.

In order to investigate further the oligomeric state of *Ec*GadB, *holo* and *apo*GadB at pH 7.5, 8.0 and 8.6 were subjected to analytical UC (AUC) and the molecular weight calculated based on the sedimentation coefficient. As shown in Table 2.3, *holo*GadB in the pH range 7.5–8.6 is mostly hexameric, though a significant increase of the dimeric species (24%) is observed when shifting toward a more alkaline value (*i.e.* 8.6). Unlike in SAXS, *apo*GadB in the AUC analysis was always detected as dimeric, regardless of the pH under investigation. We suggest that this is likely the consequence of the time required to perform the different experiments: 1 day for AUC, <1 hour for SAXS.

Table 2.3. *GadB oligomeric state in the pH range 7.5-8.6 as calculated by sedimentation velocity*

pH	GadB	
	*holo*GadB	*apo*GadB
	$s_{20,w}$/kDa (%)[a]	$s_{20,w}$/kDa (%)
7.5	*hexamer*: 13.7/308 (92) *dimer*: 6.6/104 (4)	*dimer*: 6.2/93 (99)
8.0	*hexamer*: 12.9/290 (83) *dimer*: 6.8/108 (8)	*dimer*: 6.5/100 (96)
8.6	*hexamer*: 13.3/300 (74) *dimer*: 6.9/110 (24)	*hexamer*: 13.3/302 (4) *dimer*: 6.4/100 (90)

[a]The numbers in parenthesis correspond to the percentage (%) of the species in solution.

2.3.3. Limited proteolysis as a tool for probing the sites where *apo*GadB conformational changes occur

In order to monitor where the major conformational changes probed by the Trp fluorescence emission spectra occur in *apo*GadB, with respect to *holo*GadB, limited

proteolysis analysis was employed. The same analysis was also useful to assess whether the reconstitution into the *holo* form (*holo*$_{rec}$GadB) was indeed as complete as the activity assays at pH 4.6 (Table 2.1) and the UV-Visible and fluorescence spectra were suggesting (Fig. 2.2).

To this end, *holo*GadB, *apo*GadB and *holo*$_{rec}$GadB were used at a concentration 1 mg/ml and subjected to controlled proteolysis using trypsin in a protease:target protein ratio 1:100 and at pH 8.0. The results shown in Fig. 2.5 indicate that *holo*GadB is attacked by trypsin but to a lesser extent than *apo*GadB, which after 2 h of proteolysis is significantly degraded. On the other hand, *holo*$_{rec}$GadB has significantly regained resistance to the proteolytic attack, thus displaying a proteolytic profile much resembling that of *holo*GadB. The results in Fig. 2.5A show quite clearly that PLP plays a major role in compacting the overall structure.

An MS analysis of the major bands appearing on gel during the limited proteolysis was carried out to detect where the protease attacks the protein and if this susceptibility depends on the presence/absence of PLP. Notably, it was found that in both *holo* and *apo*GadB the first attacks occur on basic residues in the N-terminal region, in particular at Arg10-Ser11 and then at Lys21- Ser22 (Fig. 2.5B). However, within the 2 h of the limited proteolysis analysis, the C-terminal tail was hardly attacked. It was interesting to find out that the two species that in *apo*GadB migrate with an apparent MW of 45 and 42 kDa are identical in sequence to the species (with an apparent MW of 50 kDa) starting with Ser22 and migrating immediately below the band corresponding to full-length GadB. These faster migrating species were hardly detectable on the *holo*GadB and *holo*$_{rec}$GadB samples. For these bands the MS analysis provided a less complete set of internal peptides, following their tryptic digestion, thus suggesting that as soon as trypsin attacks *apo*GadB at the N-terminal region, this leads to a sort of 'collapse' of the overall fold that causes the same species in terms of length to migrate as different species on the gel. After 20 min smaller peptides (<27 kDa) were detectable on the SDS-PAGE only for the *apo*GadB (data not shown), which suggests that another cleavage occurs, likely at the level of the peptide bond Arg178-Glu179, though at present the above mentioned collapse makes it difficult to provide a precise assignment.

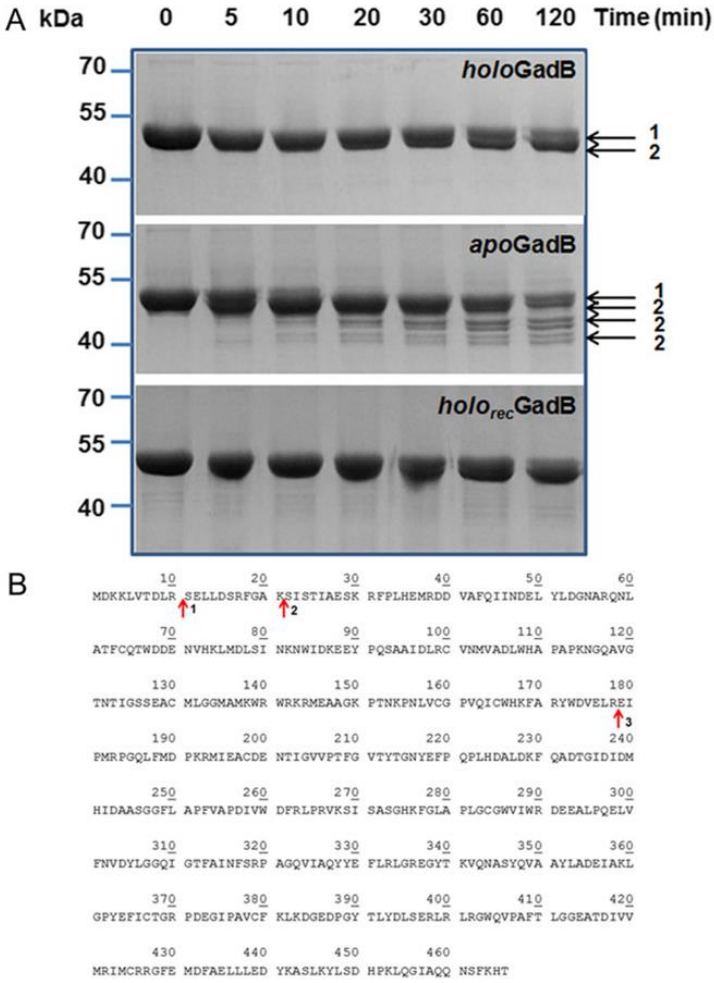

Figure 2.5. *Limited proteolysis on* Ec*GadB*. **(A)** Proteolytic pattern on *holo*GadB (upper panel), *apo*GadB (central panel) and *holo$_{rec}$*GadB (lower panel). **(B)** *Ec*GadB sequence and N-terminal amino acid of the corresponding peptide fragments. The numbers refer to the gel bands that were cut and subjected to proteomic analysis using LC-ESI (See Materials and Methods). The Band 3 is not visible on gel area presented and corresponds to a species with an MW of ~27 kDa, visible after 20 min, only in the *apo*GadB form.

Thus, trypsin cleavage has clearly a different effect on the overall fold of *holo*-, *apo*- and $holo_{rec}$GadB. Activity assays carried out on *holo*GadB and $holo_{rec}$GadB suggest that the N-terminal cleavage has only a limited effect on the activity of the enzyme (20% loss of the activity after 2 h with trypsin). However, on a longer time scale and when also the second site gets completely cleaved off, a significant disappearance of the protein from the gel (indicative of a more extensive proteolysis) and therefore of the enzymatic activity is observed (data not shown).

2.4. Discussion

The PLP-dependent enzyme glutamate decarboxylase from *E. coli* (*Ec*Gad) has been the object of many detailed biochemical and enzymological investigations especially in the 1960–1980's (for a review: Sukhareva, 1986). However, only in more recent years has significant progress been made on the study of this enzyme not only in clarifying its physiological role (in fact *Ec*Gad is a major component of the glutamate-dependent acid resistance system), but also in getting several crystal structures solved and in investigating its use for biotechnological purposes (for reviews: De Biase and Pennacchietti, 2012; Lund *et al*., 2014; Giovannercole *et al*., 2017b).

Prompted by observations mostly from transcriptomic and proteomic studies, indicating that the enzyme is often present in the bacterial cell in conditions where pH is more neutral-to-slightly alkaline than acidic, it was decided to investigate the conformational and oligomeric state of *Ec*Gad in the pH range 7.0–8.6, disregarded in the past as being too far from the range where *Ec*Gad performs its physiological activity (*i.e.* 3.8–6.0). The role of the PLP cofactor in the folding and stability of the enzyme was also investigated. This adds information on the role of PLP in affecting the folding of PLP-dependent enzymes and the consequences (even pathological) associated with a lack of cofactor (Giardina *et al.*, 2011, 2015; Angelaccio *et al.*, 2014; Cellini *et al.*, 2014; Kass *et al.*, 2014).

While some of the observations in the present work are in line with previous findings, others are novel and rather unexpected, thus setting the ground for further studies.

The dissociation of hexameric *Ec*Gad into dimers was already reported as occurring upon PLP removal and at pH > 6.0, at low temperatures and in diluted solutions (Tikhonenko *et al*., 1968; To, 1971; Sukhareva, 1986). However, because all the available crystal structures (PDB codes: 1PMO; 2DGD; 3FZ7) obtained at neutral pH from *Ec*GadB (one of the two very similar Gad isoforms expressed in *E. coli*) show that the enzyme is in a rather compact/ entangled hexameric assembly (Fig. 1.7, General Introduction), it was interesting to note that alkaline pH triggers hexamer dissociation into dimers even in the *holo* enzyme. Very recently, the isoform GadA from *E. coli* in the *holo* form was studied by SAXS together with three other enzymes involved in stationary phase metabolism (Dadinova *et al.*, 2016). Data obtained at pH 7.5 could not be fit by a combination of hexamer and dimer scattering patterns. The conformation of the dimer and of the hexamer were refined using the program SASREFMX and the authors considered a P32 symmetrical hexamer in equilibrium with dimers. This is consistent with our data on *holo*GadB (Fig. 2.3) that essentially show the presence of hexamers together with a small amount of dimers as expected at the pH 6.9 of our sample. Our data suggest a minor conformation difference with the crystal structure, certainly of much reduced amplitude than that reported by Dadinova and coll. (2016). The difference between the observations may reflect differences between protein isoforms (GadB vs GadA) and pH value (6.9 vs 7.5). In the case of the apo form, dissociation appears to be a stepwise process since the tetramer resulting from one dimer removal is stable enough to be separated from the dimer during elution and form a clear peak ahead of the dimer peak. Thanks to the use of SEC-SAXS, in the present work it was possible to separate the two species in solution and to reconstruct the scattering patterns of both species. The comparison with the curve computed from the crystal structure of the hexamer (Fig. 2.4A) suggests that the conformation of *holo*GadB in solution is very similar to that in the crystal. In contrast, the comparisons of both tetramer and dimer curves of *apo*GadB exhibit significant differences pointing to the

existence of different conformations from that of the *holo* protein in the crystal (Fig. 2.4B and C). The dimer appears to be in a more open and extended conformation with a larger Rg value as a consequence of the loss of the interactions of the protein with the PLP that contribute to stabilize the *holo* conformation. This is accompanied by an increase in the flexibility of *apo*GadB as confirmed by the large increase in Trp fluorescence emission (Fig. 2.2) and by the higher susceptibility to trypsin cleavage respect to the forms with the PLP bound, *i.e.* *holo*GadB and $holo_{rec}$GadB. The tetramer in *apo*GadB retains the global arrangement of subunits seen within the *holo* hexamer. However, the conformations of the *apo* subunits are likely less compact, *i.e.* looser than that of the subunits in the *holo* hexamer. Thus, both the dimeric and tetrameric forms of *apo*GadB seem to explore an ensemble of conformations in solution. Consequently, in the absence of additional information, we did not attempt to model any further the conformations of either *apo*GadB oligomeric form.

Trp fluorescence emission was here employed for the first time to monitor the formation of the *apo* form as well as the dissociation of *Ec*Gad into dimers during alkalinization from 7.5 to 8.6 (Fig. 2.2 and Table 2.3). At present, it is not possible to assign to specific Trp residue(s) (out of the 11 present in each protein subunit) the source for the large increase in fluorescence emission in the *apo*GadB form (Fig. 2.2). Disappointingly, the structure of *apo*GadB (PDB code: 3FZ7) does not provide additional information and it looks very similar (RMSDs 0.4%) to *holo*GadB. However, the solution studies reported here do show that changes in conformation and in the oligomeric state occur. Inspection of the *holo*GadB crystal structure at pH 7.6 (PDB code: 1PMO) suggests that while Trp67 and Trp404 are likely candidates for the observed increase in fluorescence with increasing pH (*i.e.* when dimers abundance increases), Trp139 and Trp173 directly/indirectly interacting with their counterparts in the functional dimer are likely responsible for the large increase in fluorescence that occurs upon PLP dissociation (Fig. 2.6). This hypothesis needs to be tested, but right now it is considered as a likely possibility given that Trp139 and Trp173 are not too distant from Gln163 that uses the alkyl portion of its side chain to be in stacking contact with the pyridine ring of PLP.

Thus, in the absence of the coenzyme, it is likely that the active site is not in the same compact conformation and that several residues, including Gln163, are more free to move and cause a different exposure of Trp139 and Trp173 side chains to solvent, therefore leading to the observed strong increase in Trp fluorescence.

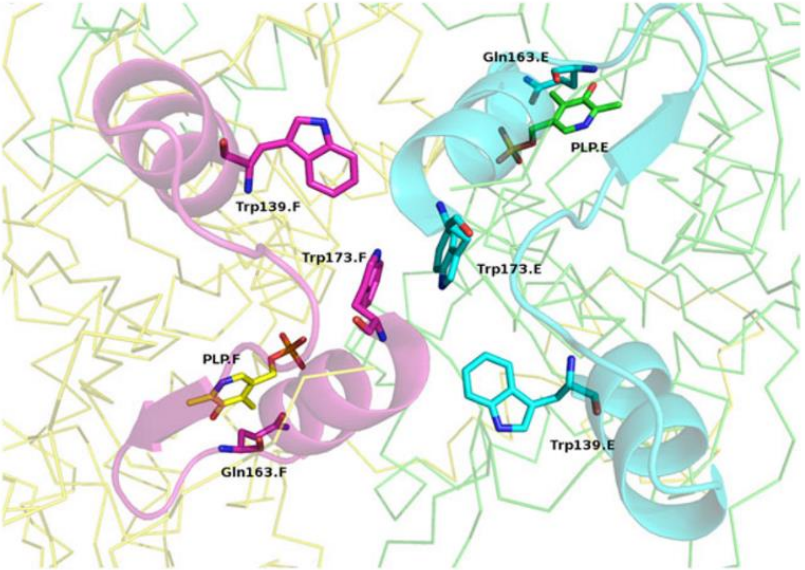

Figure 2.6. *Trp residues involved in interactions between subunits in the GadB functional dimer*. PLP is reported as stick (for chain E and chain F as named in 1PMO). Helices and loops bearing the Trp residues are depicted as ribbon (cyan for chain E and magenta for chain F). The rest of the chains are reported as backbone.

The limited proteolysis experiments using trypsin do suggest that the site that is more accessible to proteolytic attack in both *holo*GadB and *apo*GadB is the N-terminal region, in particular Arg10-Ser11 and Lys21-Ser22 bonds (Fig. 2.5B). Similar results were also obtained

with proteases, with different peptide bond specificity, such as Asp-N, chymotrypsin and thermolysin (data not shown). However, the rate at which proteolysis occurs was always faster in *apo*GadB than in *holo*GadB, thus pointing to a prominent role of PLP not only in catalysis but also in the overall stability and compactness of the fold, as also confirmed by the fact that *holo*$_{rec}$GadB is behaving as *holo*GadB (Fig. 2.5A, upper and lower panels).

Notably, the species detected in *apo*GadB run faster on SDS-PAGE than those of similar mass from *holo*GadB. This striking observation can be explained as a consequence of a collapse of the entire polypeptide chain of *apo*GadB into a more compact structure, which is hard to attack by trypsin during digestion of the protein band analysed by proteomic approaches, *i.e.* LC-ESI. This finds confirmation in the literature (Maras *et al.*, 1992): when guanidinium- HCl-denatured *Ec*Gad (resembling an *apo*Gad form) was digested with several proteases to establish its primary structure, many peptides in the region 150–330 were missing or not overlapping. Therefore, only through cloning and sequencing of the corresponding gene region was possible to overcome the lack of this information. The absence of the same 'faster-running' species in the SDS-PAGE from *holo*GadB and *holo*$_{rec}$GadB also suggests that PLP is responsible for avoiding the collapse occurring in *apo*GadB.

Further work will be necessary to establish the concentration dependence and possible cooperativity in the dimer-hexamer interconversion as well as in the transient formation of the tetramer, a species never observed in the past. This work also sets the basis for studies aiming at screening for novel activities/roles played by *Ec*GadB at pH above 7 and assessing whether the dimer-hexamer equilibrium has relevance in the cell.

CHAPTER III

Asp86 plays a key role in the catalytic mechanism of *Escherichia coli* glutamate decarboxylase

The content of this chapter is included in a manuscript in preparation for submission as:

Pennacchietti, E*., Giovannercole, F*., Grassini, G., Blanchard, J., De Biase, D. (2018) "Asp86 plays a key role in the catalytic mechanism of *Escherichia coli* glutamate decarboxylase".

*These authors contributed equally to this work

3.1. Introduction

Glutamate decarboxylase (*L*-glutamate 1-carboxy-lyase, Gad; E.C. 4.1.1.15) is a ubiquitous pyridoxal 5'-phosphate (PLP)-dependent enzyme catalyzing the irreversible α-decarboxylation of *L*-glutamate (*L*-Glu) to yield γ-aminobutyrate (GABA) and CO_2 (Scheme 3.1). In *E. coli,* two biochemically indistinguishable Gad isoforms, GadA and GadB, sharing 99% sequence identity and exhibiting an acidic pH optimum of activity (pH 3.8-5.0), are produced by the corresponding genes (De Biase *et al.*, 1996). The GadB isoform (*Ec*GadB) is the most intensively studied Gad isoform at the biochemical and structural level (Tramonti *et al.*, 2002a; Capitani *et al.*, 2003a, 2003b; Gut *et al.*, 2006; Pennacchietti *et al.*, 2009): it is a 316-kDa homohexameric enzyme, the pH-dependent activation of which can be easily monitored by the change in the absorption spectrum of its coenzyme, PLP (Tramonti *et al.*, 2002a; Pennacchietti *et al.*, 2009). As shown in the dashed box in Scheme 3.1, the PLP coenzyme typically undergoes interconversion between the active *ketoenamine* species (maximally absorbing at 420 nm) and the inactive *substituted aldamine* (maximally absorbing at 340 nm). The interconversion between the active and inactive species is a highly cooperative pH-dependent process that occurs over a very narrow range of pH (5.25-5.4). The midpoint of the spectroscopic transition is shifted to pH 5.8 in the presence of chloride ions, which act as positive allosteric modulators of the enzyme (Gut *et al.*, 2006).

The crystal structures obtained from the wild-type enzyme at different pH values and from an N-terminal deletion mutant (Capitani *et al.*, 2003a; Gut *et al.*, 2006) show that three important local structural rearrangements occur in *Ec*GadB upon changes in pH: one affects the first 15 residues of the N-terminal domain (residues 1-57), the second affects residues 300-313, which form a β-hairpin in the PLP-binding domain (residues 58-346), and the third involves the last 15 residues (hereafter named C-tail) of the C-terminal domain (residues 347-466). In the active form occurring at acidic-pH, the C-tail of each subunit was proposed to be disordered because it was not visible in the crystal structure.

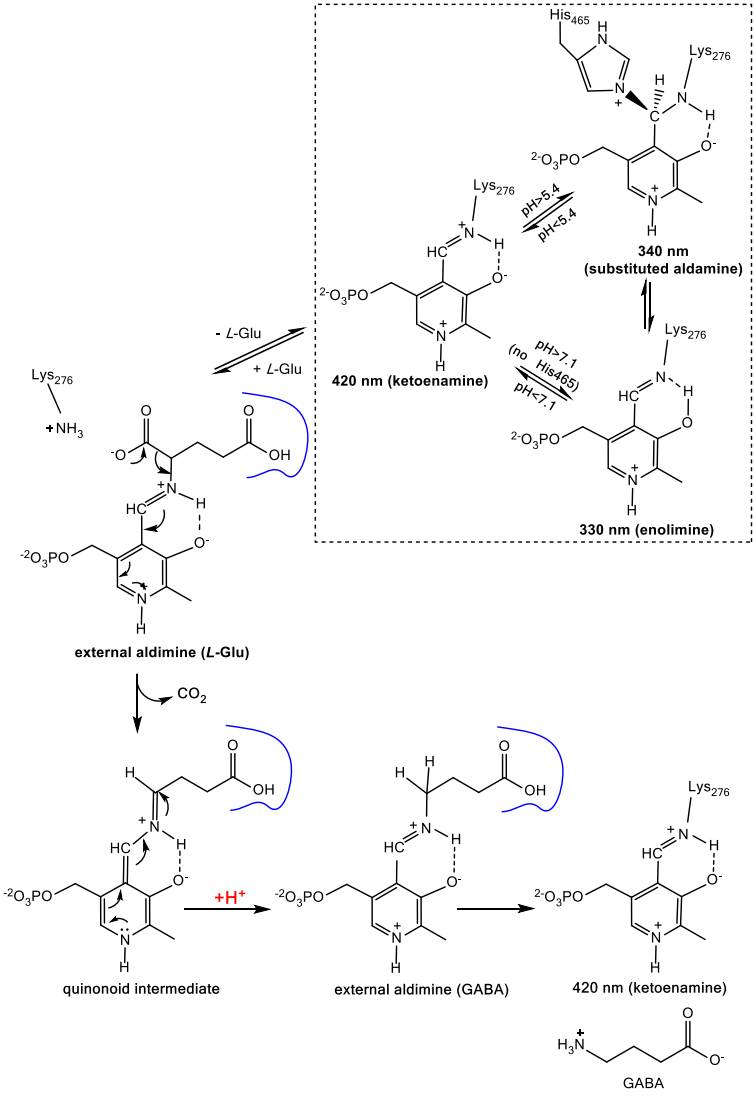

Scheme 3.1. *Catalytic intermediates in the reaction catalyzed by* Ec*GadB*. The cofactor species at the active site of the enzyme in the absence of the substrate are shown in the dashed box. The blue curve indicates the pocket where Asp86 is located and the binding of the γ-carboxylate of *L*-Glu occurs.

In contrast, in the neutral-pH inactive form, the C-tail was found to be ordered, 'plugging' the active site and reversibly inactivating the enzyme via formation of a substituted aldamine, *i.e.* the species in which the distal nitrogen of the imidazole ring of His465 forms a covalent bond with the PLP C4' of the Schiff base between PLP and the residue Lys276 at the *Ec*GadB active site (Scheme 3.1, uppermost structure and Gut *et al.*, 2006).
All these findings fit nicely with the biological role assigned to bacterial Gad, which assists in relieving bacteria from the acid stress encountered in particular, though not exclusively, during colonization of the gastrointestinal tract of the host (De Biase and Pennacchietti, 2012; De Biase and Lund, 2015; Pennacchietti *et al*., 2016). As shown in Scheme 3.1, during the catalytic mechanism, Gad takes up one proton which replaces the α–carboxylate released as CO_2. Thus, during catalysis and in the absence of sufficient buffering capacity, the pH rises and the enzyme activity naturally declines because the *ketoenamine* spontaneously converts into the *substituted aldamine* (Scheme 3.1, dashed box).

Spectroscopic analysis of different His465 mutants demonstrated that this is indeed a key residue for the reversible inactivation of *Ec*GadB at acidic pH (Pennacchietti *et al.*, 2009). On the other hand, His465 does not contribute to the cooperativity observed in *Ec*GadB activity (Pennacchietti *et al.*, 2009). The GadB_His465 mutant enzymes display a pH-activity profile broader than that of the wild-type enzyme, though their catalytic activity falls above pH 6.0, much before the spectroscopic transition midpoint (pH ≈ 7.4) occurs (Pennacchietti *et al.*, 2009). This led to speculation that the decrease of the catalytic activity as a function of increasing pH could be attributed to the deprotonation of one (or more) residue(s) involved in substrate binding or catalysis and with an expected p*K* of 6.0. A likely candidate is the side chain carboxylate of Asp86, which only in the low pH active form is suitably oriented to bind the γ-carboxylate of *L*-Glu (Capitani *et al.*, 2003a). In support of this, the Asp86 side chain was found in different conformations in *Ec*GadB at neutral and acidic pH (Fig. 3.1) and a mutant of this residue (Asp to Asn) expressed in *E. coli* was found to display Gad activity in whole cells even at neutral pH (Capitani *et al.*, 2003a; Hou *et al.*, 2018). Notably, Asp86,

strictly conserved in the pH-dependent prokaryotic and plant Gads (Gut *et al.*, 2009), is replaced by a positively charged arginine residue, forming a salt bridge with the carboxyl group of GABA in human GAD65 and GAD67 (UniProt code: Q99259), which display maximal activity at neutral pH (Fenalti *et al.*, 2007).

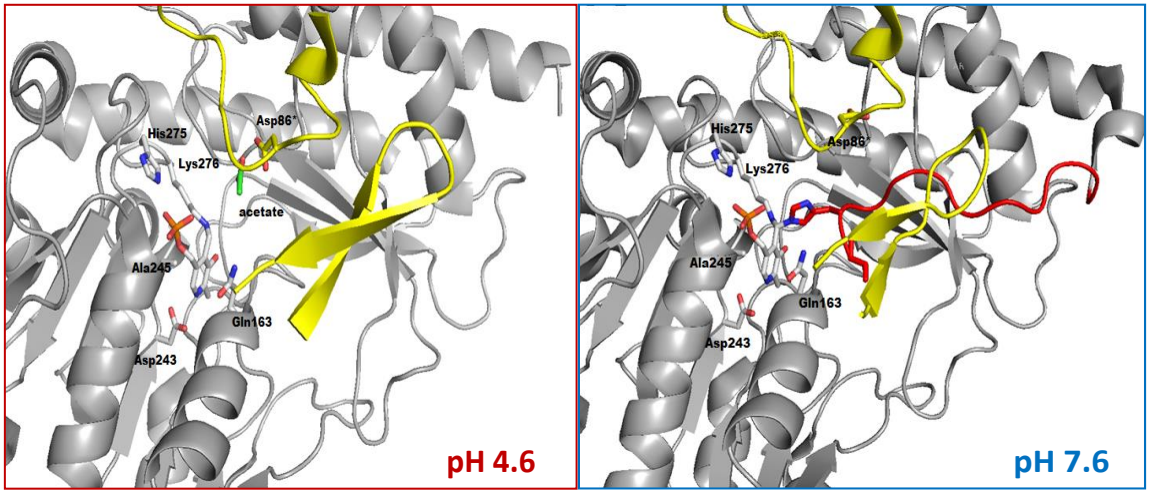

Figure 3.1. *Structure of* Ec*GadB active site at pH 4.6 (PDB: 1PMM) and pH 7.6 (PDB: 1PMO).* At pH 4.6 (open conformation), Asp86-side chain moves into the active site and interacts with acetate. The β-hairpin, that partially occupies the active site, is in yellow. At pH 7.6 (closed conformation), Asp86-side chain moves away from the active site and the β-hairpin is displaced by the C-terminal domain (last 15 residues in red).

In order to elucidate the role of Asp86, we performed a biochemical characterization of the GadB_D86N-H465A mutant (Pennacchietti *et al.*, 2009). The double mutant was required in order to fully assess the involvement of Asp86 in *Ec*GadB's catalytic activity, which is impossible when His465 is present as the pH-induced auto-inactivation of *Ec*GadB occurs above pH 5.5 (Gut *et al.*, 2006; Pennacchietti *et al.*, 2009).

In the present work, Asp86 is shown to be responsible for the large solvent kinetic isotope effect observed in *Ec*Gad (Fonda, 1972; O'Leary *et al.*, 1981). Moreover, GadB_D86N-

H465A was found to catalyze the specific α-decarboxylation of *L*-Glu at a significant rate (10-3%) in the pH range 7-8: a property that is here proposed to be exploitable in biotechnological applications aimed at producing GABA under conditions where an increase in pH is regarded as a limiting factor (Lammens *et al.*, 2009; Ho *et al.*, 2013; Kang *et al*., 2013).

3.2. Materials and methods

3.2.1. Materials

Taq platinum High Fidelity DNA polymerase, restriction enzymes, alkaline phosphatase and ampicillin were from Roche Applied Science. GeneTailor™ Site-Directed Mutagenesis system was from Invitrogen. The DNA ligation system, pre-packed HiPrep DEAE FF 16/10 (20 ml) and HiPrep™ 16/60 Sephacryl™ S-300 HR were from GE Healthcare. *Taq* DNA polymerase (used for colony screening of mutant clones) and SDS-PAGE protein markers were from Fermentas. Kits for plasmid DNA purification and for DNA extraction from agarose gel were from Macherey-Nagel. Ingredients for bacterial growth were from Difco. Streptomycin sulfate was from U.S. Biochemical Corp. (Cleveland, OH, USA). Acetic acid and hydrochloric acid and methanol (HPLC-super grade) were from VWR International. Vitamin B_6, potassium dihydrogen phosphate, dipotassium hydrogen phosphate, *L*-glutamic acid, and kanamycin were from Fluka. Sodium glutamate, sodium acetate, sodium chloride, deuterium oxide (D_2O), GABA and pyridoxal 5'-phosphate (PLP) were purchased either from Merck or from Sigma-Aldrich. Gabase was from Sigma-Aldrich. OPA (*o*-phthaldialdehyde) was from Agilent and *D,L*-norvaline was from Alfa Aesar. Vivaspin 500 (30 KDa) centrifugal concentrators were from Sartorius Stedim Lab Ltd, UK. Oligonucleotide synthesis and DNA sequencing services were from MWG Biotech.

3.2.2. Culture media

Culture media were sterilized in autoclave for 20 minutes at 121°C before use:

- **LB** 10 g/l BactoTryptone;5 g/l Yeast Extract; 5 g/l NaCl. The medium was brought to pH 7.4 by adding 5 N NaOH.
- **SB** 12 g/l BactoTryptone; 24 g/l Yeast Extract; 5g glycerol. 50 ml of 1 M potassium phosphate, pH 7.5 was added immediately before use.
- **SOB** 20 g/l BactoTryptone; 5g/l Yeast Extract; 0.5 g/l NaCL. The medium was brought to pH 7.5 by adding 5 N NaOH.

- **SOC** Modified SOB with added 0.2% glucose and 10 mM $MgCl_2$.

3.2.3. Plasmids and strains. Plasmids and bacterial strains used in this study are listed below.

Table 3.1. *Plasmids and* E. coli *strains used in this study*

Plasmids	Description	Antibiotic Resistance[1]	Source or Reference
pQE60	Expression plasmid (3429 bp): ColE1 *ori*, PT5-*lac* RBSII, *bla*	Amp	Qiagen
pQ*gad*B	pQE60 transcription vector (3429 bp): ColE1 *ori*, P_{T5}-*lac*O RBSII, *bla* (Amp^R); harboring a 1411 bp-fragment (1398 bp ORF *gadB* and 13 bp downstream) cloned into the restriction sites *Nco*I and *Hind*III	Amp	(De Biase *et al.*, 1996)
pQ*gad*B_H465A	pQ*gadB* in which the fragment *gadB Eco*RV-*Hind*III (639 bp) is replaced by a 639-bp fragment, containing the mutation H465A, obtained by PCR and digested with *Eco*RV-*Hind*III.	Amp	(Pennacchietti *et al.*, 2009)
pQgadB_D86N	pQ*gadB* in which the Asp86 has been mutated to Asn using the Gene Tailor system (Invitrogen) which inserts the mutation by amplification of the entire plasmid.	Amp	This work
pQgadB_D86N-H465A	pQ*gadB* in which the fragment gadBH465A NcoI-EcoRV (771 bp) is replaced by a 771-bp fragment, containing the mutation D86N, obtained by digestion with NcoI-EcoRV from pQgadBD86N.	Amp	This work
pREP4	A 3740 bp-vector with *lacI* gene for regulating expression from pQE vectors	Kan	Qiagen
***E. coli* strains**			
Str. K12 JM109	F' [*tra*D36, *pro*AB^+, *lac*I^q, *lacZ*(ΔM15)], *rec*A1, *end*A1, *gyr*A96(Nal^R), *thi*, *hsd*R17(r^-_k,m^+_k), *sup*E44, *rel*A1,*mcr*A, Δ(*lac*-proAB)	Nal	(Ausubel *et al.*, 1987)

[1]Amp, Ampicillin (100 µg/ml); Kan, Kanamycin (25 µg/ml); Nal, Nalidixic acid (20 µg/ml).

pQE60 (Fig. 3.2) belongs to the pDS family and derived from pDS556/RBSII plasmid. It consists of 3429 bp and contains phage T5 promoter and two *lac* operators. The regulation of the promoter/operator is very efficient: the transcription is blocked in the presence of *lac* repressor (lacI), while it is rapidly induced by the addition of IPTG, which inactivates the repressor and makes the promoter accessible. The plasmid has a polylinker immediately downstream of a synthetic ribosome binding and carries the ampicillin resistance *bla* gene. Furthermore, it possesses a sequence coding for six histidine residues (His_6-tag), which precedes the translation termination codons. This accessory protein portion can be used to purify the expressed protein, by affinity chromatography on a nickel column, which was not the case for GadB and its variants characterised in this work.

pREP4 is a 3740 bp plasmid, which contains the *lacI* gene encoding the *lac* repressor. The presence of this accessory plasmid in the cell carrying pQE60 or its derivatives provides high levels of repressor, thus increasing the efficiency in repressing the *lac* operator of pQE60. This plasmid contains also the kanamycin resistance gene (*neo*) and an origin of replication (p15A) different from that of pQE60, which allows their co-existence in the host.

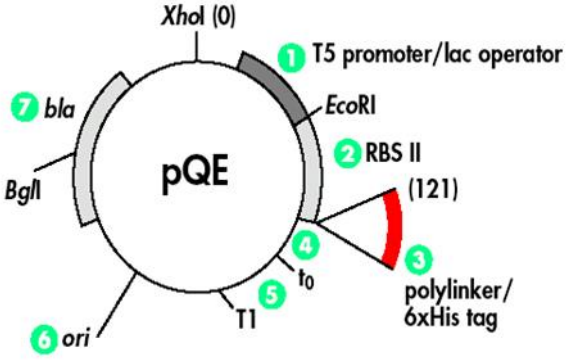

Figure 3.2. *Map of pEQ60 vector.*

3.2.4. Site-directed mutagenesis

Site-directed mutagenesis of *E. coli* GadB was carried out by overlap extension PCR on the entire plasmid pQ*gadB* (De Biase *et al.*, 1996) using the GeneTailor™ Site-Directed Mutagenesis system (Invitrogen). The single mutant plasmid pQ*gadB*-D86N was generated using two specific primers: the forward (mutagenic) oligonucleotide 5'-CCATTAACAAAAACTGGATCAACAAAGAAGAA-3', which introduces the Asp→Asn mutation (GAC in wild type *gadB*), and the reverse, partially complementary oligonucleotide 5'-GATCCAGTTTTTGTTAATGGACAAATCCAT-3'. The underlined and double underlined sequences refer to the region of oligonucleotides overlap and to the mutated codon, respectively. Plasmid pQ*gadB*_D86N-H465A was obtained by ligating a 771-bp *Nco*I-*Eco*RV DNA fragment (corresponding approximately to the first half of the gene) from plasmid pQ*gadB*_D86N into pQ*gadB*_H465A (Pennacchietti *et al.*, 2009) previously digested with the same restriction enzymes to release the corresponding wild-type fragment. The newly generated plasmid was used to transform the *E. coli* strain JM109/pREP4. Transformed colonies were screened by colony PCR and the positive clones isolated. Plasmid pQ*gadB*_D86N-H465A was purified from the positive clones and sequenced on both strands to confirm for the presence of the mutations.

3.2.5. Expression and purification of GadB_D86N-H465A

Expression and purification of GadB_D86N-H465A from *E. coli* JM109/pREP4/pQ*gadB*_D86N-H465A was essentially as described for wild type GadB (De Biase *et al.*, 1996) and GadB-H465A (Pennacchietti *et al.*, 2009) except for the pH of the potassium phosphate buffer used during the DEAE-Sepharose chromatography, pH 6.0 instead of 6.5. Following the first DEAE-chromatographic step, the enzyme was dialyzed against 0.1 M sodium acetate, pH 4.6, containing 0.1 mM DTT and concentrated to 25 mg/ml and loaded (1 ml) onto a HiPrep™ 16/60 Sephacryl™ S-300 HR column equilibrated with the

same buffer. Column equilibration and chromatography were carried out at a flow rate of 0.5 ml min^{-1}. All the chromatographic steps were carried out at 4°C.
Wild-type GadB and GadB-H465A were purified for comparative analyses. Protein purity was judged by SDS-PAGE. The enzyme concentration was calculated as previously described (De Biase *et al.*, 1996). The PLP content of the purified enzymes was determined spectrophotometrically after treating each protein with 0.1 N NaOH. Under these conditions, the molar absorption coefficient (ε) at 388 nm of the released PLP is 6.55 x 10^3 M^{-1} cm^{-1} (Peterson and Sober, 1954).

3.2.6. GAD-Gabase assay

E. coli Gad activity was assayed in 0.2 ml at 37°C at different pH values, in either 50 mM sodium acetate buffer (pH 4.5-5.8) or 50 mM potassium phosphate buffer (pH 5.9-8.3) in the presence of 40 μM PLP, 50 mM NaCl and 50 mM sodium glutamate. For each assay 2-4 μg of enzyme were used. A 5-50 μl aliquot was withdrawn from the reaction mixtures, at various time intervals and assayed with Gabase, using a slightly modified protocol than that previously described (De Biase *et al.*, 1996). Briefly, the reaction mixture was transferred into 100 μl of Gabase solution containing 1.25 μl of activated Gabase (0.02 U/μl) and the incubation was carried out for 60 min at 37°C. The specific activity is given as μmol GABA min^{-1} mg^{-1} (U/mg). Gabase (Sigma) consists of two enzymes from *P. fluorescens*, GABA transaminase (GABA-T, UniProt code: G8PZ77) and succinic semialdehyde dehydrogenase (SSADH, UniProt code: Q4K837), which sequentially convert GABA in succinic semialdehyde and succinic acid, with concomitant reduction of $NADP^+$ into NADPH + H^+. The reduced coenzyme is then quantified on the basis of the specific absorbance at 340 nm. Under the conditions of the assay both reactions are irreversible.

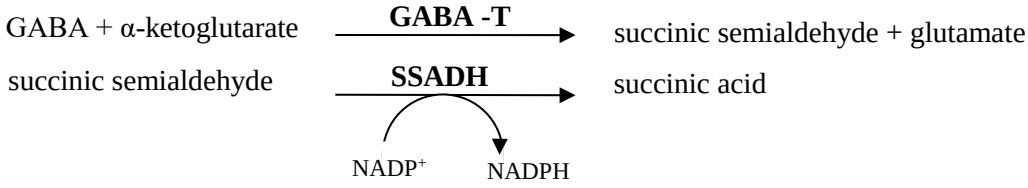

GABA production at pH 7.0 was assayed over a period of 3 hours. The reaction was conducted at 30°C in 4 ml of 50 mM potassium phosphate buffer, pH 7.0, in the presence of 40 μM PLP and 50 mM sodium glutamate. Protein concentration was 2 μM (referred to monomer concentration). At time intervals, aliquots (100 μl) of the reaction mixture were withdrawn and mixed with 400 μl of 0.1 M HEPPS, pH 8.6, followed by vigorous vortexing. A 5-50 μl aliquot was then analyzed for GABA content with the Gabase assay, as above.

3.2.7. Solvent kinetic isotope effects (SKIEs) and Proton inventory

SKIE is a type of kinetic isotope effect (KIE) in which the change in kinetic parameters is due to the replacement of H_2O with D_2O in an enzyme-catalyzed reaction. This typically affects V only, V/K_m only or both. SKIE is usually employed where an isotopic exchange of one or more protons coming from the solvent is relevant in the rate-limiting step for acid-base catalysis. SKIE is generally normal (*i.e.* V in H_2O faster than V in D_2O), which reflects the slower cleavage of N-D or O-D bonds compared to N-H or O-H bonds.

The isotopic effect is measured in terms of isotopic fractionation factor: $k_D/k_H = \varphi^{TS}/\varphi^{RS}$, and the distribution of an isotope for a particular site is dictated by the following role: the heavier isotope (*e.g.* deuterium) will accumulate in the site where binding to the isotopic center is the strongest; the greatest the difference in this binding, the higher is fractionation. The isotopic fractionation, in a reactant (φ^{RS}) or transition-state (φ^{TS}), measures the contribution of a particular site in a particular molecular state defining the deuterium preference to that site relative to water as standard. A large fractionation factor for a site

means that binding at that site is stronger than in bulk-water. The isotopic fractionation factor depends only on the molecular state in the immediate neighbourhood of the site, and this is particularly useful in proton inventory studies. The values of most of the fractionation factors and their biochemical implications are reported in Venkatasubban and Schowen, 1984.

The isotope effect allows to address the transition-state structures occurring in a chemical reaction. Unfortunately, in most biochemical reactions the number of exchangeable protons, and thus the number of transition-state structures, can be very high, making extremely difficult the interpretation of the results. This is the reason why a proton inventory for individual kinetic constants (k_{cat} or k_{cat}/K_m) is usually carried out to determine the number of protons that are being transferred in the rate-limiting steps, from which it is possible to derive the transition-state structures. The experimental procedure consists of determining the reaction kinetics (k_{cat} or k_{cat}/K_m) in a series of isotopic water solvents in which, starting from pure (100%) H_2O, D_2O is mixed with H_2O and increased up to pure (100%) D_2O. The result is a series of kinetic parameters as a function of the atom fraction of deuterium (n) in the solvent. This is described by the Gross-Butler equation (Venkatasubban and Schowen, 1984):

$$V_n = V_0 \frac{\prod_i (1 - n + n\varphi^{TSi})}{\prod_j (1 - n + n\varphi^{RSj})} \quad (1)$$

Where:

- n is the atom fraction of deuterium in mixed isotopic solvent;
- V_n is the velocity in solvent with atom fraction of deuterium (n);
- V_0 is the velocity in pure (100%) H_2O;
- φ_{TSi} is the transition-state fractionation factor;
- φ_{RSj} is the reactant-state fractionation factor.

The form of the curve, that relates the kinetic parameters to n, indicates the number of active protons involved in the rate-limiting steps. The simpler result is a linear plot, which suggests that the observed isotope effect comes from only one transition-state (*i.e.* only one

proton exchanged with the solvent). Often the proton inventory plot is nonlinear (*i.e.* bowl-shaped plot), thus indicating the contribution of two, three or even "infinite-site" to the isotope effect. The "infinite-site" model means the involvement of a very large number of sites, each with a small contribution to the overall isotope effect. Under these conditions, the plot becomes exponential (see eq. 4).

Sometimes the bowl-shaped plot exhibits more than an exponential degree of curvature involving more than one reaction process, *i.e.* a multichannel model (see eq. 5). This usually occurs in the presence of either two parallel reactions, both proceeding with a multiproton mechanism, or two steps in succession both contributing to the isotope effect.

The proton inventory has two main limitations: *i*) the generated models are never unique, and *ii*) the structural site of the isotope effect cannot be identified. This inevitably implies that the proton inventory is only one part of a larger biochemical investigation (Venkatasubban and Schowen, 1984).

Experimental procedure: SKIEs on k_{cat} and k_{cat}/K_m of wild-type *Ec*GadB, GadB_H465A and GadB_D86N-H465A mutants (0.075 μM in buffer prepared in H_2O or 0.151 μM in buffer prepared in D_2O) were determined in either 100% H_2O or 97% D_2O. The reaction was carried out at 25°C in 250 μl of 50 mM sodium acetate, containing 40 μM PLP and different glutamate concentrations, from 0.3 mM to 20 mM, for wild-type *Ec*GadB and GadB_H465A, or from 0.3 mM to 80 mM, for GadB_D86N-H465A. SKIEs were measured in the pL (L= H or D) range 4.4 - 5.0 (Table 3.3). At various intervals, aliquots (50 μl) of the reaction mixture were withdrawn, quenched in 200 μl of 0.1 M HEPPS, pH 8.6, and the GABA content was analyzed by the Gabase assay (see above).

For the experiments performed in buffers prepared with D_2O, the pH values of the buffer solutions were adjusted according to the relationship: pD = pH + 0.4.

To mimic the viscosity effect caused by D_2O, a viscosity control was performed by assaying the enzyme activity in buffer containing 9% (w/w) glycerol. These assays provided evidence that solvent viscosity has no effect on the reaction rate (data not shown).

A proton inventory on k_{cat} and k_{cat}/K_m for wild-type *Ec*GadB and GadB_D86N-H465A was performed by varying the atom fraction of deuterium oxide at pL 4.8. The reaction conditions were the same as those for the SKIEs, except that sodium glutamate was kept constant at 50 mM (*Ec*GadB) or 80 mM (GadB_D86N-H465A) for the proton inventory on k_{cat} and 40 µM (*Ec*GadB) or 250 µM (GadB_D86N-H465A) for the proton inventory on k_{cat}/K_m. Protein concentration for the proton inventory on k_{cat}/K_m was 0.0375 µM and 0.225 µM for *Ec*GadB and GadB_D86N-H465A, respectively. GABA was quantified using the Gabase assay (see above) for the proton inventory on k_{cat}, whereas HPLC was used to measure GABA production for the proton inventory on k_{cat}/K_m. The k_{cat} value was derived from the Michaelis-Menten equation reduced to a zero-order kinetics (eq. 2). The k_{cat}/K_m value was calculated using the Michaelis-Menten equation reduced to a first-order equation as in eq. 3.

$$k_{cat} = \frac{V_{max}}{[E]_t} \quad (2)$$

$$v = \frac{k_{cat}}{K_m} [E]_t [S] \quad (3)$$

The best fitting for the proton inventory on k_{cat}/K_m and k_{cat} for wild-type *Ec*GadB and GadB_D86N-H465A was obtained with eq. 4, whereas the best fitting for the proton inventory on k_{cat} for wild-type GadB was obtained with eq. 5.

$$k_n = k_0 \, \varphi_i^{TS} \quad (4)$$

$$k_n = k_0 \, [f \, (\varphi_i^{TS1})^n + (1 - f) \, (\varphi_j^{TS2})^n] \quad (5)$$

In both eqs, k_n is k_{cat} or k_{cat}/K_m at each atom fraction of D_2O (n) while k_0 is k_{cat} or k_{cat}/K_m in 100% H_2O. φ_i^{TS} represents the transition-state isotopic fractionation factor and f and (1-f) are the fraction of the contribution to φ_i^{TS1} and φ_j^{TS2}, respectively.

3.2.8. GABA quantification by HPLC

Samples from k_{cat}/K_m proton inventory experiments were analyzed by HPLC on an Agilent 1260 series system (Agilent Technologies, USA) equipped with a quaternary pump and a fluorescence detector. GABA, Glu and the internal standard, norvaline, were separated under a mix of isocratic and gradient elution using an Agilent Poroshell 120 HPH-C18, 4.6 x150 mm, 2.7 µm LC column (Agilent Technologies) and an Agilent InfinityLab Poroshell UHPLC-C18 guard column (4.6 x 5 mm, 2.7 µm particle size). The mobile phase consisted of Solvent A (50 mM sodium acetate buffer:methanol; 50:50, v/v) adjusted to pH 4.18 with HCl and Solvent B (100% methanol). Prior to methanol addition, all solutions were filtered through 0.2-µm nitrocellulose Whatman filters (Ø 47 mm).

Pre-column derivatization of standard amino acids and samples with *o*-phtalaldehyde (OPA) reagent solution (Agilent, 10 mg/ml) was set to be carried out automatically in the HPLC autosampler. Briefly, the derivatization was performed with a programmable automatic injector (Agilent) by mixing 80 µl of sample (or standard solution) with 8 µl of OPA. After 1 min at room temperature, an 80-µl aliquot of the derivatised sample was directly injected into the HPLC column equilibrated with Solvent A. The elution was carried out at RT and a flow rate of 1 ml min^{-1} with the following program: from 0 to 18 min in 100 % Solvent A (isocratic step), from 18.1 to 25 min a linear gradient step to 100 % Solvent B. The column was then washed for 7 min at 100% Solvent B and equilibrated back into 100% Solvent A with a 4-min gradient step and kept in the same solvent for 10 min, ready for the next injection. The fluorescence detector was set at an excitation wavelength of 240 nm and an emission wavelength of 450 nm, as published elsewhere (Perucho *et al.*, 2015).

Using the above HPLC program, Glu, GABA and norvaline displayed the following retention times: Glu, 4.46 ± 0.06 min; GABA, 12.15 ± 0.20 min; norvaline, 23.42 ± 0.05 min. The software used for analysis and peak integration was OpenLab (Agilent). Sample peak areas were typically measured by the automatic integration system, though in some circumstances a manual correction of the baseline was required. GABA (µM) was quantified

by comparing the peak area with those obtained from an external calibration curve (1-10 µM GABA) obtained in the same conditions as above.

Preparation of stock and working solutions. 300 mM stock solutions of either GABA or Glu or norvaline were prepared in HPLC-grade water, aliquoted out and stored at 4°C. Working solutions (10 µM) were prepared weekly (every 3 days for norvaline) by diluting the stock solutions in HPLC-grade water, aliquoted out and stored at 4°C until use.

3.2.9. Spectroscopic measurements and data analysis

Absorption spectra were recorded at the indicated temperatures on a Hewlett-Packard Agilent model 8453 diode array spectrophotometer.

The absorption spectra were resolved into their component absorption bands (deconvolution) by nonlinear least square fit of the experimental data to the sum of a variable number of log normal curves, each having independent parameters (Metzler *et al.*, 1973). Deconvolution of spectra was performed with Scientist (Micromath, Salt Lake City, UT).

Curve fitting and statistical analyses were carried out with GraphPad Prism 4.00 (GraphPad Software, San Diego, CA). The pH-dependent variation in absorbance and activity of the wild type and mutant enzymes was analyzed using the Hill equation (eq. 6):

$$Y = \text{Bottom} + \frac{(Top - Bottom)}{1 + 10^{(pK - pH)n}} \qquad (6)$$

Where: *Bottom* is the Y value at the bottom plateau; *Top* is the Y value at the top plateau; p*K* is the pH value at the midpoint of the sigmoid; *n* is the Hill coefficient corresponding to the (minimum) number of protons required for the transition.

3.3. Results

3.3.1. Purification and spectroscopic properties of GadB_D86N-H465A

The double mutant GadB_D86N-H465A was generated by incorporating the Asp86Asn mutation into the single mutant GadB_H465A, already available in the laboratory (Pennacchietti *et al.*, 2009). GadB_D86N-H465A was overexpressed in *E. coli* and purified as previously described (De Biase *et al.*, 1996) except for the DEAE-Sepharose chromatography, which was carried out in phosphate buffer at pH 6.0, instead of pH 6.5, since GadB_D86N-H465A was found not to bind the resin at the latter pH value. During DEAE chromatography a yellow band was observed on the column, indicating that, like GadB_H465A, at pH 6.0-6.5 GadB_D86N-H465A is mostly in the ketoenamine (active) form (Scheme 3.1). The Gad-containing fractions were pooled, incubated for 1 h at room temperature with a 5-fold molar excess of PLP with respect to the protein concentration (to increase the *holo*enzyme/*apo*enzyme ratio, which was 70% after the DEAE chromatography), and then further purified by gel-filtration chromatography on a Sephacryl S-300 HR column in acetate buffer at pH 4.6. Following the purification, GadB_D86N-H465A was judged to be ≥ 95 % pure by SDS-PAGE (data not shown). The PLP content was 90-95%, as confirmed by the reduced absorbance at 420 nm compared to that of wild-type *Ec*GadB (Fig. 3.3).

The yield of the purified enzyme from a standard purification (2 L bacterial culture) was 30 mg. The specific activity towards *L*-Glu (assayed at 37°C in 0.2 M pyridine/HCl buffer, pH 4.6, containing 0.1 mM PLP) was 140 U/mg, corresponding to 64 % and 80 % of the specific activity of wild-type *Ec*GadB and GadB_H465A, respectively (Pennacchietti *et al.*, 2009).

When assayed with aspartate or glutamine, GadB_D86N-H465A did not show any activity, thus indicating that the D86N mutation in the active site did not affect the substrate specificity of the enzyme.

As shown in Figure 3.4A, the UV-Visible absorption spectra recorded in the pH range 4.5 - 9.1, provide an indication that a 420 nm → 332 nm spectroscopic transition occurs. This

transition, however, does not go to completion and the 420 nm-absorbing ketoenamine species (Scheme 3.1, dashed box) is still detected at pH ≥ 9.

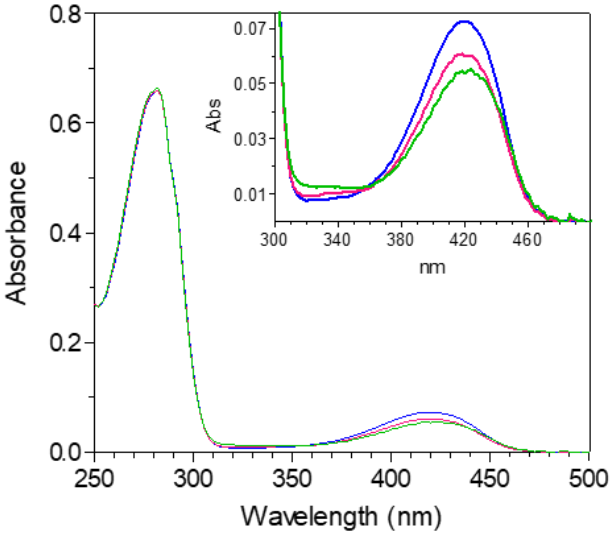

Figure 3.3. *UV-Visible absorbance spectra*. The spectra of GadB_D86N-H465A (green), wild-type *Ec*GadB (blue), and GadB_H465A (magenta) were recorded in 50 mM sodium acetate buffer, pH 4.6. Protein concentration was 7.7 μM (referred to the monomer; 0.41 mg/ml)**.** Inset: the 300 - 500 nm region of cofactor absorbance is expanded.

This is significantly different from what is reported for wild-type *Ec*GadB (Tramonti *et al.*, 2002a; Pennacchietti *et al.*, 2009), while resembling the spectroscopic transition occurring in GadB_H465A (Pennacchietti *et al.*, 2009). The 420-nm absorbance readings at each pH value were used to generate a titration curve using the Hill equation (Fig. 3.4B). and the p*K* of the spectroscopic transition as well as the Hill coefficient [*i.e.* representing the minimum number of protons involved (*n*)] were calculated (Table 3.2).

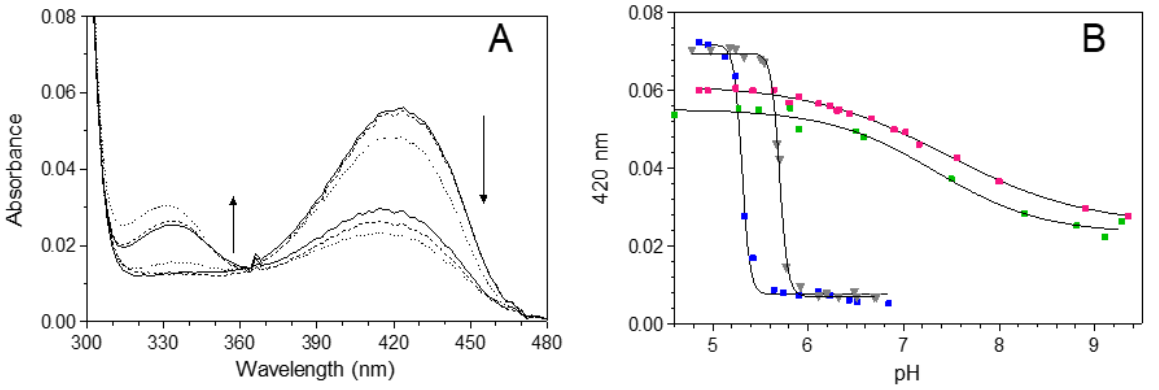

Figure 3.4. *pH-dependent absorbance changes*. **(A)** Spectra of GadB-D86N-H465A were recorded in 50 mM sodium acetate buffer at pH values of 4.6, 5.48 and in 50 mM potassium phosphate buffer at pH 6.58, 8.26, 8.81, 9.1. The protein concentration was 7.7 μM and the arrows indicate the direction of the changes in absorbance at 420 nm and at 332 nm upon increasing pH. **(B)** The pH-dependent readings at 420 nm are reported for GadB-D86N-H465A (green squares), for GadB_H465A (magenta squares) and wild type *Ec*GadB in the absence (blue squares) and presence (gray triangles) of 50 mM NaCl. The solid lines through the experimental points represent the theoretical curves obtained using the Hill equation (eq. 6 in Material and Methods).

Table 3.2. *Midpoint (p*K*) and Hill coefficient (*n*) of the spectroscopic transition in wild-type and mutant forms of* Ec*GadB.*

	p*K*	***n***
GadB	5.31 ± 0.01	10.52 ± 1.49
GadB + NaCl	5.70 ± 0.01	10.14 ± 1.04
GadB_H465A	7.44 ± 0.01	0.60 ± 0.05
GadB_D86N-H465A	7.23 ± 0.14	0.77 ± 0.17

In GadB_D86N-H465A, the midpoint of the spectroscopic transition is at pH 7.23, 2 pH units higher than that observed for wild-type *Ec*GadB. Chloride ions, known to act as positive allosteric activators of *Ec*GadB (Fig. 3.4B; (Gut *et al.*, 2006)), did not further affect the spectroscopic transition in both mutants (data not shown).

These results resemble those obtained with GadB_H465A (Fig. 3.4B and Table 3.2), except for the isosbestic point of the spectroscopic transition, that in GadB_D86N-H465A occurs at 360 nm (Fig. 3.4A) as in wild type *Ec*GadB, whereas it is blue-shifted to 348 nm in GadB_H465A (Pennacchietti *et al.*, 2009).

In order to identify more precisely the species contributing to the absorbance spectra, the spectrum of GadB_D86N-H465A at pH 8.8 (Fig. 3.5) was resolved into single component absorption bands by non-linear least-square fit (deconvolution). It is important to understand that in wild-type *Ec*GadB, the spectrum at pH 6.8 (or higher), where the enzyme is inactive, arises from the sum of three species, with maxima at 330, 341.5 and 410 nm (Fig. 3.5, inset on the left). In particular, the 341.5 nm component band, corresponding to the substituted aldamine (see Scheme 3.1 and (Pennacchietti *et al.*, 2009)), is prevailing over the other two species.

Spectra deconvolution of GadB_D86N-H465A yielded only two species with maxima at 330 nm (enolimine) and 418 nm (ketoenamine) (Fig. 3.5; Scheme 3.1), regardless of the pH (4.6, data not shown, or 8.8). This analysis confirmed that the aldamine is absent in GadB_D86N-H465A, alike in GadB-H465A. The only difference observed between GadB_D86N-H465A and GadB-H465A is in the intensity of the enolimine peak at 330 nm, which at pH 8.5 is more intense in GadB_D86N-H465A than in GadB_H465A (Fig. 3.5, inset on the right).

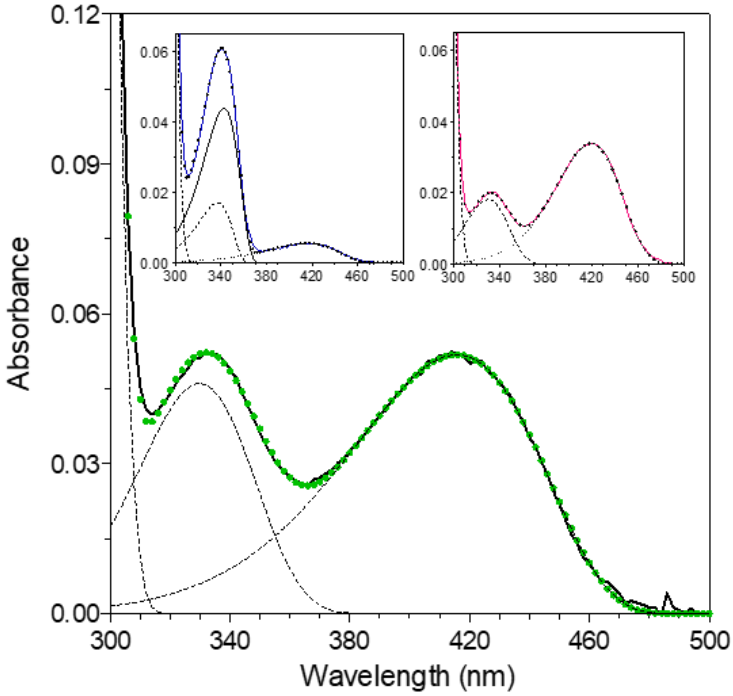

Figure 3.5. *Deconvolution of spectra of* Ec*GadB, GadB_H465A and GadB_D86N-H465A.* The absorbance spectrum of GadB_D86N-H465A at pH 8.8 was resolved into its component absorption bands. For comparison in the insets are reported the spectra of wild type *Ec*GadB at pH 6.84 (left panel) and GadB_H465A at pH 8.5 (right panel) resolved into their component absorption bands. The spectra were recorded in 50 mM potassium phosphate buffer at the indicated pH. The solid lines represent the experimental spectra, the dashed lines are the component bands, and the dotted colored curve is the theoretical curve obtained by nonlinear least-square fit of the experimental points to the sum of a variable number of log-normal curves, each having independent parameters.

In conclusion, the UV-Visible spectrophotometric analysis, combined with the spectra deconvolution, suggest that the spectroscopic properties of GadB_D86N-H465A can be primarily assigned to the H465A mutation. In fact, the spectroscopic properties of the single

mutant GadB_H465A are almost superimposable with those of the double mutant GadB_D86N-H465A. The H465A mutation appears to be primarily responsible for the observed replacement of the substituted aldamine in the active site of *Ec*GadB with the enolimine tautomer of the PLP-Lys276 Schiff base (Scheme 3.1).

3.3.2. Catalytic properties: kinetic parameters and solvent isotopic effect

SKIEs on k_{cat} and k_{cat}/K_m of wild-type *Ec*GadB, GadB_H465A and GadB_D86N-H465A mutants were determined in buffers prepared in either 100% H_2O or 97% D_2O. The reactions were carried out at 25°C and with different glutamate concentrations (see Materials and Methods, par. 3.2.7). SKIEs were measured in the pL (L= H or D) range 4.4 - 5.0 (Table 3.3).

Table 3.3. *Kinetic parameters of wild type EcGadB, GadB_H465A and Gad_D86N-H465A at different pLs.*

		H_2O			**D_2O**		
***Ec*GadB**	**pL**	**k_{cat} (s^{-1})**	**K_m (mM)**	**k_{cat}/K_m (s^{-1} mM^{-1})**	**k_{cat} (s^{-1})**	**K_m (mM)**	**k_{cat}/K_m (s^{-1} mM^{-1})**
Wild-Type	4.60	14.98 ± 0.71	1.220 ± 0.183	12.28 ± 2.46	2.07 ± 0.09	0.271 ± 0.050	7.64 ± 1.46
	4.80	16.63 ± 0.74	1.191 ± 0.169	14.01 ± 2.08	2.22 ± 0.07	0.312 ± 0.044	7.11 ± 1.03
	5.00	13.40 ± 0.68	0.937 ± 0.166	14.30 ± 2.64	1.90 ± 0.08	0.281 ± 0.047	6.77 ± 1.17
	5.20	17.28 ± 0.99	1.250 ± 0.226	13.82 ± 2.62			
H465A	4.60	18.39 ± 1.05	0.870 ± 0.175	21.14 ± 5.50	2.51 ± 0.12	0.281 ± 0.062	8.93 ± 2.41
	4.80	15.17 ± 0.36	0.767 ± 0.066	19.78 ± 1.77	2.30 ± 0.12	0.221 ± 0.044	10.41 ± 2.60
	5.00	17.83 ± 0.88	0.982 ± 0.166	18.16 ± 4.00	2.58 ± 0.11	0.174 ± 0.036	14.83 ± 3.71
D86N-H465A	4.40	35.60 ± 0.57	4.397 ± 0.235	8.10 ± 1.96	16.98 ± 1.13	3.201 ± 0.739	5.30 ± 1.27
	4.60	30.84 ± 1.32	2.636 ± 0.580	11.70 ± 2.62	14.92 ± 0.53	1.224 ± 0.197	12.19 ± 2.01
	4.80	40.24 ± 1.72	4.157 ± 0.581	9.68 ± 1.41	12.93 ± 0.24	1.448 ± 0.081	8.93 ± 0.47
	5.00	38.67 ± 0.99	2.690 ± 0.464	14.38 ± 2.51	10.33 ± 0.14	0.959 ± 0.053	10.77 ± 0.61

The data at pL 4.8, which was selected for the proton inventory studies (see paragraph 3.3.3) are reported in Table 3.4 for a straightforward observation. As shown in Table 3.4 (first three columns) the K_m and k_{cat} of GadB_D86N-H465A are 4 times and 3 times higher than those of the other two enzyme forms, respectively. This gives rise to a specificity constant (k_{cat}/K_m) 30 % and 50 % lower than that of *Ec*GadB and GadB_H465A, respectively.

Table 3.4. *Kinetic parameters of GadB_D86N-H465A at pL 4.8 (and at pL 6.2 for values in brackets) compared to wild type* Ec*GadB and GadB_H465A.*

	H_2O			D_2O		
	k_{cat} (s^{-1})	K_m (mM)	k_{cat}/K_m (s^{-1} mM^{-1})	k_{cat} (s^{-1})	K_m (mM)	k_{cat}/K_m (s^{-1} mM^{-1})
GadB	16.63 ± 0.74	1.19 ± 0.17	14.01 ± 2.08	2.22 ± 0.07	0.31 ± 0.04	7.11 ± 1.03
GadB_H465A	15.17 ± 0.36 (17.99 ± 0.81)	0.77 ± 0.07 (7.19 ± 1.14)	19.78 ± 1.77 (2.50 ± 0.41)	2.30 ± 0.12	0.22 ± 0.04	10.41 ± 2.60
GadB_ D86N-H465A	40.24 ± 1.72 (33.93 ± 0.51)	4.16 ± 0.58 (6.70 ± 0.36)	9.68 ± 1.41 (5.07 ± 0.28)	12.93 ± 0.24	1.45 ± 0.08	8.93 ± 0.47

When the same constants were measured at pH 6.2 (Table 3.4, values in parenthesis), pH at which Asp86, according to our hypothesis, is expected to be fully deprotonated and therefore unable to bind the distal carboxylate group of *L*-glutamate, only the single mutant GadB_H465A displays a significant increase in the K_m, compared to that at pL 4.8, whereas this same parameter is only slightly increased in the double mutant GadB_D86N-H465A, respect to that at pL 4.8. This observation strongly supports the original idea that the decrease of the catalytic activity in *Ec*GadB is due, at least in part, to the deprotonation of a residue involved in substrate binding, the side chain of which has an expected p*K* of 6.0, and Asp86 was proposed as a likely candidate.

The decarboxylation reaction in GadB_D86N-H465A, GadB_H465A and wild-type *Ec*GadB was also carried out in deuterium oxide (D_2O) at pL 4.8 (Table 3.4, last three columns) and the kinetic parameters were calculated. As expected from previous studies, carried out with isotopically labeled water (O'Leary *et al*., 1981), the k_{cat} in H_2O and D_2O for wild-type *Ec*GadB are significantly different and this results in a very high solvent isotope effect ($^{D2O}k_{cat}$, Table 3.5) of 7-8, rarely observed in enzymes, including PLP-dependent enzymes. This result was proposed to arise from two contributions of solvent exchangeable protons *i)* at the Schiff-base exchange step (*i.e.* transaldimination step) occurring upon substrate binding and, later, *ii)* during decarboxylation, with a conformational change possibly involved (O'Leary *et al*., 1981). Data in Table 3.5 show that the solvent isotope effect on k_{cat} observed in *Ec*GadB is unchanged in the single mutant, whereas it is more than halved in the double mutant. On the other hand, the isotope effect on k_{cat}/K_m ($^{D2O}k_{cat}/K_m$, Table 3.5) was 1.9-2.0 for both *Ec*GadB and GadB_H465A, whereas in the double mutant GadB_D86N-H465A this value is near unity. In *Ec*GadB k_{cat}/K_m includes all the rate constants for the catalytic steps up to the irreversible decarboxylation (*i.e.* from k_1 to k_5 as in Scheme 3.2). The k_{cat} value instead contains all the rate constants for the steps, following substrate binding, leading to the release of GABA (*i.e.* from k_3 to k_9 as reported in Scheme 3.2).

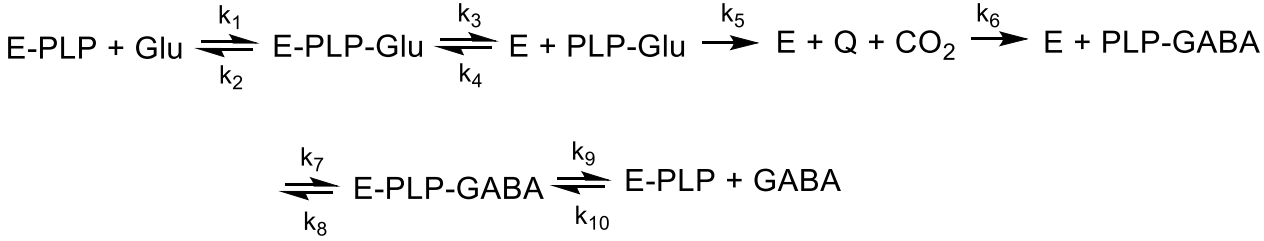

Scheme 3.2. *Catalytic steps in the decarboxylation of L-Glu in* Ec*GadB.* Q is the quinonoid intermediate, *i.e.* the short-living cofactor-substrate intermediate following the decarboxylation, which is then quickly reprotonated into the external aldimine with GABA (PLP-GABA).

In the double mutant both $^{D2O}k_{cat}$ and $^{D2O}k_{cat}/K_m$ are affected (Table 3.5), suggesting that Asp86 plays a role in both substrate binding and GABA release.
This is further supported by the values of the kinetic parameters measured in H_2O at pH 6.2 (Table 3.4), where the K_m of the single mutant GadB_H465A increase 10 times, whereas that of GadB_D86N-H465A increases by 50%.

Table 3.5. *Isotope effect at pL 4.8.*

	$^{D2O}k_{cat}$	$^{D2O}k_{cat}/K_m$
GadB	7.49 ± 0.41	1.97 ± 0.41
GadB_H465A	6.60 ± 0.38	1.90 ± 0.50
GadB_D86N-H465A	3.11 ± 0.15	1.08 ± 0.17

3.3.3. Proton inventory

A proton inventory study was conducted to obtain additional information on the solvent isotope effect on k_{cat} and k_{cat}/K_m for wild-type GadB and GadB_D86N-H465A (Fig. 3.6). The GadB_H465A variant was excluded from this study because its kinetic constants, both in H_2O and D_2O are substantially similar to those of wild-type GadB (Table 3.4). Experiments were performed at pL 4.8 since the k_{cat} and k_{cat}/K_m versus pL profiles for wild-type and GadB_D86N-H465A are relatively independent of pL over the assayed range, *i.e.* pL 4.4-5.0 (Table 3.3). The $^{D2O}k_{cat}$ was studied at 50 mM and 80 mM *L*-Glu for wild-type GadB and GadB_D86N-H465A, respectively. These values are well above the K_m calculated in both H_2O and D_2O buffers for each enzyme (Table 3.3). For wild-type GadB, the proton inventory revealed a pronounced downward-bowing curve indicating the occurrence of multiple proton transfer contributing to $^{D2O}k_{cat}$ (Fig. 3.6A), in line with previous reports (O'Leary *et al.*, 1981). The best non-linear fit was obtained using eq. 5 (Materials and Methods) with a "multichannel" model assuming the reactant state fractionation factor (φ^{RS}) equals 1 and

predicting contributions from two transition-state fractionation factors ($\varphi^{TS1} = 0.5089$ and $\varphi^{TS2} = <0.01$), each contributing with an "infinite" number of protons to the overall isotopic effect, unlike what was previously suggested (O'Leary *et al*,, 1981). The fractionation factor with value <0.01 is consistent with proton tunneling. Based on the above, the likely scenario would imply transition-state hydrogen bridges for proton transfer, with tunneling (Venkatasubban and Schowen, 1984). This is mechanistically described by proton transfer(s) to or from carbons during the catalysis of the fission of C-H bonds, activated by a neighboring carbonyl or similar functional group. The first pathway (described by φ^{TS1}) is expected to contribute by 23 ± 3% (derived from "*f*" in eq. 5), while the second (described by φ^{TS2}) by 77 ± 3% (derived from "(1-*f*)" in eq. 5) giving rise to a calculated SKIE of 8.59 ± 0.95, similar to $^{D2O}k_{cat}$ reported above (Table 3.5).

The proton inventory for GadB_D86N_H465A also revealed a downward-bowing curve, but much less pronounced than the wild-type *Ec*GadB curve. The former curve was easily fitted with several different forms of eq. 4 (Materials and Methods), revealing the involvement of only one transition-state fractionation factor. The best fit was obtained with a model predicting an "infinite" number of transition state protons ($\varphi^{TS} = 0.2652 \pm 0.0136$) that accounts for an isotopic effect of 3.77 ± 0.09, a little bit higher but consistent with the SKIE value (3.11 ± 0.07). This slight difference may derive from the nature of the equation applied for proton inventory studies (zero-order kinetics) and could also be accounted for slight differences in the homogeneity of different enzyme preparations. Transition-state hydrogens bridges in solvation catalysis are likely responsible for this isotopic effect. Transition-state stabilization by proton bridges can occur in an acid-base catalysis when, following formation or fission of covalent bond(s), there is a proton transfer amongst electronegative atoms, such as oxygen, nitrogen and sulfur, which stabilizes the transition-state. In this condition, the isotope effect usually observed is between 1.5 and 4. However the involvement of transition-state hydrogen bridges for proton transfer, alike the wild-type, but without tunneling, cannot be excluded (Venkatasubban and Schowen, 1984).

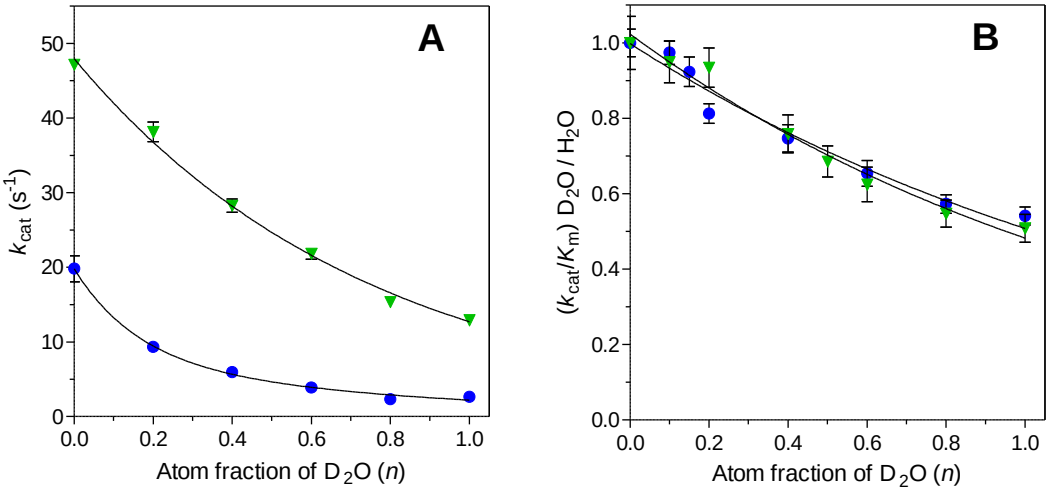

Figure 3.6. *Proton inventory for wild-type* Ec*GadB (blue) and* Ec*GadB_D86N-H465A (green).* Solvent deuterium dependence on k_{cat} **(A)** and k_{cat}/K_m **(B)** on the fraction of deuterium (*n*) in solvent. **(A)** Reactions were carried out in the presence saturating concentration of Glu (50 mM and 80 mM for wild-type and *Ec*GadB_D86N-H465A, respectively). Data were fitted to eq. 4 (for *Ec*GadB_D86N-H465A) and to eq. 5 (for wild-type). **(B)** Reactions were carried out with limited concentration of Glu (40 µM and 250 µM for wild-type and *Ec*GadB_D86N-H465A, respectively) and data were fitted to eq. 4 for both enzymes. k_{cat}/K_m values at each atom fraction of D_2O were then normalized for k_{cat}/K_m in 100% H_2O and plotted.

Hence, the effect of the D86N substitution consists in suppressing the proton tunneling observed in the wild-type enzyme, thus decreasing the overall isotope effect by a factor of 2.7.

A proton inventory on k_{cat}/K_m was also performed to assess the involvement of Asp86 in the initial steps of the reaction (Fig. 3.6B). For both wild type GadB and GadB_D86N_H465A, the data could be fitted with eq. 1 assuming one, two, three, four or "infinite" protons exchanged. Unfortunately, the level of variation (error) required to allow for fitting was >2% and this impaired the assignment of our data to a specific model, *i.e.* single, two or three-or-more protons. As a matter of fact, the fitting shown in Fig. 3.6B was possible with all the models considered.

3.3.4. Catalytic properties: effect of pH on specific activity

All the above findings suggest that Asp86 plays a negative role on GABA release, but positively affects substrate binding at acidic pH, as originally suspected. It was hypothesized that the replacement of Asp86 with an Asn residue, as in GadB_D86N-H465A, could be exploited for GABA synthesis at neutral pH, where the wild type GadB is totally inactive and the single mutant GadB_H465A is drastically affected (Table 3.4, values in parenthesis).

Thus, the activity profile of GadB_D86N-H465A in the pH range 4.5-8.3 was compared with those of wild-type GadB and GadB_H465A (Fig. 3.7A). The results indicate that GadB_D86N-H465A still retains activity at pH > 7, whereas that of wild-type GadB and GadB_H465A is undetectable (Fig. 3.7A and (Pennacchietti *et al.*, 2009)). Notably, GadB_D86N-H465A retains 10% and 6% of the starting activity at pH 7.0 and 8.0, respectively.

Given that GadB_D86N-H465A is still active at pH close to 7-8, GABA production was measured in phosphate buffer at pH 7.0 in the presence of 50 mM *L*-Glu over a period of 3 hours (Fig. 3.7B). For comparative purposes, the time-course of GABA production was analyzed also for GadB_H465A and wild-type GadB. As shown in Figure 3.7B, GadB_D86N-H465A converts 86 % and 96 % of *L*-Glu into GABA after 2 and 3 hours of reaction, respectively. Following the first 30 min of reaction, the rate of GABA production gradually decreased due to pH increase (Fig. 3.7B inset) and the concomitant consumption of *L*-Glu, which after 3 hours is only 2 mM. These results are remarkable if compared with those obtained with GadB_H465A, which converts only 25 % of *L*-Glu into GABA after 3 hours. As expected, wild-type GadB decarboxylates only <1 % of *L*-Glu after 3 hours at pH 7.0.
During the reaction, the pH of the solutions was monitored: after 3 hours the pH increased by 0.2 and 0.4 pH units in GadB_H465A and GadB_D86N-H465A reactions, respectively. This is consistent with H^+ consumption occurring during the decarboxylation reaction in a buffer system at a 50 mM, *i.e.* similar to that of the substrate. In wild-type GadB no pH change was

detected. In conclusion, the D86N mutation leads to a noticeable expansion of GadB activity towards alkaline pHs.

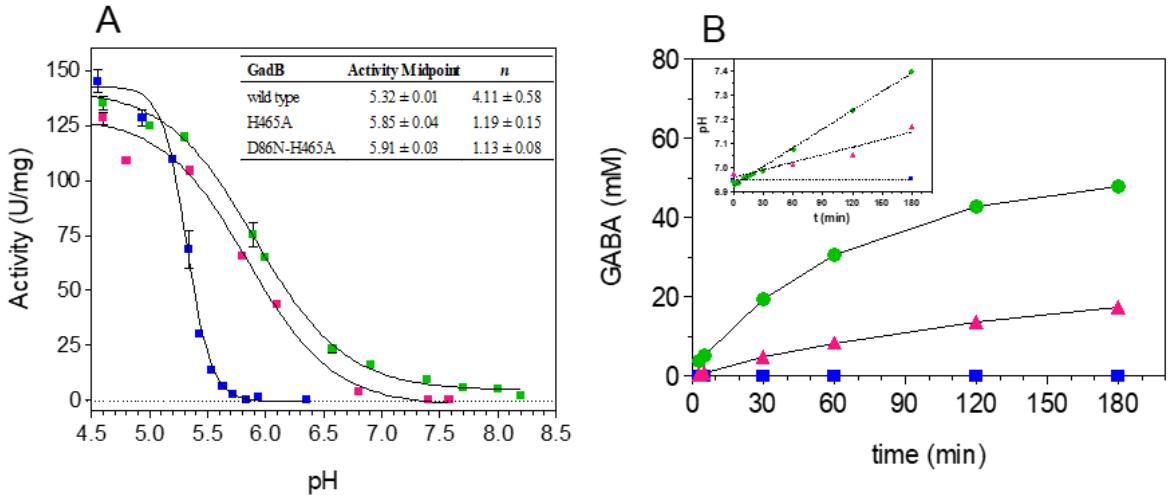

Figure 3.7. *Effect of pH on the specific activity and time course of GABA production.* Blue squares, wild type GadB; magenta squares, GadB-H465A; green squares, GadB-D86N-H465A. **(A)** Activity assays were carried out at 37°C in 50 mM acetate (pH 4.5 - 5.8) or phosphate (pH 5.9 – 8.3) buffer in presence of 40 µM PLP, 50 mM NaCl and 50 mM *L*-Glu. Protein concentration was 0.9-2 µM. The solid lines through the experimental points represent the theoretical curves obtained using the Hill equation. The reported data are the means of three independent experiments, with a standard deviation < 10 % of the given value. The *n* and Activity Midpoint values retrieved from curve fitting are given in the inset Table. **(B)** GABA production was analyzed over a period of 3 hours. The reaction was carried out at 30°C in 4 ml of 50 mM potassium phosphate buffer, pH 7.0, containing 40 µM PLP and 50 mM *L*-Glu. The protein concentration was 2 µM. At each time point aliquots (100 µl) were withdrawn and analyzed for GABA content with the Gabase assay. The pH changes during the reaction were also recorded (inset).

3.4. Discussion

In many enteric bacteria Gad is a major structural component of a very potent acid resistance system, *i.e.* the glutamate-dependent acid resistance system, which was shown to protect them from extremely acidic stress, such as that encountered during transit through the host stomach (De Biase and Pennacchietti, 2012). Examples of bacteria employing this system include commensal and pathogenic strains of *E. coli*, *S. flexneri*, *L. monocytogenes*, *B. microti* and several other *Brucella* species (amongst those evolutionary most ancient), *L. reuteri* and *L. lactis* (Lund *et al*., 2014; Damiano *et al.*, 2015). Therefore, it is not surprising that in bacterial Gad many residues are strictly conserved, suggesting that this enzyme has evolved to accomplish the proton-consuming decarboxylation reaction only when the intracellular pH falls below a life-threatening threshold level, as the consequence of the low external pH and proton "leakage" into the cell. Clearly, some amino acid residues in the Gad "signature" (De Biase and Pennacchietti, 2012) are of crucial importance from the functional point of view. Asp86 was hypothesized to be amongst these and therefore in this work its contribution to the spectroscopic and catalytic properties of GadB is described.

Asp86 is provided by the neighboring subunit in the functional dimer (GadB in *E. coli* is a trimer of dimers (Capitani *et al.*, 2003a)) and that, in order to bind the γ-carboxyl group of *L*-Glu, it undergoes a significant side chain reorientation during the pH-dependent conformational change that accompanies the activation of the enzyme at acidic pH (Capitani *et al.*, 2003a). Only at acidic pH the side-chain of Asp86 is oriented towards the active site and, based on the binding of acetate ions, the Asp86 β-carboxylate was proposed to interact with the γ-carboxylate of the substrate *L*-Glu (Capitani *et al.*, 2003a). Clearly, for this interaction to occur, at least one (if not both) of the two carboxylate groups must be protonated, otherwise they would repel each other.

In this work Asp86 was replaced with a similarly sized but neutral Asn residue. This mutation was expected not to affect hydrophilicity in the GadB active site, while abolishing the charge repulsion between the β-carboxylate of Asp86 and the γ-carboxylate of *L*-Glu at

non- permissive pH values (> 5.5 in wild-type GadB), thus allowing substrate binding at pH values well above 6.

To assess the role of Asp86 in GadB, the GadB_D86N-H465A double mutant was produced. This was performed to assess the contribution of Asp86 in substrate binding and the catalytic mechanism at pH > 5.5, an interaction otherwise undetectable due to the presence of His465 in the active site at pH > 5.5. While the D86N mutation in the double mutant GadB_D86N-H465A does not affect the spectroscopic properties with respect to the single mutant GadB_H465A, the data obtained in this work show that GadB_D86N-H465A *i)* displays reduced SKIEs on both k_{cat} and k_{cat}/K_m and *ii)* has an expanded pH-range of activity with respect to both wild-type GadB and GadB_H465A.

Notably, the decrease in the SKIE was observed only in the double mutant and not in the single GadB_H465A mutant, pointing to a prominent role of Asp86 in the solvent isotope sensitivity of GadB. This turned out to be an unpredicted finding because when Asp86 was mutated into Asn, it was expected to affect the binding of the substrate at neutral pH. However, the data presented in this work suggest that Asp86 has indeed a notable effect on the high SKIE observed for wild-type GadB, an unusually high number, rarely found in enzymes (Venkatasubban and Schowen, 1984). We propose that Asp86 plays a key role in both substrate binding and GABA release, by altering the hydrogen bonds network in both cases. A non-optimal initial interaction with γ-carboxylate group of *L*-Glu might explain the increase in K_m value. However, following binding, *L*-Glu might be in a more favorable position for the subsequent reaction steps (*i.e.* increased k_{cat}). The kinetic parameters and isotope effect discrepancies between GadB_D86N-H465A and both wild-type GadB and GadB_H465A mutants suggest that the above are indeed likely possibilities. No significant differences in H_2O and D_2O were detected between wild-type GadB and GadB_H465A, suggesting that His465 is involved neither in the binding of *L*-Glu nor in any of the catalytic steps involved in the decarboxylation and the release of the product. This agrees with previously published work (Pennacchietti *et al.*, 2009). Interestingly, the Asp86Asn

substitution strongly decreased the isotope effect on k_{cat} to ~3. Thus, we propose that Asp86 is intimately involved in the binding and in the orientation of *L*-Glu, however its major role is in controlling the release of the product. This came as a totally unexpected finding respect to our original idea when we conceived the Asp86Asn substitution.
It must be pointed out here that the SKIE and the proton inventory results were completed only very close to the conclusion of this PhD thesis work and therefore a complete and more thoughtful interpretation of the results is still underway.

Of interest is the finding that GadB_D86N-H465A is able to catalyze *L*-Glu decarboxylation reaction at a significant rate at pH 7-8, where the activity of both GadB-H465A and wild-type GadB is either significantly lower or undetectable, respectively. It is important here to recall that *L*-Glu is a non-essential amino acid, abundant in many plant proteins, including those present in waste streams from biofuel production. This amino acid is therefore considered an interesting starting material for the industrial synthesis of nitrogen-containing chemicals, including GABA, the precursor of 2-pyrrolidone, which is an important industrial solvent (Lammens, 2011). The enzymatic conversion of *L*-Glu to GABA via GadB, carried out in bioreactors at the industrial level, was proposed as a strategy to decrease the dependence on fossil fuels, allowing the production of chemicals from renewable resources, such as biomass (Lammens *et al.*, 2009). However, during decarboxylation GadB activity is slowed down by the pH rise caused by the consumption of protons (Lammens *et al.*, 2009; Pennacchietti *et al.*, 2009). Engineered *E. coli* GadB, such as a C-terminal truncated mutant (Yu *et al.*, 2012), His465 mutants (Pennacchietti *et al.*, 2009) and Glu89/His465 mutants (Ho *et al.*, 2013) were designed with the aim of improving and enhancing the enzymatic properties of GadB and the reaction conditions for potential industrial applications. The GadB_D86N-H465A mutant characterized in this work is expected to be useful in biotechnological applications because, unlike GadB and much better than GadB-H465A, it is able to catalyze the decarboxylation reaction across a wide pH range, extending above pH > 8.0, thereby rendering the pH of the reaction no longer a limiting parameter.

CHAPTER IV

Preliminary biochemical characterization of a glutamate decarboxylase from *Mycobacterium tuberculosis*

This work is included in a project funded in 2018 by Istituto Pasteur-Fondazione Cenci Bolognetti and carried out in collaboration with the Fundacao Oswaldo Cruz – Institute Pasteur Brazil:

1) *Whole transcriptome (RNA-Seq) combined with biochemical studies to evaluate the contribution of the metabolism of glutamate and GABA in* Mycobacterium tuberculosis *strains circulating in Salvador, Bahia, Brazil.*

4.1. Introduction

Tuberculosis (TB) is a disease caused by the bacillus *Mycobacterium tuberculosis* isolated in 1882 by Dr. Robert Koch, known as Koch's bacillus. TB mostly affects the lungs (pulmonary TB) but infections can spread through the blood stream and the lymphatic system to many other sites (extra-pulmonary TB) (Raviglione, 2015). The World Health Organization (WHO) reports that, amongst HIV-negative people, 1.3 million died of TB, while the deaths amongst HIV-positive people were 374.000. Overall, WHO estimates that 1.7 billion of people will be affected by TB in their life. In this contest, TB is the leading cause of death from a single infection agent, above malaria and HIV (World Health Organization, 2017).

The causative agent of TB, *M. tuberculosis*, is an obligate aerobic mycobacterium which belongs to the family Mycobacteriaceae and the actinobacteria class. At the cellular level it presents a rod-shaped curvature and possesses a complex cell-wall made of fatty acids, waxes and mycolic acids linked to the underlying peptidoglycan and arabinogalactan which make the cell totally impermeable to Gram-staining. Such a complex cell-wall composition is also responsible for the slow generation time, 15-20 hours, and resistance to common antibiotics, detergents and immune system (Raviglione, 2015).

M. tuberculosis is an obligate intracellular pathogen for humans and relies on the host nutrients for its replication and survival. Therefore, it is adapted to survive within the host and evade successfully the immune response (Raviglione, 2015; Mishra and Surolia, 2018). Usually, the infection starts with the inoculum of air droplets harboring the microbe, which invades the lower respiratory tract where it is phagocytized by the alveolar macrophages and dendritic cells. Here, it resides in the phagosome, and strategically avoids its acidification by halting the phagosome-lysosome fusion (Armstrong and Hart, 1971). Characteristics of *M. tuberculosis* phagosome are: *i*) incomplete acidification of the phagosomal lumen obtained by inhibiting the host recruitment of vacuolar-H^+-ATPase (V-ATPase); *ii*) absence of mature lysosome hydrolases (Vergne *et al.*, 2004). The bactericidal property of phagolysosome

compartment is represented by a hypoxic, nitro-oxidative and nutrient-limiting environment, in which *M. tuberculosis* persists (active infection) by activating an array of molecular responses and starts to replicate exploiting the nutrients derived from the host cell (Ehrt and Schnappinger, 2009; Mishra and Surolia, 2018). In response to this, the host immune system activates the infected macrophages through IFN-γ (Fig. 4.1) that overrides phagosome-arrest and delivers *M. tuberculosis* to increasingly inhospitable compartments, mainly represented by low pH (4.5-5.0), lysosomal hydrolases, ubiquitin-derived peptides and reactive oxygen and nitrogen intermediates (ROI and RNI) (Vandal *et al.*, 2009a). Nonetheless, the pathogen can survive (Schaible *et al.*, 1998).

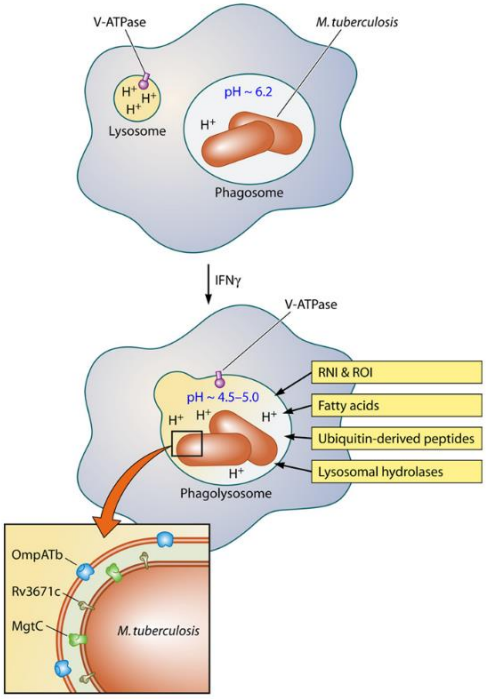

Figure 4.1. M. tuberculosis *within the macrophage.* In resting macrophages *M. tuberculosis* impairs the lysosome-phagosome fusion and resides in a mildly acidic environment. Activation with IFN-γ triggers the formation of phagolysosome that exposes *M. tuberculosis* to host-derived stress, such as vacuolar-ATPase (V-ATPase), RNI and ROI, lysosomal hydrolases, free fatty acids, ubiquitin-derived peptides and to a more acidic pH (pH 4.5-5.0). The Rv3671c-encoded membrane-bound serine protease (MarP, see text), the putative magnesium transporter MgtC, and the pore-forming *M. tuberculosis* outer membrane protein (OmpATb) help *M. tuberculosis* to deal with the acidic environment (the latter two not reported in the text) through unknown mechanisms.
Image from Vandal *et al.*, 2009a.

On the other end, in most individuals the infection does not proceed with the disease since the host immune system response, unable to kill the pathogen, confines it into a self-limited granulomatous lesion, *i.e.* tuberculous granuloma, where the infection is contained and cannot spread (latent infection) (Raviglione, 2015). In this case, the infection has not symptoms and it is not contagious, but *M. tuberculosis* is still alive. How the pathogen persists in this latent infection is not understood and it is much debated. For many years it was thought that *M. tuberculosis* enters a non-replicative dormant stage (quiescence) due to the high toxic environment of the granuloma; more recently it has been assumed that the host-pathogen interaction in the granuloma is more dynamic than previously thought and involves continuous loss of cells by cell death and tissue remodeling. In this scenario, *M. tuberculosis* divides slowly but it is metabolically active and, together with the immune infiltration, it is assumed to shape progressively the granuloma to its advantage (Ehlers and Schaible, 2012).

The granuloma can last from several months to years (dormancy), or even decades (latency), and usually the reactivation of the infection takes place during immune senescence and suppression (Raviglione, 2015); in this regard, significant is the connection with HIV coinfections (World Health Organization, 2018).

The first chemotherapeutic agent found to be effective against TB was streptomycin. It was quickly followed by the identification of isoniazid (INH; 1952), pyrazinamide (PZA; 1954), rifampicin (RIF; 1957) and ethambutol (ETH; 1960). The combination of these latter four drugs was recommended as the standard "short-course" therapy (6 months) for drug-sensitive TB. However, the long course of antibiotic treatments can require 6-9 months to fully clear the infection and the numerous side effects, such as hepatotoxicity and peripheral neuropathy, often cause premature treatment arrest (World Health Organization, 2017). To date, the only vaccine available, the Bacille Calmette Guerin (BCG) vaccine, confers protections only to infants and children but there is a lack of evidence over its efficacy against different *M. tuberculosis* strains (World Health Organization, 2018).

Despite globally the mortality rate is decreasing by 3% per year, drug-resistant TB represents an important threat. Three main categories are observed: *i*) MDR (multi drug resistant)-TB which is a TB resistance to both rifampicin and isoniazid, thereby it requires the treatment with a second-line regimen; *ii*) RR (rifampicin resistant)-TB which also required a second line-regimen; *iii*) XDR (extensively drug resistant)-TB which combines MDR plus resistance to at least one drug between either fluoroquinolones or second-line injectable agent (kanamycin, amikacin or capreomycin) (World Health Organization, 2017). Starting from the late 1990's, strains of *M. tuberculosis* resistant to isoniazid and rifampicin began to appear and in the last 8-10 years the specter of XDR-TB has emerged. Finally, totally drug-resistant strains of *M. tuberculosis* were first identified in Italy in 2003 (Migliori *et al.*, 2007). Therefore, the research of new strategies and molecular targets constitutes a global priority.

4.1.1. Metabolic adaptation of *M. tuberculosis* to stress

By arresting the phagosome maturation, *M. tuberculosis* is able to establish a life-long infection in resting macrophages; however, even in this state, the phagosome environment may provide a critical cue for adaptation, especially in IFN-γ-activated macrophages; thereby our understanding of the survival strategies, metabolism and physiology of *M. tuberculosis* during intracellular growth, though still incomplete, may represent a successful strategy to find new molecular targets (Rhee *et al.*, 2011).

Over the last years, several studies have been conducted in order to investigate at the genomic and molecular level how *M. tuberculosis* responds and adapts to the environmental cues during the infection (Rohde *et al*., 2007, 2012; McKinney *et al.*, 2000; Fisher *et al*., 2002; Saviola *et al*., 2003; Rengarajan *et al*., 2005; Fontán *et al.*, 2008; Pandey and Sassetti, 2008; Rhee *et al.*, 2011; Galagan *et al.*, 2014; Baker and Abramovitch, 2018). Transcriptome and microarray analysis, supported by knock-out lethal strains of infection in mice or guinea pigs, seem to converge towards an over-expression of genes involved in lipid metabolism, such as β-oxidation, acetate and glyoxylate cycle metabolism, propionate metabolism, amino

acid biosynthesis, gluconeogenesis, starvation responses, oxidative stress, remodeling of cell-wall and in uptake and consumption of cholesterol. In clear agreement with this, *M. tuberculosis* perceives the phagosome as a fatty acids-rich environment with severe limitations in sugars, oxygen (hypoxia) and amino acids availability, with a potential to damage DNA and cell envelope through ROS and RNI. This switches the microbial metabolism toward the utilization of the host fatty acids and cholesterol as main carbon sources, which fuel the TCA and glyoxylate cycles and are converted into carbohydrates through gluconeogenesis. This model is strongly supported by the overexpression of genes involved in β-oxidation, gluconeogenesis and glyoxylate cycle when *M. tuberculosis* is within the macrophages, and by the observation that mutant strains of these genes exhibit attenuated virulence in mice. Some of these mutants included isocitrate lyase (Icl, UniProt code*: P9WKK7) encoded by *icl1* and *icl2*, phosphoenolpyruvate carboxykinase (PEPECK, UniProt code: P9WIH3) encoded by *pckA*, lipoamide dehydrogenase (Lpd, UniProt code: P9WHH9) encoded by *lpdC*, dihydrolipoamide acyltransferase (DlaT, UniProt code: P9WIS7) and *mce4*-encoded cholesterol transporter (McKinney *et al.*, 2000; Pandey and Sassetti, 2008; Rhee *et al.*, 2011; Mukhopadhyay *et al*., 2012; Ghazaei, 2018). *Notably, hereafter the UniProt codes refer to *M. tuberculosis* ATCC 25618/H37Rv).

Amino acids play also a key role in the microbial survival (Mishra and Surolia, 2018). For example, by up-regulating the amino acid biosynthesis genes, *M. tuberculosis* evades the amino acid starvation exploited by the host cell as a defense mechanism. In this respect, glutamate levels constitute a significant determinant of bacterial survival since glutamate serves as scaffold for amino acid biosynthesis; as such its regulation elicits interest in light of new antitubercular drugs (Cowley *et al.*, 2004; Viljoen *et al.*, 2013; Gallant *et al.*, 2016; Rieck *et al.*, 2017). Together with glutamate, arginine plays a critical role as a central metabolite in the phagosome since *i*) it is the main substrate of the host inducible nitric oxide synthase (iNOS), which synthetizes nitric oxide (NO), a strong inhibitor of bacterial growth, and *ii*) it

is the precursor of the polyamines putrescine and spermidine, which strongly favor and support the infection (Duque-Correa *et al.*, 2014; Tiwari *et al.*, 2018).

Overall, it is established that *M. tuberculosis* takes advantage of different metabolic pathways of the central carbon metabolism (CCM) to adapt and cope with the numerous harsh conditions that it encounters while invading the host; as such, the enzymes of the CCM are regarded with interest as potential drug targets and might be exploited for new therapeutic strategies (Rhee *et al.*, 2011).

4.1.2. Acid resistance strategies in *M. tuberculosis*

As described in the "General Introduction", the acid stress is one of the most harmful condition that bacteria have to cope with in order to survive; as such, many efforts have been made to investigate the molecular strategies responsible for the survival to acidity. The most successful responses to acidity have been extensively studied in enteric bacteria, such as *E. coli* and *L. monocytogenes*, but much less is known in intracellular pathogens, like *M. tuberculosis*, for which the acid environment is mostly represented by the phagosome/phagolysosome or the tuberculous granuloma (Fig. 4.1) (Vandal *et al.*, 2009a); Indeed, in resting macrophages, the phagosomal pH is ~6.2, whereas it falls to 4.5-5.0 when the phagosome fuses with lysosome in response to IFN-γ (Ehrt and Schnappinger, 2009). Apart from severely altering the cellular homeostasis, the acidity of the phagosome supports additional antimicrobial mechanisms, such as the activation of acid-dependent lysosomal hydrolases and the dismutation of nitrite to form NO and nitrogen dioxide, both highly toxic radicals. However, following one day of exposure to pH 4.5, *M. tuberculosis* slows it growth but controls its intracellular pH at neutrality even in activated macrophages (Vandal *et al.*, 2008, 2009a), suggesting that some acid resistance mechanisms may be also conserved in *M. tuberculosis.*

Interestingly, several transcriptomic studies found that the drop in pH experienced within resting macrophages serves as a dominant signal for the early transcriptional adaptation of *M.*

tuberculosis to this intracellular niche. Hence it is thought to represent a protection to other form of stress and to sustain the long-term infection (Rohde *et al*., 2007, 2012; Baker and Abramovitch, 2018). The upregulation of some two-component signal transduction systems (TCSs) in the phagosome *in vivo* plays surely a key role in this. A significant overlap was found with the TCS PhoPQ regulon, in which PhoP (UniProt code: P71814) serves a sensor histidine kinase and autophosphorylates itself on a specific histidine residue under specific environmental signals; once phosphorylated, it transfers the phosphate signal to the aspartate residue in the receiver domain of the transcriptional regulator, PhoQ (UniProt code: A0A1K3EIS2). Over 100 genes are under the regulation of the PhoPQ system, and several of them are associated with lipid metabolism at low pH, suggesting that lipids are an important player of the acid resistance (Rohde *et al*., 2007). Notably, PhoPQ signal is also involved in the activation of the GDAR system in *E. coli* (General Introduction).

Consistent with this, a recent study found that the PhoPQ regulon is a key mediator of the redox homeostasis of *M. tuberculosis* at low pH by redirecting the carbon metabolism towards the lipid anabolism, which results in the accumulation of methyl-branched lipids, such as sulfolipids, the main role of which is thought to relieve the reductive stress caused by the hypoxic environment within the phagosome (Baker *et al*., 2014). Indeed, as corroborated by a recent study (Mehta *et al*., 2016), the acidic pH perturbs the redox physiology of *M. tuberculosis* by reducing the electrogenic potential across the membrane, which, if not properly counteracted, leads bacterial death. This pH-mediated reductive shift triggers and enhances the expression of several genes involved in mitigating the redox stress, with the highest degree exhibited by the transcriptional regulator, WhiB3 (UniProt code: P9WF41). WhiB3, an Actinomycete-specific protein, is a Fe-S cluster-containing transcriptional factor early induced in response to acidic pH (Rohde *et al*., 2007). Notably, by acting as an intracellular redox sensor, it was found to mount an antioxidant response to promote the survival within macrophages by upregulating several genes involved in cell wall lipid composition and redox balance as well as genes coding for virulence factors that impair the

phagosome maturation (Mehta *et al*., 2016). Notably, the pH-dependent activation of WhiB3 was recently reported to be mediated by PhoPQ (Feng *et al*., 2018).

Another significant overlap is represented by the pH-driven transcriptional activation of the Acid Phagosome Regulated *aprABC* operon (Abramovitch *et al.*, 2011). This locus, whose gene products have not been fully characterized yet, operates downstream of the PhoPQ regulon and it is required for the optimal growth of *M. tuberculosis* at acidic pH since it genetically modules the expression of hundreds of genes mainly involved in the integrity of the bacterial cell envelope.

Overall, the microarray and transcriptome data of the above studies, along with *M. tuberculosis* acid-sensitive mutants with defects in genes involved in cell-wall lipids biosynthesis, clearly depict a model in which the physical and molecular composition of the cell wall is an effective primary defense against the entry of protons. In strong agreement with this, the disruption of the gene Rv3671 via transposon mutagenesis impaired *M. tuberculosis* ability to maintain the intracellular pH to neutrality when exposed to low pH, and the growth of the mutant was compromised in mice. Rv3671c was found to code for a serine protease MarP (UniProt code: A0A2Z4TVS8) that cleaves the peptidoglycan hydrolase RipA (UniProt code: O53168), the activity of which was shown to mediate the peptidoglycan hydrolysis at low pH, thus allowing cell division in acidic environments (Vandal *et al.*, 2008; Botella *et al.*, 2017). Therefore, the remodeling of the cell envelope constitutes a successful response to phagosome acidification by acting as a formidable permeability barrier for antibacterial (Vandal *et al.*, 2008, 2009b).

Unlike enteropathogenic bacteria, *M. tuberculosis* does not appear to possess many of the most common acid-resistance mechanisms; nevertheless, some recent studies report that an overlap between acidity, oxidative stress and heat shock seems to occur in *M. tuberculosis.* In fact, low pH, together with oxidative stress and heat shock, was found to induce the expression of the stress-responsive transcriptional regulators SigB (UniProt code: P9WGI5)

and SigH (UniProt code: P9WGH9), two alternative sigma factors, which enable the activation of several stress response genes (Rohde *et al*., 2007).

Although none of the *M. tuberculosis* mutants isolated so far is involved in mechanisms exploited by neutralophilic bacteria to counteract the acid stress (Lund *et al*., 2014), the urea breakdown with the concomitant release of ammonia, a biochemical process catalyzed by the enzyme urease, may be involved in neutralizing the acidic environment of the phagosome and/or in preventing the phagosome acidification (Gordon *et al*., 1980). However, in another study, the urease activity assayed in IFN-γ activated macrophages failed to counteract efficiently the acidity of the phagolysosome compartment and, furthermore, it did not confer significant capability to *M. tuberculosis* to replicate and survive *in vivo*. Conversely, the same study suggested another possible involvement of urea in *M. tuberculosis* physiology, *i.e.* as a potential nitrogen source, since it sustains the bacterial growth when provided as sole nitrogen source *in vitro* (Lin *et al.*, 2012). In support of this, urease activity was found to be increased under nitrogen starvation (Clemens *et al*., 1995). On the other hand, in *M. tuberculosis* amino acids represent an important nitrogen source (Lin *et al.*, 2012). Indeed, they have been recognized to support *M. tuberculosis* growth *in vitro* by functioning as both nitrogen and carbon sources (Gouzy *et al*., 2014c). This is clearly highlighted by a high number of amino acids transporters coding genes (Cole *et al.*, 1998), which actively import the host-derived amino acids, as well as by the increased amount in the tubercular granuloma of some amino acids, such as alanine, aspartate and glutamate (Shin *et al*., 2011; Somashekar *et al.*, 2011). Of considerable importance are asparagine and aspartate, which were found to couple nitrogen assimilation to acid resistance in *M. tuberculosis* during the infection (Fig. 4.2). This is possible due to the asparagine deamination into aspartate with concomitant release of ammonia, which acts as proton acceptor, yielding the ammonium ion, and raises the intracellular pH *in vitro*. Key players of such protective system are the aspartate and asparagine importers AnsP1 (UniProt code: P9WQM9) and its paralogue AnsP2 (UniProt code: P9WQM7), together with the asparaginase AnsA (UniProt code: A0A1K3L398)

(Gouzy *et al.*, 2014a, 2014b). On this subject, it is not surprising that proteins involved in the uptake, biosynthesis or hydrolysis of amino acids may represent also an attractive field for new drug targets (Harth and Horwitz, 2003; Mowbray *et al.*, 2014).

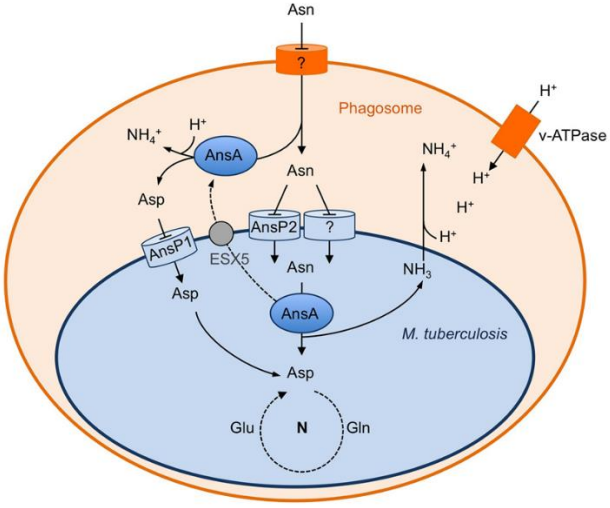

Figure 4.2. *Schematic representation of the role of asparagine catabolism in nitrogen incorporation, resistance to acid and intracellular survival.* Asparagine (Asn) enters the phagosome through an unknown transporter and it is captured by AnsP2 and other transporters that deliver Asn in the cytoplasm of *M. tuberculosis*. Here it is deaminated to Aspartate (Asp), freeing ammonia (NH_3) that relieves the acidity of the phagosome and contributes to nitrogen assimilation. AnsA can also deaminates Asn to Asp in the phagosome; Asp is then imported by AsnP1 for nitrogen assimilation. Image from Gouzy *et al.*, 2014a.

4.1.3. The GABA-shunt pathway as hypothetical route to restore the TCA cycle

With the publication of the complete genome of *M. tuberculosis* in 1998 by the Cole group (Cole *et al.*, 1998), it became possible for the first time to explore the genome for open reading frames that had homology to known enzymes. Even after 20 years, the vast majority of *M. tuberculosis* protein functions is solely assigned through the homology-based modeling and bioinformatic comparison *in silico* with orthologues proteins from other *Mycobacterium*

species, such as *M. bovis;* whereas only a small fraction of proteins has been expressed and purified. As a matter of fact, *M. tuberculosis* proteome needs to be complemented with experimental evidences in order to confirm the biochemical properties and thus avoiding possible mistakes in the annotation (Rhee *et al.*, 2011).

A significant example comes from the enzymes of the CCM. The enzymatic activity of *M. tuberculosis* α-ketoglutarate dehydrogenase (KDH, UniProt code: P9WIS5) complex was assayed in cell extract and was reported to require $NADP^+$ but not CoA as a cofactor (Murthy *et al*., 1962). In full disagreement with this unprecedented finding, *M. tuberculosis* cell extracts were recently found to lack KDH activity and that was corroborated by biochemical studies of the purified E2 and E3 recombinant subunits, DlaT and Lpd respectively, which were instead reassigned as components of the pyruvate dehydrogenase (PDH) (Tian *et al.*, 2005a). Therefore, the TCA cycle of *M. tuberculosis* appears to be interrupted by the lack of KDH, a feature shared by *M. bovis* and *M. smegmatis* (Tian *et al.*, 2005a).

Split TCA cycles with or without interconnecting pathways are quite common amongst bacteria since the two half-cycles can be joined in several ways. One in particular leads to the production of α-ketoglutarate and succinate through the oxidative and reductive branches respectively, and it may be the strategy adapted by *M. tuberculosis* to survive in hypoxia. In this regard, it has been proposed an alternative scenario in which α-ketoglutarate is converted into succinate, thus refilling the TCA cycle, by the concerted action of the α-ketoglutarate decarboxylase (KGD) and succinic semialdehyde dehydrogenase (SSADH) (Fig. 4.3A). In the proposed model, SucA (UniProt code: P9WIS5), previously annotated as E1 component of KDH, reacts with α-ketoglutarate in the presence of TPP and Mg^{2+}, whereas showing no dependence on CoA, NAD^+ or $NADP^+$; GabD1 and/or GabD2 are instead the source of SSADH activity and they use $NADP^+$ as cofactor, in strong agreement with other bacterial SSADH. Given that KGD is not present in humans, it may represent a new attractive antitubercular target (Tian *et al.*, 2005b). Interestingly, the biochemical function of the hypothetical KGD was recently revisited by the same group and it turned out to not be a

decarboxylase but a synthase. Through activity-based metabolomic profile (ABMP), KGD was reassigned as 2-hydroxy-3-oxoadipate-synthase (HOAS), which catalyzes the C-C bond formation between the aldehyde, obtained by the decarboxylation of α-ketoglutarate, and glyoxylate to yield 2-hydroxy-3-oxoadipate (HOA) (Fig. 4.3B). HOA then undergoes spontaneous decarboxylation, thus forming 5-hydroxy-levulinate (HLA). HOAS may be involved in glutamate/glutamine metabolism, or in detoxifying the surplus of glyoxylate, or in producing precursors (HOA and HLA) of important microbial metabolites (de Carvalho *et al.*, 2010).

Moreover, succinate can derive from glutamate via the GABA-shunt pathway (Fig. 4.3A), an alternative biochemical route which channels glutamate into the TCA cycle bypassing the KDH and the succinate tiokinase (*i.e.* succinyl-CoA synthetase (SCS, UniProt code: P9QGC5/7). The GABA-shunt pathway consists of three biochemical steps acting in concert: glutamate is firstly converted into GABA by Gad; GABA is then transaminated into succinate semialdehyde (with α-ketoglutarate as acceptor of the amino group, yielding glutamate) by the enzyme GABA-aminotransferase (GABA-AT) and finally oxidized into succinate via SSADH with concomitant production of $NAD(P)H + H^+$.

Although not extensively studied in bacteria, the GABA-shunt pathway has been found to be involved in several important processes, such as carbon and nitrogen assimilation, but there is growing evidence that it may play a more prominent role in terms of bacterial virulence or survival to stress (Feehily and Karatzas, 2013). A remarkable example is provided by *L. monocytogenes*, which, alike *M. tuberculosis*, lacks a set of genes required for the TCA cycle and, therefore, it takes advantage of the GABA-shunt pathway to compensate this. Additionally, being the GABA-shunt pathway coupled to Gad activity, it was demonstrated to play also a significant role in the acid resistance, thus linking *L. monocytogenes* metabolism with acid tolerance (Feehily *et al*., 2013). A similar scenario has never been addressed for *M. tuberculosis*, in which the only enzyme of the GABA-shunt pathway biochemically investigated is *Mt*GabD1 (UniProt code: P9WNX9) (de Carvalho *et al.*, 2011).

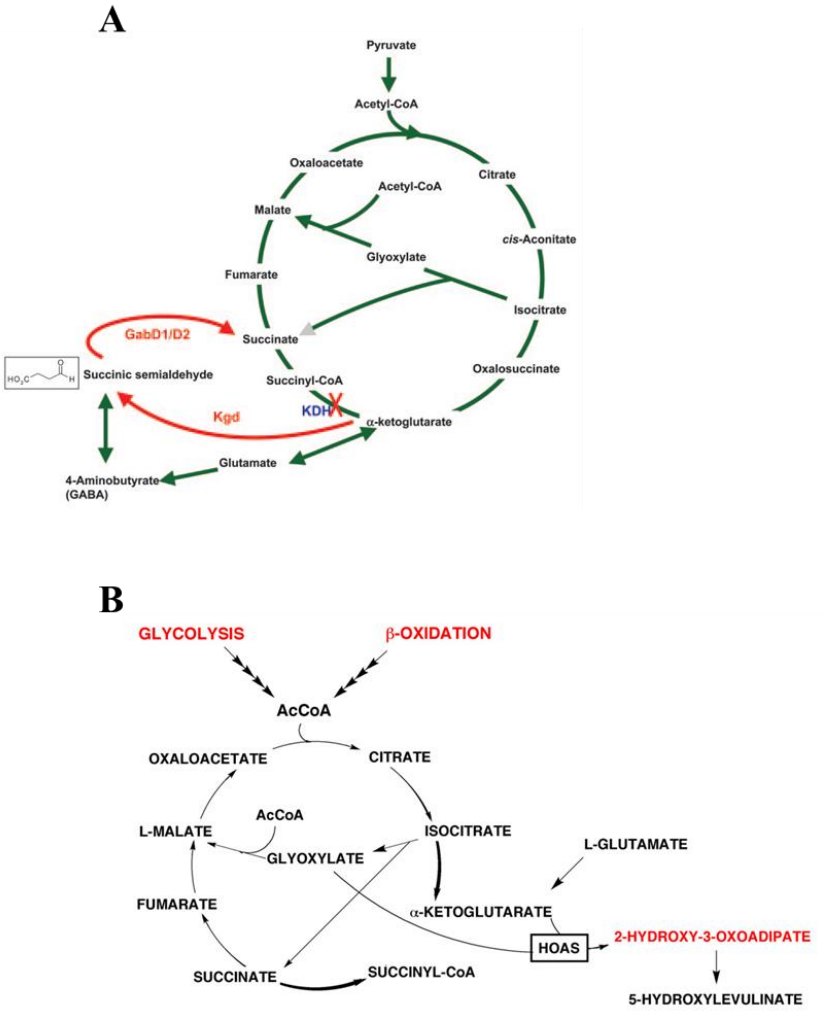

Figure 4.3. M. tuberculosis *interrupted TCA cycle with alternative routes to produce succinate* ***(A)*** *or 2-hydroxy-3-oxoadipate* ***(B)***, *from α-ketoglutarate*. Image **(A)** from Tian *et al*., 2005b; image **(B)** from de Carvalho *et al.*, 2010.

4.1.4. Aims

To date, with some exceptions represented by the production of ammonia by urease (Vandal *et al.*, 2009a) and by asparaginase (Gouzy *et al.*, 2014a, 2014b), the most common protective mechanisms for acid resistance/tolerance, in Gram-positive and Gram-negative bacterial pathogens, have not been found to play a role in *M. tuberculosis* acid resistance. Hence discovering how the microorganism adapts within the acidic environment of the phagosome may push the development of new drugs. In this respect, the serine protease MarP could be an interesting target since *M. tuberculosis* mutant strains for MarP are hypersensitive to acidic pH and are unable to maintain the intracellular pH at neutrality when challenged at pH 4.5 *in vitro* and *in vivo* (Botella *et al.*, 2017).

Attractive candidates might be the enzymes of the GABA-shunt pathway, an alternative route to the TCA cycle, whose involvement may compensate for the lack of KDH activity in *M. tuberculosis* through the conversion of glutamate to succinate in three enzymatic steps. Moreover, apart from refilling the TCA cycle, the GABA-shunt pathway may play a deeper role in *M. tuberculosis* physiology, such as resistance to acidity in analogy to *L. monocytogenes* (Feehily *et al*., 2013). In this contest, the mediator role between microbial metabolism and adaptation to hostile environment could be played by Gad. To date, the few available data on the *MtgadB* gene, derived from transposon mutagenesis, seem to suggest that it is not an essential gene for *M. tuberculosis* growth *in vitro* (Sassetti *et al*., 2001; Griffin *et al.*, 2011; DeJesus *et al.*, 2017); however more research is required.

To date, despite the growing emergence worldwide represented by TB and the publication of the complete genome of *M. tuberculosis* (Cole *et al.*, 1998), only limited high-throughput screens against individual enzymes thought or known to be essential for growth of the organism have been carried out; a significant example is represented by the enzymes of the GABA-shunt pathway, in which the only enzyme purified and so far characterized in depth is *Mt*GabD1 (de Carvalho *et al.*, 2011).

Given the evidence that Gad plays a key role in the acid resistance phenotype in other eubacteria, it seems plausible that *M. tuberculosis* may also use this mechanism for acid resistance within the macrophage or, alternatively, that the GABA produced serves signalling functions.

Taking all of this into account, with the current study we propose to investigate the biochemical properties of GadB from *M. tuberculosis*, herein *Mt*GadB, in order to provide a framework for assessing the differences with the *E. coli* homologue, very well characterised in our laboratory, and the relevance of glutamate decarboxylase to acid resistance in TB or to GABA production. To accomplish this, the *MtgadB* gene was cloned and expressed under several different inducing conditions, in order to define the best expression condition. Afterwards, *Mt*GadB was purified and preliminary characterized at the biochemical level.

4.2. Materials and methods

4.2.1. Materials

DNA ladder and SDS-PAGE protein markers were from Fermentas and Thermo Fisher Scientific. Kits for plasmid DNA purification was from GEL Extraction & PCR Clean Up kit (Fisher Molecular Biology, FMB). HisTrap HP (1 ml) and HiPrep^{TM} 16/60 Sephacryl^{TM} S-300 HR for affinity and gel filtration chromatography respectively, were from GE Healthcare. Ingredients for bacterial growth were from Difco. IPTG was from VWR International. Vitamin B_6, potassium dihydrogen phosphate, dipotassium hydrogen phosphate, *L*-glutamic acid and kanamycin were from Fluka. *D*-glucose was from CARLO ERBA Reagents Srl. Sodium glutamate, sodium acetate, sodium chloride, imidazole and pyridoxal 5'-phosphate (PLP) were purchased either from Merck or from Sigma-Aldrich. Gabase was from Sigma-Aldrich. Thrombin Restriction Grade was from Novagen®. All the other reagents were from Sigma-Aldrich.

4.2.2. Culture media

Bacteria were cultivated in the following media, which were sterilized in autoclave for 20 minutes at 121°C before use unless otherwise specified:

- **LB** 10 g/l BactoTryptone;5 g/l Yeast Extract; 5 g/l NaCl. The medium was brought to pH 7.4 by adding 5N NaOH.
- **SB** 12 g/l BactoTryptone; 24 g/l Yeast Extract; 5g glycerol. 50 ml of 1 M potassium phosphate, pH 7.5 was added immediately before use.
- **2x XL** BactoTryptone 20 g/l; Yeast Extract 10 g/l; NaCl 1 g/l. The medium is brought to pH 7.5 with 5 N NaOH.
- **SOB** 20 g/l BactoTryptone; 5g/l Yeast Extract; 0.5 g/l NaCL. The medium was brought to pH 7.5 by adding 5N NaOH.
- **SOC** Modified SOB with added 0.2% glucose and 10 mM $MgCl_2$.
- **LB-Agar** LB with added 15 g/l of BactoAgar.

When required, antibiotics were added at the following concentrations: Ampicillin (100 µg/ml); Kanamycin (25 µg/ml).

4.2.3. Plasmids and strains

Plasmids and bacterial strains used in this study are listed in Table 4.1.

Table 4.1. *Plasmids and* E. coli *strains used in this study*

Plasmid	Description	Antibiotic Resistance[1]	Source or Reference[2]
pET23(+)*Mtgad*B	pET23(+) transcription vector (3592 bp) with *Mtgad*B gene cloned into the restriction sites	Amp	JSB
pET28a(+)*Mtgad*B	pET28a(+) transcription vector (5369 bp) with *Mtgad*B gene cloned into the restriction sites	Kan	JSB
***E. coli* strain**			
Str. B BL21(λDE3)	F^- *ompT*, *gal dcm lon hsd*S_B($r_B^- m_B^-$) λ(DE3 [*lacI lacUV5-T7p07 ind1 sam7 nin5*])[*malB*$^+$]$_{K\text{-}12}$(λ^S)	None	(Studier *et al.*, 1990)

[1]Amp, Ampicillin; Kan, Kanamycin. [2]JSB, from John S Blanchard, Albert Einstein College of Medicine.

pET-23(+) and -28a(+) (Fig. 4.4A and B, respectively). The pET System is a powerful system for the cloning and expression of recombinant proteins in *E. coli*. Target genes are cloned in pET plasmids under control of strong bacteriophage T7 transcription and (optionally) translation signals; expression is induced by providing a source of T7 RNA polymerase in the host cell that selectively transcribes the target genes. Target genes are initially cloned using hosts that do not contain the T7 RNA polymerase gene, thus eliminating plasmid instability due to the production of proteins potentially toxic to the host cell. Once established in a non-expression host (*e.g. E. coli* DH5α), plasmids are then transferred into the expression hosts containing a chromosomal copy of the T7 RNA polymerase gene under lacUV5 control (*e.g. E. coli* BL21(λDE3)). Gene expression is thus induced by the addition of isopropyl-β-D-thiogalactoside (IPTG), an analogue of lactose.

The pET28a vector possess a sequence coding for six histidine residues (His_6-tag) which precedes the translation start codon, thus generating a N-terminal tag. The His_6-tag allows the protein to be purified by affinity chromatography on a nickel column. A thrombin cleavage site is between the His_6-tag and the start codon sequences, allowing, if necessary, the removal of the His_6-tag.

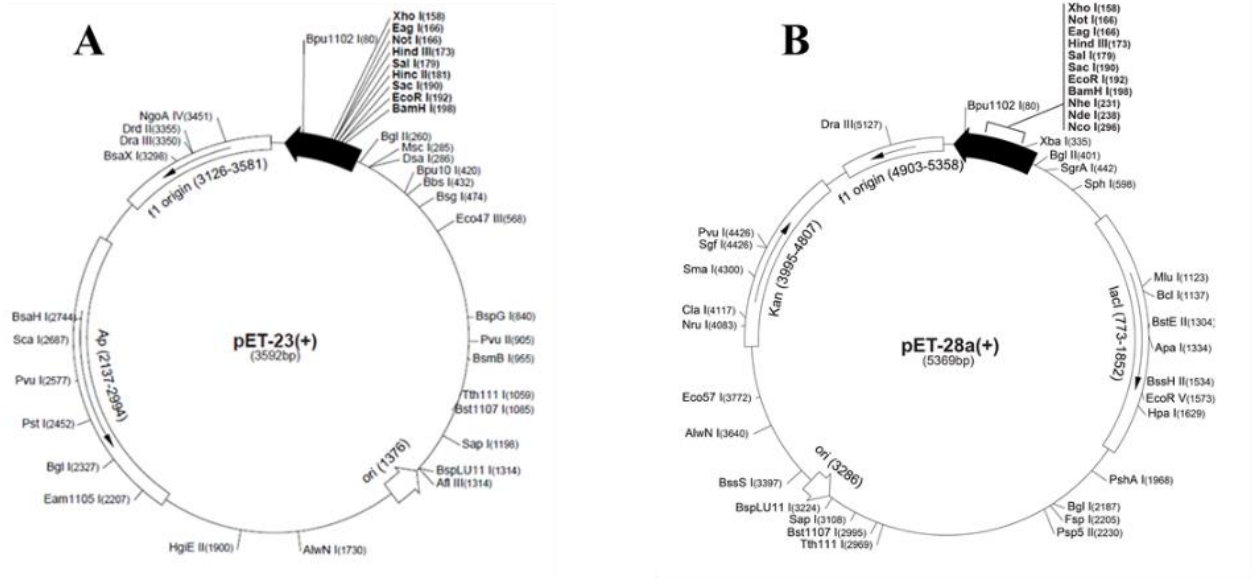

Figure 4.4. *Maps of plasmids used in this work.* **(A)** pET-23(+); **(B)** pET-28a(+).

4.2.4. Preparation, transformation, expression and purification of *Mt*GadB

Preparation of competent cells. *E. coli* BL21(λDE) competent cells (Table 4.1) were prepared by inoculating few colonies from a LB plate in 50 ml 2x XL. Cells were grown at 37°C up to $O.D._{600}$ = 0.5 and then kept on ice for 90 minutes. Following centrifugation at 4000 rpm for 15 minutes at 4°C, the cell pellet was resuspended in 20 ml of buffer containing

100 mM $CaCl_2$, 70 mM $MnCl_2$, 40 mM sodium acetate, pH 5.5 and kept on ice for 45 minutes. After a further centrifugation as described above, the cell pellet was resuspended in 3 ml of the same buffer containing 80% glycerol, split into 220 µl-aliquots and stored at -80°C for no more than 6 months.

Transformation. *E. coli* BL21(λDE3) competent cells (100 µl) were transformed with 20-50 ng of supercoiled plasmid DNA. The mixture was incubated on ice for 30 minutes, then at 37°C (thermal shock) for 4 minutes and finally back on ice for 2 minutes. SOC medium (1.05 ml) was added and the incubation was prolonged for additional 15 minutes at room temperature. The incubation was continued for 100 minutes at 37°C. To select transformed colonies, an aliquot (50-100 µl) of the transformation was plated on LB agar containing the required antibiotic and incubated at 37°C overnight.

Small scale cultures. The conditions to test the best protein expression levels included assaying the following: different IPTG concentrations, temperature pre and post-induction with IPTG and time (hours) of growth after induction. Briefly, transformed colonies from LB-Agar plate were inoculated in 10 ml of LB pH 7.4 containing 0.5% *D*-glucose and 0.1 g/L vitamin B_6 and supplemented with ampicillin (100 µg/ml) or kanamycin (25 µg/ml) (depending on the pET vector) and grown at 37°C by vigorous shaking up to $O.D._{600}$ = 0.5-0.6; then IPTG was added to the medium for the induction of *MtgadB*. Before induction, the temperature was brought to the desired value and the cultures were adapted to the new temperature for 30 minutes. At time intervals, aliquots from the induced bacterial cultures were withdrawn. After induction, the bacterial cultures were centrifuged at 3500 rpm for 30 minutes at 15°C and the cell pellet was resuspended in 1 ml of 1 mM PLP/1 mM DTT solution and transferred into a 2 ml-eppendorf tube. Cells were disrupted by sonication on ice using a small tip-probe (6 mm) at the following conditions:

- 50% Amplitude;
- 8 Pulses, 15 seconds ON/60 seconds OFF.

After a further centrifugation step, carried out at 10000 rpm for 30 minutes at 8°C, the supernatant was transferred into a 1 ml-eppendorf tube, whereas the cell pellet was resuspended in 1 ml of Milli-Q water. To judge the amount of soluble expressed protein, aliquots from the cell cultures and cell lysis were boiled for 5 minutes and run on SDS-PAGE. The successful expression of active *Mt*GadB was assessed through a colorimetric activity assay (see Rice test).

Large scale cultures. The purification of *Mt*GadB was carried out from 3 L of bacterial cultures, carrying the His_6-tag construct, by immobilized metal ion affinity chromatography (IMAC). Briefly, 3 cultures of 1 L each were grown and the corresponding bacterial pellet stored at -80°C. For each culture, from an overnight culture (50 ml) of *E. coli* BL21(λDE3) carrying pET28 plasmid, 10 ml of cells were inoculated into 1 L (1:100) of LB pH 7.4 with 0.5% *D*-glucose and 0.1 g/L of vitamin B_6 and supplemented with kanamycin (25 µg/ml). Cell growth and IPTG-induction were optimized to the following conditions:

- 0.1 mM IPTG for induction;
- temperature for expression: 16°C;
- induction time: 14 hours.

The next day, the cells were collected by centrifugation at 3500 rpm for 30 minutes at 4°C and stored at -80°C. The bacterial pellet from a total of 3 L cultures was slowly thawed on ice and resuspended in 20 ml of *binding buffer*: 20 mM potassium phosphate, pH 7.4, containing 80 mM imidazole, 300 mM NaCl, 1 mM PLP and 1 mM DTT. Two tablets of protease inhibitors (cOmplete EDTA-free, Roche) were dissolved in the *binding buffer*. Cells were then disrupted by incubation with lysozyme (0.1 g) for 30 minutes on ice, followed by sonication as already described for *Ec*GadB (De Biase *et al.*, 1996) and cell debris were removed by centrifugation at 10000 rpm for 30 minutes at 4°C. The supernatant was loaded onto a HisTrap HP (1 ml) column and after washing with 15 column volumes (CV) with the same buffer, *Mt*GadB was eluted in isocratic mode with an elution buffer of the same

composition as the binding buffer, but with 500 mM imidazole and without PLP. The flow rate was 0.5 ml min^{-1} for both the loading and the elution steps, which were carried out at RT. Fractions (500 µl) were collected in 1 ml-eppendorf tubes and the purity of *Mt*GadB in each fraction was judged by 12% SDS-PAGE. Fractions with the highest purity were pooled and dialyzed overnight at 4°C against 3 L of 50 mM potassium phosphate, pH 7.4, containing 100 mM NaCl and 1 mM DTT. After dialysis, any precipitate was removed by centrifugation (10000 rpm for 30 minutes) and *Mt*GadB was concentrated to 2 mg/ml using Vivaspin® 500 (Sartorius) with a 30 kDa cut-off before being loaded (1 ml) onto a HiPrep™ 16/60 Sephacryl™ S-300 HR column equilibrated with a buffer consisting of 50 mM potassium phosphate, pH 6.5, containing 150 mM NaCl and 1 mM DTT. Equilibration and chromatography were carried out at 4°C and at a flow rate of 0.5 ml min^{-1}. Fractions (3 ml) were collected and analyzed by 12% SDS-PAGE. Fractions with the highest purity were pooled and concentrated to a final volume of 1-2 ml.

The protein was stored at 4°C for several days in the same buffer.

The final yield and purity were judged as for *Ec*GadB (De Biase *et al.*, 1996), whereas the protein concentration was calculated by using $\varepsilon_{280\ nm}$ = 72000, as estimated by ProtParam (Gasteiger *et al.*, 2005).

4.2.5. Rapid *Mt*GadB-activity detection: Rice test

Glutamate decarboxylase activity was qualitatively detected as described elsewhere (Rice *et al.*, 1993). The solution (100 ml) for the assay consisted of: 2 mM glutamic acid, 0.002% (w/v) BCG (BromoCresol Green), brought to pH 4.4 by a small addition of 1 N KOH. The solution was protected from light with alufoil and stored at 4°C until use.

*Mt*GadB activity was assayed by using 5-10 µl of the supernatant from the small-scale cultures (section 4.2.4) in 500 µl (final volume) of the above solution. The negative control was with 5-10 µl of supernatant from uninduced cells. Samples were incubated at 37°C for 1 h. The test was judged positive if, following the neutralization of the medium due to the

proton-consuming decarboxylation of glutamate, the color of the supernatant changed from green to blue.

4.2.6. *Mt*GadB pH-dependent absorption and fluorescence spectra

Absorption spectra were recorded at RT on a Hewlett-Packard Agilent model 8453 diode array spectrophotometer. The buffer was 50 mM potassium phosphate with 150 mM NaCl, brought to the following pH values: 3.88, 4.01, 4.60, 4.80, 5.00, 5.20, 5.40, 5.60, 5.80, 5.99 and 6.50. The protein concentration was 110 µM (referred to monomer). When necessary, spectra were normalized to the same absorbance at 280 nm (starting values were ± 10% with respect to that used for normalization) using GraphPad Prism 4.0 (GraphPad Software, San Diego, CA).

Fluorescence spectra were acquired at RT on a FluoroMax-3 spectrofluorometer (Horiba Jobin–Yvon) using 3 nm bandwidth on both slits and at a scan speed of 100 nm/min. The buffer was as the one used for the UV-Visible spectroscopy but restricted to pH 4.0 and 7.0. The protein concentration was 2 µM. The spectra were corrected by subtracting the corresponding buffer emission spectrum (blank).

4.2.7. Removal of the His_6-tag and *Mt*GadB activity assay

The cleavage of the His_6-tag was carried out by thrombin and was firstly investigated by setting up a time course digestion experiment performed in the conditions reported below:

1.6 µl (10 µg) *Mt*GadB
5.0 µl Thrombin Buffer 10X (200 mM Tris-HCl; 1.5 M NaCl; 25 mM $CaCl_2$, pH 8.4)
1.0 µl Thrombin (0.0132 U/µl)
42.4 µl Milli-Q water

The final volume was 50 µl. The reaction was allowed to proceed at 24°C for 16 hours.

In parallel, *Mt*GadB was also cleaved in another eppendorf tube under the following conditions:

2.4 µl (15 µg) *Mt*GadB
2.5 µl Thrombin Buffer 10X (200 mM Tris-HCl; 1.5 M NaCl; 25 mM $CaCl_2$, pH 8.4)
1.5 µl Thrombin (0.0132 U/µl)
18.6 µl Milli-Q water

The final volume was 25 µl. Notably, in this case the reaction was incubated at 24°C for 6 hours and then moved to 4°C for additional 10 hours (16 hours in total) to keep the protein over a long period of time in a condition more compatible for its stability.

Aliquots (10 µl) from the first reaction, corresponding to ~2 µg of protein, were withdrawn at time intervals, halted in 3 µl of SDS-sample buffer (4X) and run on 10% SDS-PAGE.

*Mt*GadB (2-4 µg) activity with or without the His_6-tag was assayed in 0.2 ml at 37°C in 50 mM potassium phosphate buffer, pH 4.6, containing 150 mM NaCl, 40 µM PLP, with 50 mM sodium glutamate. *Ec*GadB (2-4 µg) was assayed as a control under the same conditions. Aliquots (25 µl) were withdrawn from the reaction mixtures, halted in 0.1 M EPPS pH 8.6 (100 µl) and assayed with Gabase as previously described (Materials and Methods in Chapter II).

4.3. Results and Discussion

4.3.1. Sequence alignment of *Mt*GadB with *Ec*GadB

The *Mt*GadB sequence (Rv3432c) was retrieved from the NCBI database and aligned with *Ec*GadB by using Clustal Omega (version 1.2.1). The result of the alignment is shown in Fig. 4.5. *Mt*GadB and *Ec*GadB, 460 and 466 amino acids in length, respectively, share 48% of sequence identity and the full conservation of the GAD-signature residues (marked in red in Fig. 4.5) (De Biase and Pennacchietti, 2012 and General Introduction of this thesis). respectively.

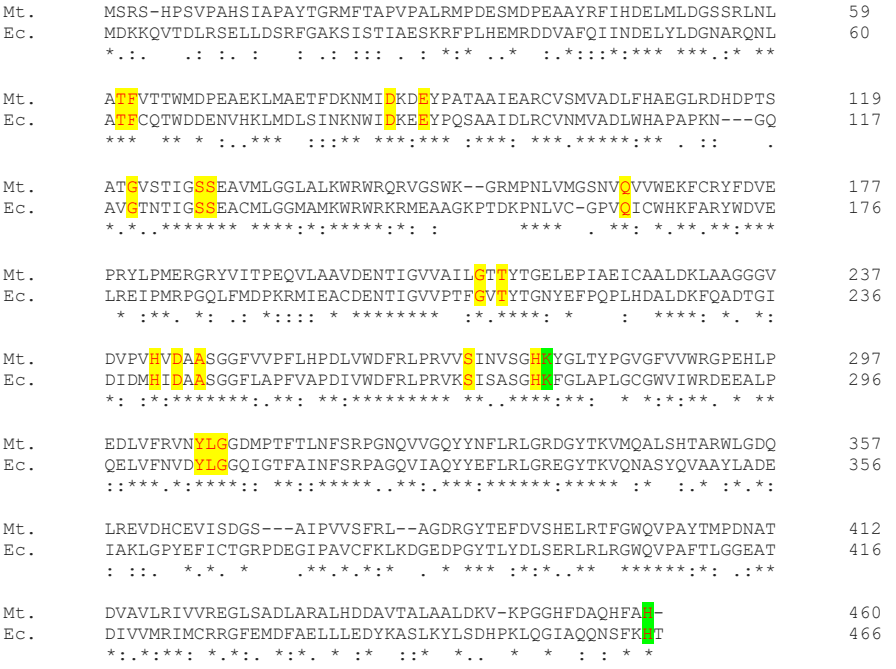

Figure 4.5. *Sequence alignment of* Mt*GadB* **(Mt)** *and* Ec*GadB* **(Ec)**. The residues of the GAD-signature are marked in red and in a yellow background, except *Mt*GadB Lys277 and His460 which are in green background.

These residues include *M*tGadB Lys277 and His460 (highlighted in green), likely involved in the Schiff-base formation with the PLP cofactor and in the closure of the active site at neutral pH.

Using ProtParam, in the ExPASy server (Gasteiger *et al.*, 2005), the estimated molecular weight of *Mt*GadB is 51.000 Da and the theoretical isoelectric point (pI) is 5.37.

Notably, while *E. coli gadB* is well-known to be part of the operon *gadBC*, where the gene coding for the decarboxylase is co-transcribed with the Glu/GABA antiporter encoded by the gene *gadC* (De Biase and Pennacchietti, 2012), the *MtgadB* gene is not in operon arrangement with neighbouring genes and the *gadC* homologue seems not to be present in *M. tuberculosis* genome (based on the current assignments).

4.3.2. *MtgadB* cloning and small-scale expression experiments

The *MtgadB* gene (Rv3432c), previously inserted into two different pET expression plasmids provided by Professor J.S. Blanchard's team (Albert Einstein College of Medicine, New York), was transformed into *E. coli* BL21(λDE) strain (section 4.2.4), a common laboratory strain suitable for heterologous expression of recombinant proteins from pET vectors, which guarantees high efficiency of expression. The pET plasmids were pET23 and pET28; the latter providing an N-terminal hexahistidine-tag (His_6-tag), which enables the purification of the recombinant protein by IMAC. On the contrary, the purification of the protein from the pET23 system can be performed through the standard purification protocol employing an ion exchange chromatography, as successfully carried out for the purification of *E. coli* and *B. microti* GadB (UniProt code: C7LHI0_BRUMC) (De Biase *et al.*, 1996; Grassini *et al.*, 2015).

The expression efficiency and the soluble protein yield were established by testing different *i*) growth media, *ii*) concentration of IPTG for induction, *iii*) temperature of growth during induction and *iv*) the induction time (Table 4.2). The conditions tested were also in line

with some published articles where *M. tuberculosis* enzymes were successfully expressed for biochemical studies (Sikora *et al*., 2010; Xu *et al*., 2011; Hazra *et al.*, 2015).

Table 4.2. *Small-scale experiments to test* MtgadB *expression from pET23 and pET28 plasmids.* The highest yield of soluble protein was obtained in the conditions highlighted in red bold.

Medium	IPTG (mM)	Temperature (°C)	Hours of Induction
SB pH 7.0	0.5	25	3
LB pH 7.4	0.5	25	3
LB pH 7.4	0.5	25	>12 (ON)
LB pH 7.4	0.1	25	up to 5, 6 or 7
LB pH 7.4	0.1	16	>12 (ON)
LB pH 7.4	**0.1**	**16**	**14**

As shown in Table 4.2, to achieve this, small-scale (10 ml) cultures of *E. coli* BL21(λDE) harbouring either pET23_*MtgadB* or pET28_*MtgadB* were set up.

At the end of the induction period, the cultures were harvested and sonicated and the amount of soluble and insoluble proteins was judged by 12% SDS-PAGE (Fig. 4.6), which allowed also to detect the expression of the recombinant *Mt*GadB.

Gad activity was assayed in parallel through the Rice test (section 4.2.5), a colorimetric assay in which the alkalinisation resulting from the consumption of protons as part of glutamate decarboxylase activity is quickly detected from the green to blue colour shift of the BGC, a pH indicator. Fig. 4.7 shows that, though the expression from pET23_*MtgadB* yields less soluble protein (Fig. 4.6), *Mt*GadB is more active than the His_6-tag enzyme expressed from pET28_*MtgadB*, even though the $O.D._{600}$ at 14° h of the culture carrying pET28_*MtgadB* was 2.5 times higher than that of pET23_*MtgadB*. In fact, the color shift is

incomplete after 1 hour of incubation, while that from the native enzyme (pET23_*MtgadB*) has already reached completion. This result may find an explanation in the involvement of the N-terminal region in stabilizing the hexameric structure of *Ec*GadB (Capitani *et al*., 2003a and General Introduction of this thesis). Therefore, it is reasonable to hypothesise that, given the central role of the N-terminal region in *Ec*GadB, the His_6-tag may negatively affect the contacts of the N-terminal portions in the oligomeric structure of *Mt*GadB, thereby resulting in a less active enzyme than the native counterpart.

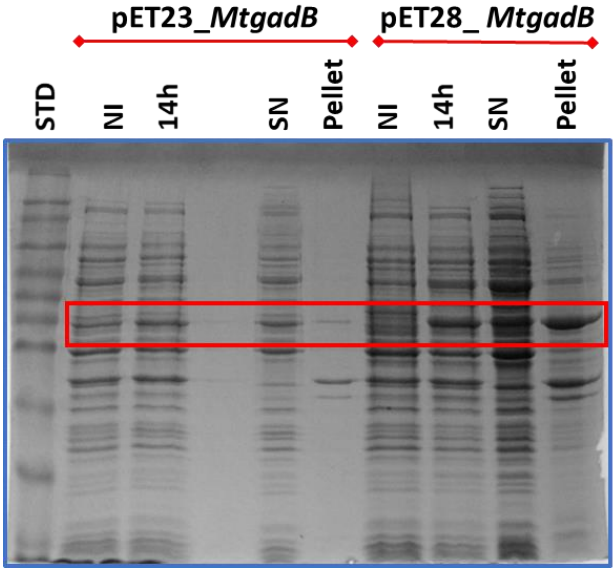

Figure 4.6. *Small-scale experiments* for Mt*GadB expression*. 12% SDS-PAGE stained with Coomassie Blue. Abbreviations used: **STD**, molecular weight standard; **NI**, total cell extract from the IPTG-induced cell cultures; **14h**, total cell extract after 14 hours of induction with IPTG (0.1 mM); **SN**, supernatant of cell lysate clarified by low-speed centrifugation; **Pellet**, pellet from cell lysate clarified by low-speed centrifugation and resuspended in 1 ml of Milli-Q water. In the red box, the protein band associated to *Mt*GadB.

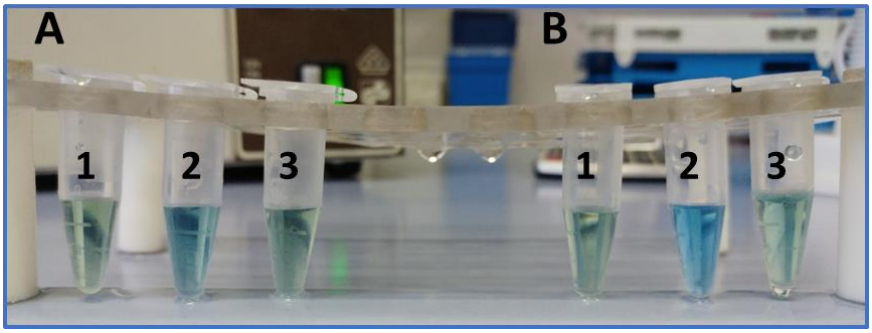

Figure 4.7. *Rice test of small-scale expression experiments*. **1**, negative control; **2** supernatants from *E coli* carrying pET23_*MtgadB*; **3**, supernatants from *E coli* carrying pET28_*MtgadB*, after clarification by low-speed centrifugation. The reaction was carried out for 1 h at 37°C. **(A)** and **(B)** are referred to the same samples but using 5 or 10 µl from the supernatants, respectively.

4.3.3. Expression and purification of His_6-tag *Mt*GadB

Although the expression of *Mt*GadB using the pET23 plasmid resulted in a more active enzyme, on the other end it gave a lower amount of soluble protein in comparison to the other plasmid. Therefore, if purified through the classical purification protocol which employs an ion-exchange chromatography, as for *Ec*GadB (De Biase *et al.*, 1996), it would result in a very low amount, unlikely to be enough for a full biochemical characterization. Based on the above, we decided to purify *Mt*GadB carrying the His_6-tag via IMAC and set up a large-scale cell culture. The idea behind is to give priority to maximal yield of pure protein, though keeping in mind that the removal of the His_6-tag by thrombin cleavage is necessary to yield a fully active enzyme. The last step of the purification, described in section 4.2.4, was a gel-filtration chromatography which, apart from improving the purity of the protein, provided information on the quaternary structure of *Mt*GadB (Fig. 4.8). Interestingly, compared to *Ec*GadB elution (Fig. 4.8, inset), *Mt*GadB elution occurred over a broader peak, suggesting that it exists only in part as hexamer, the typical oligomeric assembly of *Ec*GadB (Capitani *et*

al., 2003a and General Introduction of this thesis). Thus, given that the elution profile of *Mt*GadB was not fully coinciding to that of *Ec*GadB (Fig. 4.8, inset), the occurrence of tetramers or dimers cannot be excluded. As discussed in Chapter II of this thesis, several environmental conditions favor the dissociation of *Ec*GadB from hexamer into dimers, with a tetrameric species probably occurring in this process (Giovannercole *et al.*, 2017a). It is reasonable therefore to suggest that the N-terminal His_6-tag interferes with the oligomerization of *Mt*GadB, thus causing the dissociation of the hexamer into tetramers and, likely, into dimers. This result is in line with the fact that the activity of *Mt*GadB carrying the His_6-tag is lower than that of the native enzyme expressed with plasmid pET23 (Fig. 4.7). However, it cannot be excluded that part of the dissociation (tetramers and dimers) may be assigned also to the pH at which the chromatography was performed, pH 6.5, respect to that used for *Ec*GadB (pH 4.6). We are planning to perform the gel-filtration chromatography of *Mt*GadB at pH 4.6, which will provide a stronger evidence on the real contribution of pH and His_6-tag to the oligomerization of *Mt*GadB.

The UV-Visible absorption spectrum of *Mt*GadB was recorded at pH 4.6 (Fig. 4.9, left) and the purity of the protein was judged by 12% SDS-PAGE to be ≥ 95% (Fig. 4.9, right). Indeed, some the protein bands still detected in the top part of the SDS-PAGE in Fig. 4.9 were also assigned to aggregates of *Mt*GadB, not fully removed because the sample was not boiled before the SDS-PAGE, due to the presence Asp-Pro bonds in the sequence which brake during boiling.

The final yield was ~1.3 mg/L of induced culture. The pure protein was kept a 4°C for several days in a buffer consisting of 50 mM potassium phosphate, 150 mM NaCl, pH 6.5. Interestingly, in clear contrast to *Ec*GadB, it was not possible to store the protein in 0.1 M acetate buffer pH 4.6 since this buffer caused the precipitation of *Mt*GadB.

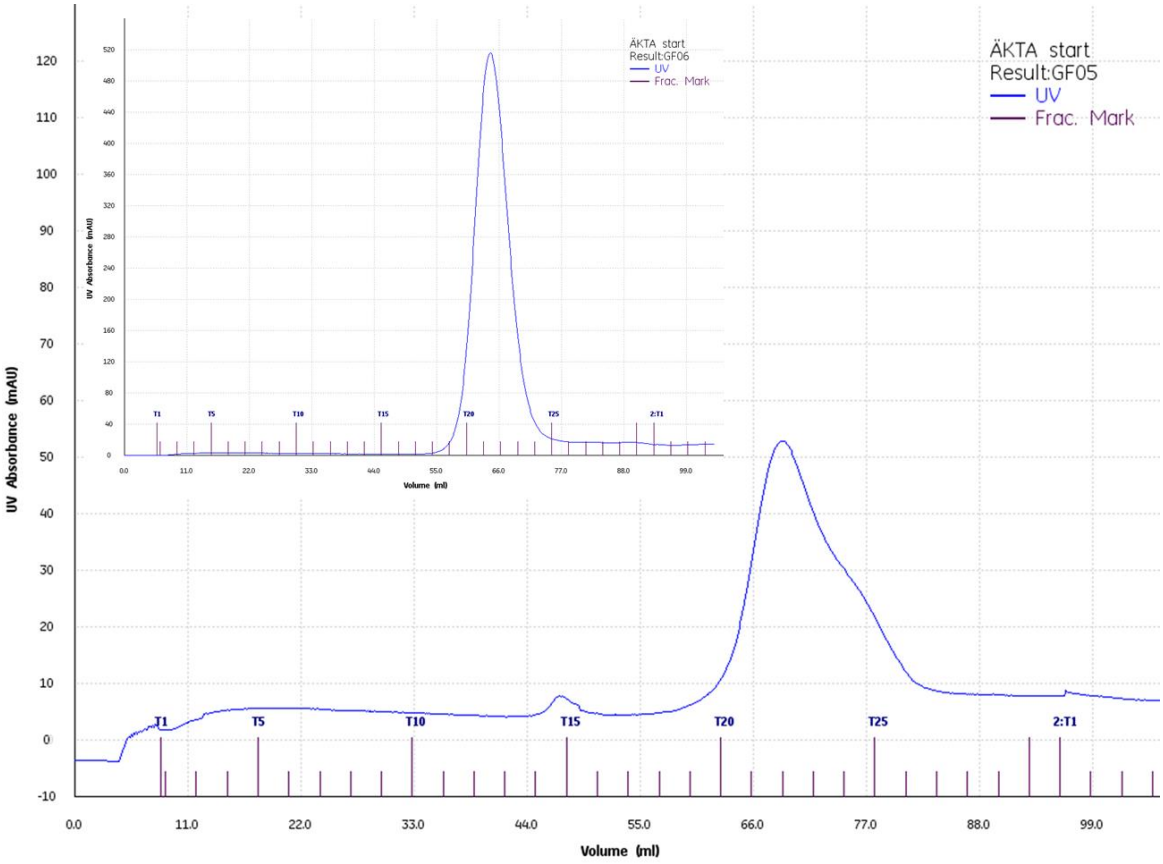

Figure 4.8. *Gel filtration chromatography of* Mt*GadB carrying the N-ter His$_6$-tag.* The chromatography was carried out on a HiPrep^{TM} 16/60 Sephacryl^{TM} S-300 HR column equilibrated with a buffer consisting of 50 mM potassium phosphate, 150 mM NaCl, 1 mM DTT, pH 6.5. The temperature was set at 4°C and the flow rate was 0.5 ml min^{-1}. Inset panel: elution of *Ec*GadB in the same conditions but in acetate buffer at pH 4.6.

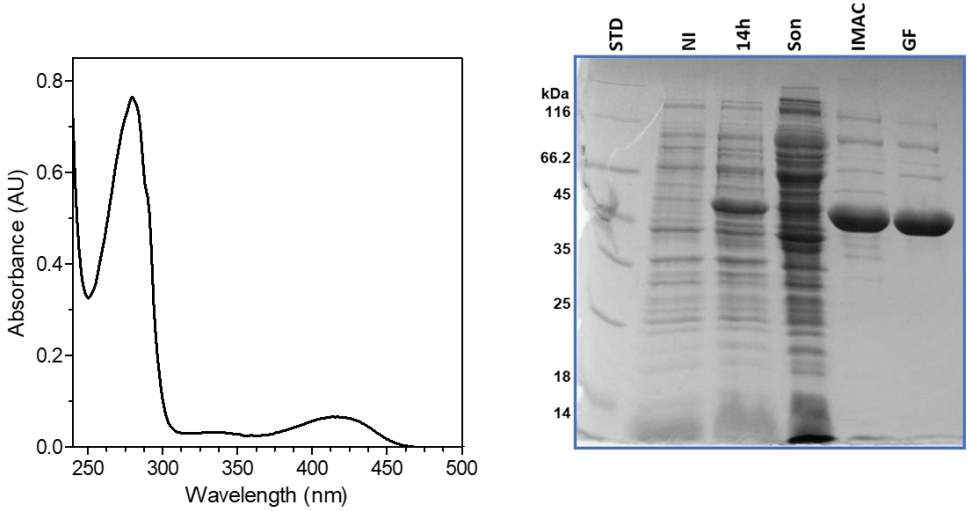

Figure 4.9. *Spectrum and purity of* Mt*GadB*. **(Left)** UV-Visible spectrum of *Mt*GadB recorded in 50 mM potassium phosphate, 150 mM NaCl, pH 4.6. **(Right)** 12% SDS-PAGE of *Mt*GadB purification stained with Coomasie Blue. Abbreviations used: **STD**, molecular weight standard; **NI**, total cell extract from the IPTG-induced cell cultures; **14h**, total cell extract after 14 hours of induction with IPTG (0.1 mM); **Son**, supernatant of cell lysate clarified by low-speed centrifugation; **IMAC**, pooled fractions after affinity chromatography; **GF**, pooled fractions of purified *Mt*GadB after gel filtration chromatography.

4.3.4. pH-dependent absorbance and fluorescence properties of *Mt*GadB

When analysed in a pH range between 3.8 and 6.5 (Fig. 4.10A), *Mt*GadB undergoes a pH-dependent spectroscopic change of the cofactor (PLP), alike *Ec*GadB and *Bm*GadB (Pennacchietti *et al.*, 2009; Grassini *et al.*, 2015). This corresponds to the interconversion from the active into the inactive form of the enzyme. The 420 ↔ 340 nm interconversion occurs in the pH range 5.0-5.6, with a clear isosbestic point at 361 nm (Fig. 4.10A). The absorbance at 420 nm corresponds to the *ketoenamine* (*i.e.* the active form of the PLP), whereas the *substituted aldamine* (*i.e.* the inactive form of the PLP) absorbs at 340 nm (O'Leary and Brummund, 1974; Gut *et al.*, 2006; Pennacchietti *et al.*, 2009; Grassini *et al.*,

2015). Notably, unlike *Ec*GadB, the 340 nm-absorbing species was still detectable at pH 3.9, an indication that the *substituted aldamine* or the *enolimine* (Fig. 1.6 in the General Introduction) are still present at this pH.

Based on the UV-Visible spectra, the absorbance values at 420 nm as a function of pH were plotted, and the resulting curve was compared to that obtained with *Ec*GadB under similar conditions (Pennacchietti *et al.*, 2009) (Fig. 4.10B). As expected, *Mt*GadB exhibits a sigmoidal pH-dependent spectroscopic transition, which can be fitted with Hill equation (see Chapter III). The estimated Hill-coefficient was 2.40, much less than that found for *Ec*GadB (7-10). This value corresponds to the minimum number (*n*) of protons involved in the pH-dependent spectroscopic transition (420 to 340 nm). In the same Hill equation, the p*K* is the pH value of the transition midpoint, which was 5.49 and 5.7 for *Mt*GadB and *Ec*GadB, respectively (both calculated in the presence of NaCl).

A lower Hill-coefficient for *Mt*GadB suggests that the 420 $\leftrightarrow$ 340 nm spectroscopic transition is less cooperative compared to that occurring in the *E. coli* counterpart, whereas the pH value at the midpoint of this transition is not much different. In addition, in *Mt*GadB the *ketoenamine* species becomes undetectable only at pH $\geq$ 6.5, which suggests a persistence of this cofactor species at a more neutral pH respect to what is observed in *Ec*GadB (Fig. 4.10B).

When tryptophan residues are excited at 295 nm, the fluorescence emission spectra provide also useful insights into the chemical state of the cofactor (due to FRET), embedded in the active site, at different pHs. The emission at 490 nm is typical of the *ketoenamine* species, whereas it disappears in the presence of the *substituted aldamine* (Pennacchietti *et al.*, 2009; Grassini *et al.*, 2015). To this purpose, *Mt*GadB emission spectra were obtained at acidic and neutral pH by exciting at a fixed wavelength (295 nm) and recording the fluorescence emission signal from 305 to 550 nm (Fig. 4.11). When analysed at pH 4.0 the protein exhibited two peaks centred at 340 and 490 nm, with the latter disappearing at pH 7.0, in clear agreement with *Ec*GadB and *Bm*GadB (Pennacchietti *et al.*, 2009; Grassini *et al*., 2015). This

result, along with the UV-Visible spectra, confirms that the active form of *Mt*GadB has the *ketoenamine* at acidic pH, a prerequisite to be catalytically competent, whereas it the *aldamine species* is prevailing at neutral pH.

To conclude, the UV-Visible and fluorescence spectra analysis indicates that *Mt*GadB likely undergoes the same pH-dependent conformational changes reported for *Ec*GadB and that this is a common feature shared also with *Bm*GadB (Grassini *et al.*, 2015).

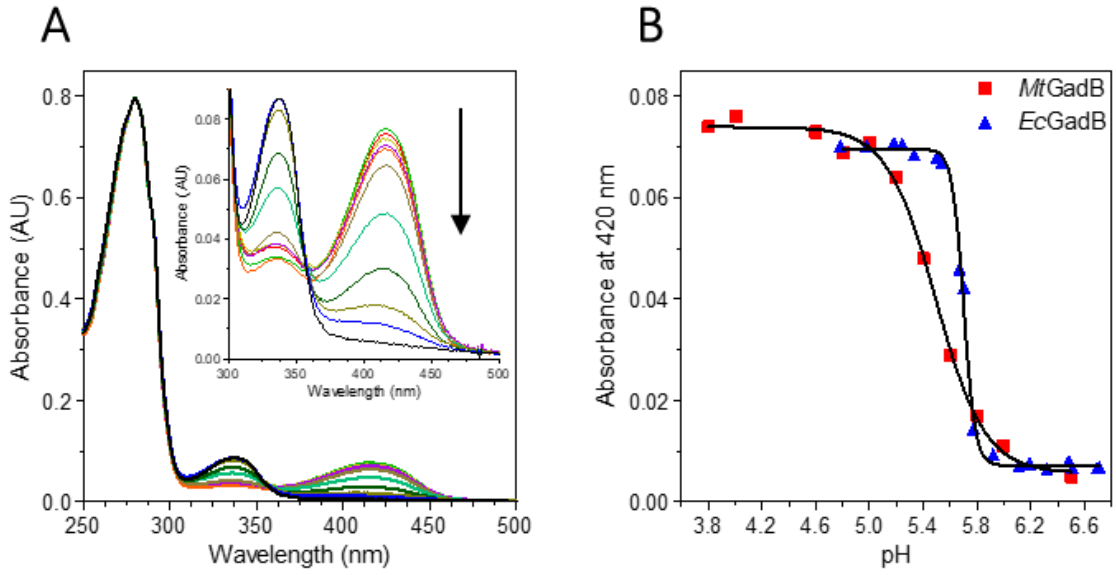

Figure 4.10. *pH-dependent absorption spectra and 420 nm-titration curve of* Mt*GadB*. **(A)** Absorption spectra of *Mt*GadB were recorded in 50 mM potassium phosphate buffer with 150 mM NaCl at pH values of 3.88, 4.01, 4.60, 4.80, 5.0, 5.2, 5.4, 5.6, 5.8, 6.0 and 6.5. Spectra were normalized to the 280-nm value. The arrow indicates the change in absorbance at 420 nm upon increasing pH. **(B)** pH-dependent change in absorbance at 420 nm of *Mt*GadB (red squares) and *Ec*GadB (blue triangles). The solid lines through the experimental points show the theoretical curves obtained using the Hill equation.

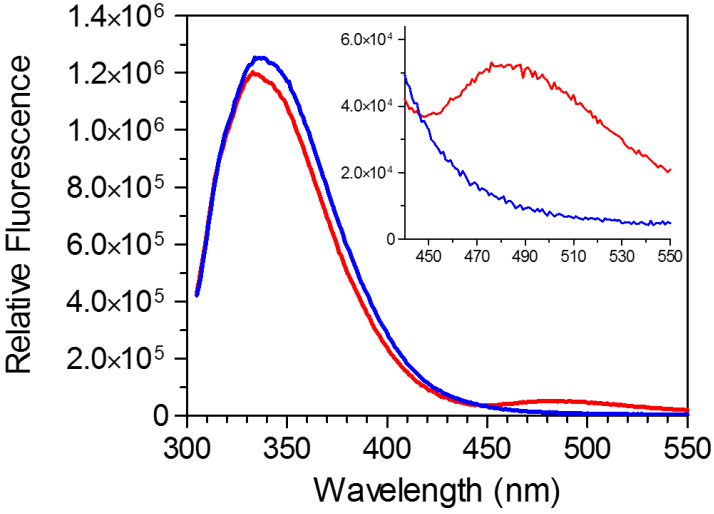

Figure 4.11. *Tryptophan fluorescence emission spectra of* Mt*GadB*. Fluorescence spectra were obtained at pH 4.0 (red line) and 7.0 (blue line) by exciting at 295 nm and recording the fluorescence emission from 305 to 550 nm. Inset panel: expansion of the emission region where the *ketoenamine* is detected. The protein concentration was 2 µM and the buffer was 50 mM potassium phosphate containing 150 mM NaCl.

4.3.5. Time-course of His_6-tag cleavage and effect on *Mt*GadB activity

The results obtained from Rice test and gel filtration chromatography suggested that the N-terminal His_6-tag could negatively affect the oligomeric assembly and the catalytic activity of *Mt*GadB. With this in mind, the His_6-tag was removed (treated sample) and the enzymatic activity of the treated sample was compared to that of the untreated one.

To assess the efficiency in His-tag removal by thrombin, a preliminary time-course experiment was carried out according to manufacturer's instructions and the aliquots withdrawn at different time intervals were run on 10% SDS-PAGE (see section 4.2.7). As

reported in Fig. 4.12, the His_6-tag was already completely removed after 1 hour of incubation, when compared to the untreated sample.

Table 4.3 shows that the enzymatic activity of *Mt*GadB following the His_6-tag cleavage increases by approximately 30% when compared to the untreated sample. Although a deeper investigation will be required, this evidence clearly suggests that, not only the N-terminal tag negatively impacts the oligomeric assembly of *Mt*GadB, but also its catalytic activity. Therefore, the His_6-tag removal step needs to be included in the purification protocol of *Mt*GadB. This could be done by treating the protein with thrombin before the gel filtration and then loading the cleaved protein onto the size exclusion column, thereby achieving both removal of thrombin and His_6-tag and purification from residual contaminants.

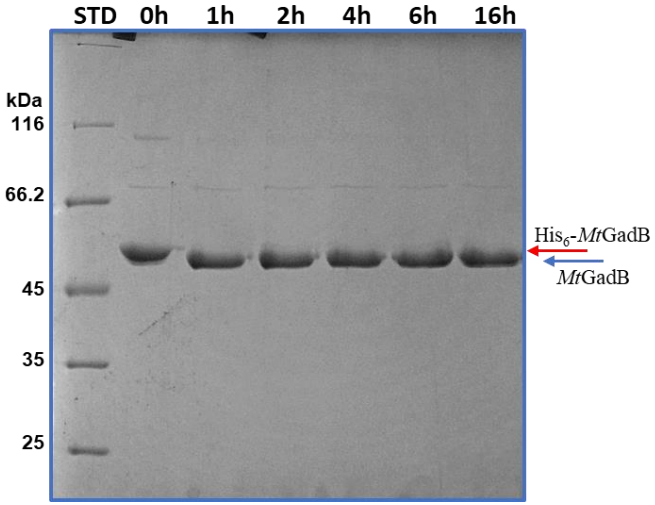

Figure 4.12. Analysis of the *time-course of thrombin cleavage*. Aliquots (2 µg) were withdrawn at different times and run on 10% SDS-PAGE. **STD**, molecular weight standard. Red and blue arrows indicate the bands corresponding to *Mt*GadB with/without the His_6-tag, respectively.

Table 4.3. *Enzymatic activity assay of* Mt*GadB before and after* His_6*-tag cleavage by thrombin*

	***Mt*GadB**		***Ec*GadB***
	Untreated	Treated	
Activity (U/mg)	183	253	93

*Enzymatic activity assay of *Ec*GadB was carried out for comparison

4.4. Conclusions

The present work reports for the first time the purification and spectroscopic analysis of glutamate decarboxylase from *M. tuberculosis*. This is also the first glutamate decarboxylase purified from the genus *Mycobacterium*, where Gad activity was reported and partially characterized from suspensions of *M. leprae,* purified from the organs of experimentally-infected armadillos (Prabhakaran *et al*., 1983).

In this study, we developed a successful protocol for the expression and purification of *Mt*GadB (carrying an N-terminal His_6-tag), which resulted in a purity ≥ 95% and a final yield of approximately 4 mg from 3 L of bacterial culture, which allowed the investigation of the biochemical and spectroscopic properties of the enzyme and the comparison of these properties with those of the extensively studied *Ec*GadB.

The N-terminal His_6-tag seems to influence the oligomeric structure and the enzymatic activity. These results may find an explanation on the flexible nature of the N-terminal domain in *Ec*GadB, which plays a key role in the oligomeric assembly and stability of the hexamer (Capitani *et al.*, 2003a). With this in mind, the His_6-tag cleavage step will be introduced in the future in the purification protocol of *Mt*GadB.

Regarding the spectroscopic properties of *Mt*GadB, the enzyme shares with the *Ec*GadB counterpart many similarities. In the *E. coli* enzyme, His465 plays a key role in controlling

the accessibility of the active site in a pH-dependent manner (Gut *et al.*, 2006; Pennacchietti *et al.*, 2009). This avoids the futile consumption of protons, which, otherwise, would cause a not physiological rise in the intracellular pH in a cell no longer exposed to acidic pH. A likely candidate for the formation of the *substituted aldamine* in *Mt*GadB is His460 which, indeed, occupies the same position in the sequence alignment (Fig. 4.5). An in deep biochemical characterization of this residue, along with the pH-dependent activity profile of the enzyme, not yet performed as part of this study, will elucidate the pH-dependent inactivation of *Mt*GadB.

To conclude, it is possible to speculate that *M. tuberculosis* possesses an acid pH-active glutamate decarboxylase as part of the arsenal evolved by the pathogen to cope with the acidity in the phagosome/phagolysosome. However, to the best of your knowledge, the Glu/GABA orthologue antiporter in *M. tuberculosis* has not been detected yet and therefore GABA production may be linked to other function, but not to export as in many other enteric bacteria (De Biase and Pennacchietti, 2012).

Another possible role of *Mt*GadB would be as a key component of the GABA-shunt which allows glutamate to feed the split TCA cycle of *M. tuberculosis*, thus by-passing the KDH missing step. Hence, the current study sets the basis for a better understanding of the *M. tuberculosis* GABA-shunt enzymes of which to date the only enzyme characterised to a significant extent is *Mt*GabD1 (de Carvalho *et al.*, 2011).

Taken all of this together, this work has the potentiality to extends our comprehension on *M. tuberculosis* acid resistance phenotype and if *Mt*GadB serves as a novel virulence factor; moreover, it can push further our knowledge on *M. tuberculosis* resistance to drugs.

CHAPTER V

Analogues and derivatives of dicarboxylic acids as antibacterial

Italian patent application:

De Biase, D., Pennacchietti, E., Giovannercole, F. Analogues and derivatives of dicarboxylic acids as antibacterial. Patent number: 102016000098005. Deposited on September 29 2016.

As part of my thesis, I also supported the group in developing the following italian patent, which refers to analogues and derivatives of dicarboxylic acids to be exploited as potential antibiotics in treating bacterial infections and in counteracting the antibiotic resistance.

The invention reported in the patent has been deposited on September 29 2016 and the evaluation for its acceptance is in progress.

Herein the information on the italian patent application from Ufficio Italiano Brevetti e Marchi (UIBM) and the graphic sheet from Office for Technology Transfer is enclosed.

MINISTERO DELLO SVILUPPO ECONOMICO
DIREZIONE GENERALE PER LA LOTTA ALLA CONTRAFFAZIONE
UFFICIO ITALIANO BREVETTI E MARCHI

UIBM

Informazioni identificative della domanda di brevetto per invenzione industriale numero 102016000098005 presentata il 29/09/2016

Data deposito	Tipo domanda	Stato	Tipo deposito
29/09/2016	Ordinaria	da assegnare	deposito on line

Titolo

Analoghi e derivati di amminoacidi dicarbossilici come antibatterici

Inventori 3

Cognome	Nome
De Biase	Daniela
Giovannercole	Fabio
Pennacchietti	Eugenia

Classificazione IPC 3

Sezione	Classe	Sottoclasse	Gruppo	Sottogruppo
A	61	K		
A	61	P	31	04
A	61	K	31	662

Richiedente 1

Denominazione/Cognome	Nome	Tipo società	Diritti %	CAP	Città	Provincia	Nazione
Università degli Studi di Roma La Sapienza		le universita'	100				Italia

Mandatari 4

Cognome e nome	Codice Albo
Cavattoni Claudia	1296
Cavattoni Fabio	24
Primiceri Maria Vittoria	465

Raimondi Adriana	22

Domicilio Elettivo 1

Denominazione/Cognome e nome	CAP	Città	Provincia	Nazione
Maria Vittoria Primiceri	00197	Roma	Roma	non presente

Istanza 1

Numero	Data	Tipo
782018000037051	28/06/2018	Risposta a rapporto di ricerca

MINISTERO DELLO SVILUPPO ECONOMICO (http://www.mise.gov.it)
Direzione generale per la lotta alla contraffazione - UIBM (http://www.uibm.gov.it)
Via Molise 19
0187 Roma

Analogues and derivatives of dicarboxylic amino acids as antibacterials

KEYWORDS

- ANTIBIOTICS
- MULTIDRUG RESISTANCE
- PATHOGENIC BACTERIA
- ENZYME INHIBITORS
- PHOSPHINIC COMPOUNDS
- DISINFECTANTS
- ANTISEPTICS

AREA

- PHARMACEUTICAL

CONTACTS

➢ PHONE NUMBERS
+39.06.49910888
+39.06.49910855

➢ EMAIL
u_brevetti@uniroma1.it

Priority Number
n. 102016000098005 of the 29.09.2016

Patent Type
Patent for invention.

Ownership
Sapienza University of Rome 100%

Inventors
Daniela De Biase, Fabio Giovannercole, Eugenia Pennacchietti.

Industrial & Commercial Reference

Pharma companies interested in novel molecules for the treatment of infections/surfaces by multidrug-resistant bacteria.

Time to Market

The most interesting molecules have been synthesized and their efficacy tested on many pathogenic bacteria. Preclinical investigation not available yet.

Availability

Research, Development, Experimentation and Collaboration.

THE ONU AGAINST RESISTANCE TO ANTIBIOTICS
The threat of antibiotic-resistant bacteria has become so concrete to enter the agenda of the United Nations National Assembly

Abstract

This invention relates to the fight against "bad bugs", i.e. bacteria that are resistant to a large spectrum of antibiotics available in the market, mostly chemically-related compounds.

The invention is about compounds that derive from a "lead compound" and that are antibacterials to various degrees and act on the bacterial central metabolism.

Preliminary data suggest that they are not endowed with toxicity for humans, which would prevent their systemic/topic use.

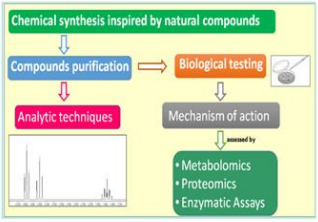

SAPIENZA UNIVERSITÀ DI ROMA

ASuRTT _ UFFICIO VALORIZZAZIONE E TRASFERIMENTO TECNOLOGICO
SETTORE BREVETTI E TRASFERIMENTO TECNOLOGICO
➢ http://uniroma1.it/ricerca/brevetti

Analogues and derivatives of dicarboxylic amino acids as antibacterials

Technical Description

The invention relates with the employment of novel chemical compounds in the fight against the infections caused by multi-drug resistant bacteria. The mechanism underlying the antibiotic activity has still to be fully elucidated in the molecular details. The data collected so far suggest that they could find an application as antibiotics to bring into the market. The novelty of the invention resides in the fact that the different compounds (all derived from a "lead molecule") penetrate the bacterial cell through different transporters thereby increasing the chance of successful penetration. Because of their chemical nature, the bacterial detoxification from these compounds would be a more rare event because the molecules and their derivatives are very unlikely to be excreted from the cell, as they mimic intracellular metabolites.

E. coli ESBL

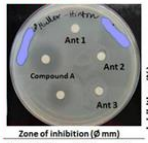

Zone of inhibition (Ø mm)

Compound A (amount)	EPEC (mm)	ESBL (mm)
2X (µg)	16	20
X (µg)	12	17

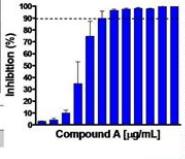

Technologies & Advantages

Key point of this innovation resides on the chemical nature of these compounds.

The sole substitution of a carbon with another non-toxic element gives rise to compounds that, being analogs of dicarboxylic-amino acids, can be substrates or inhibitors of enzymes in the bacterial central metabolism, therefore compromising the cellular viability.

On this regard, despite all the available antibacterial molecules, these compounds constitute a novelty in the field as such, and can be employed in the treatment to bacterial infections, especially against multi-drug resistant bacteria, that represent one of the most dramatic emergencies in the world.

An additional novelty of the invention resides in the ability of these compounds to enter the bacterial cell through diverse transporters.

This expands the entry points into the cell and, as such, might interfere with the development of bacterial resistances over time.

Applications

The compounds of the invention can be employed as antibacterials, alone or in combination with other antibiotics to fight infections caused by Gram-positive e Gram-negative bacteria.

These compounds can be also used in the formulation of disinfectants of the skin or of the oral cavity, as well as of the external genitals.

They could also well be employed in the treatment of materials/surfaces/ containers/ medical devices.

Formulations may include creams, gels, oils, powders, sprays, solutions, bandage, plasters, etc.

CONTACTS

- PHONE NUMBERS
+39.06.49910888
+39.06.49910855
- EMAIL
u_brevetti@uniroma1.it

SAPIENZA
UNIVERSITÀ DI ROMA

ASuRTT _ UFFICIO VALORIZZAZIONE E TRASFERIMENTO TECNOLOGICO
SETTORE BREVETTI E TRASFERIMENTO TECNOLOGICO
- http://uniroma1.it/ricerca/brevetti

GENERAL CONCLUSIONS AND PERSPECTIVES

With the work presented in this thesis, I provided new intriguing insights into the influence of the coenzyme (PLP) and pH on the oligomeric assembly of the enzyme glutamate decarboxylase from *E. coli* (*Ec*GadB); moreover, the mechanism of the pH-dependent regulation of the enzymatic catalysis of *Ec*GadB was investigated at the molecular level through the implementation of mutants for key amino acids.

As part of a project recently funded by Istituto Pasteur-Fondazione Cenci Bolognetti, I also carried out a preliminary biochemical investigation of a glutamate decarboxylase from *Mycobacterium tuberculosis* (*Mt*GadB). As such, the study of the biochemical and biophysical properties of bacterial Gad enzymes represents the connecting point of the projects presented in this thesis.

In Chapter II I demonstrated that *Ec*GadB dissociates from hexamer to tetramer and dimer not only in the *apo*-form, *i.e.* following the loss of PLP from the active site as previously reported (Sukhareva, 1986), but also in *holo*-form (*i.e.* with a full complement of PLP) when it is exposed to neutral-alkaline pH environments. This was accompanied by a significant increase in Trp fluorescence in *apo*GadB compared to *holo*GadB, which is a clear indication of consistent structural changes. Moreover, the Trp fluorescence signal in *holo*GadB increases following the exposure to more neutral-alkaline pHs (pH 7.5, 8.0 and 8.6). AUC, SAXS and limited proteolysis studies highlighted that the observed increase in fluorescence in *holo*- and *apo*GadB was due to the dissociation of the hexamer to tetramer and dimer. Further work will establish the concentration dependence and possible cooperativity in the dimer-hexamer interconversion as well as in the transient formation of the tetramer, a species never detected for *Ec*GadB, in order to understand whether the tetrameric/dimeric *Ec*GadB has a biological significance within the cell.

In Chapter III I studied the biochemical role of Asp86, a residue that is part of the Gad signature, as a key player in the pH-dependent regulation of the *Ec*GadB enzymatic activity.

This was achieved by incorporating the Asp86Asn in the single mutant *Ec*GadB_H465A, thus generating the double mutant *Ec*GadB_D86N-H465A, which was purified and investigated at the biochemical level. The comparison of the biochemical properties of this mutant with the wild-type enzyme and the single mutant showed that *Ec*GadB_D86N-H465A retains activity at pH 7.5-8.0 in strong contrast with the wild-type enzyme and the single mutant *Ec*GadB_H465A. In addition, I demonstrated that Asp86 is not only involved in the binding of glutamate, as originally thought, but also plays a major and unforeseen role in the release of the product, GABA. Notably, the extended pH-range of enzymatic activity of *Ec*GadB_D86N-H465A makes it exploitable for biotechnological applications as a source of GABA at neutral pH, an experimental condition suitable for industry.

In Chapter IV I carried out a preliminary investigation of the biochemical properties of *Mt*GadB as part of a project aimed at understanding the role of glutamate and GABA in metabolism of drug resistant *M. tuberculosis* strains. *Mt*GadB displayed part of the biochemical features of *Ec*GadB, therefore it may be part of molecular strategies exploited by *M. tuberculosis* to cope with the acidic environment of the phagosome/phagolysosome within macrophages during an infectious process. On the other hand, *Mt*GadB could play a key role in refilling the TCA cycle as part of the GABA-shunt, contributing to the conversion of α-ketoglutarate to succinate. Further work will be necessary to investigate the pH-dependent activity of *Mt*GadB and the oligomeric assembly of the enzyme. This information will provide a contribution to our understanding of the biological role of *Mt*GadB in *M. tuberculosis.*

In the last Chapter of this thesis, Chapter V, I reported a patent application focused on the use of analogues and derivatives of dicarboxylic acids as antibacterial. To date, the patent is under final evaluation for deposit.

REFERENCES

Abramovitch, R. B. *et al.* (2011) 'aprABC: A Mycobacterium tuberculosis complex-specific locus that modulates pH-driven adaptation to the macrophage phagosome', *Molecular Microbiology*, 80(3), pp. 678–694. doi: 10.1111/j.1365-2958.2011.07601.x.

Accardi, A. and Miller, C. (2004) 'Secondary active transport mediated by a prokaryotic homologue of ClC Cl-channels', *Nature*, 427(6977), pp. 803–807. doi: 10.1038/nature02314.

Aiso, T., Murata, M. and Gamou, S. (2011) 'Transcription of an antisense RNA of a gadE mRNA is regulated by GadE, the central activator of the acid resistance system in Escherichia coli', *Genes to Cells*, 16(6), pp. 670–680. doi: 10.1111/j.1365-2443.2011.01516.x.

Andréll, J. *et al.* (2009) 'Crystal structure of the acid-induced arginine decarboxylase from Escherichia coli: reversible decamer assembly controls enzyme cctivity', *Biochemistry*. American Chemical Society, 48(18), pp. 3915–3927. doi: 10.1021/bi900075d.

Angelaccio, S. *et al.* (2014) 'Conformational transitions driven by pyridoxal-5′-phosphate uptake in the psychrophilic serine hydroxymethyltransferase from Psychromonas ingrahamii', *Proteins: Structure, Function and Bioinformatics*, 82(10), pp. 2831–2841. doi: 10.1002/prot.24646.

Aquino, P. *et al.* (2017) 'Coordinated regulation of acid resistance in Escherichia coli', *BMC Systems Biology*, 11(1). doi: 10.1186/s12918-016-0376-y.

Armstrong, J. A. and Hart, P. D. (1971) 'Response of cultured macrophages to Mycobacterium tuberculosis, with observations on fusion of lysosomes with phagosomes.', *The Journal of experimental medicine*, 134(3 Pt 1), pp. 713–40. doi: 10.1084/jem.134.3.713.

Ausubel, F. M. *et al.* (1987) *Current Protocols in Molecular Biology*, *John Wiley Sons New York N Y*.

Baker, J. J. and Abramovitch, R. B. (2018) 'Genetic and metabolic regulation of Mycobacterium tuberculosis acid growth arrest', *Scientific Reports*. Springer US, 8(1), pp. 1–16. doi: 10.1038/s41598-018-22343-4.

Baker, J. J., Johnson, B. K. and Abramovitch, R. B. (2014) ‘Slow growth of Mycobacterium tuberculosis at acidic pH is regulated by phoPR and host-associated carbon sources’, *Molecular Microbiology*, 94(1), pp. 56–69. doi: 10.1111/mmi.12688.

Bennet, P. M. (2004) ‘Genome plasticity’, in Woodford, N. and Johnson, A. (eds) *Genomics, Proteomics, and Clinical Bacteriology: methods in molecular biology*. Totowa, N.J. : Humana Press, pp. 71–113.

Bennett, B. D. *et al.* (2009) ‘Absolute metabolite concentrations and implied enzyme active site occupancy in Escherichia coli’, *Nature Chemical Biology*, 5(8), pp. 593–599. doi: 10.1038/nchembio.186.

Bertoldi, M. *et al.* (2002) ‘Mutation of tyrosine 332 to phenylalanine converts dopa decarboxylase into a decarboxylation-dependent oxidative deaminase’, *Journal of Biological Chemistry*, 277(39), pp. 36357–36362. doi: 10.1074/jbc.M204867200.

Blanchet, C. E. and Svergun, D. I. (2013) ‘Small-Angle X-ray scattering on biological macromolecules and nanocomposites in solution’, *Annual Review of Physical Chemistry*, 64(1), pp. 37–54. doi: 10.1146/annurev-physchem-040412-110132.

Blankenhorn, D., Phillips, J. and Slonczewski, J. (1999) ‘Acid- and base-induced proteins during aerobic and anaerobic growth of Escherichia coli revealed by two-dimensional gel electrophoresis.’, *Journal of Bacteriology*, 181(7), pp. 2209–2216.

Botella, H. *et al.* (2017) ‘*Mycobacterium tuberculosis* protease MarP activates a peptidoglycan hydrolase during acid stress’, *The EMBO Journal*, 36(4), pp. 536–548. doi: 10.15252/embj.201695028.

Brookes, E. *et al.* (2013) ‘Fibrinogen species as resolved by HPLC-SAXS data processing within the UltraScan Solution Modeler (US-SOMO) enhanced SAS module’, *Journal of Applied Crystallography*, 46(6), pp. 1823–1833. doi: 10.1107/S0021889813027751.

Brookes, E. *et al.* (2016) ‘US-SOMO HPLC-SAXS module: Dealing with capillary fouling and extraction of pure component patterns from poorly resolved SEC-SAXS data’, *Journal of Applied Crystallography*, 49(5), pp. 1827–1841. doi: 10.1107/S1600576716011201.

Capitani, G. *et al.* (2003a) 'Crystal structure and functional analysis of Escherichia coli glutamate decarboxylase', *The EMBO Journal*, 22(16), pp. 4027–4037. doi: 10.1093/emboj/cdg403.

Capitani, G. *et al.* (2003b) 'The critical structural role of a highly conserved histidine residue in group II amino acid decarboxylases', *FEBS Letters*. No longer published by Elsevier, 554(1–2), pp. 41–44. doi: 10.1016/S0014-5793(03)01079-2.

Castanie-Cornet, M. P. *et al.* (1999) 'Control of acid resistance in Escherichia coli.', *Journal of bacteriology*, 181(11), pp. 3525–3535.

Cellini, B. *et al.* (2014) 'The chaperone role of the pyridoxal 5'-phosphate and its implications for rare diseases involving B6-dependent enzymes', *Clinical Biochemistry*. Elsevier B.V., 47(3), pp. 158–165. doi: 10.1016/j.clinbiochem.2013.11.021.

Clemens, D. L., Lee, B. Y. and Horwitz, M. a (1995) 'Purification, characterization, and genetic analysis of Mycobacterium tuberculosis urease, a potentially critical determinant of host-pathogen interaction', *J Bacteriol*, 177(19), pp. 5644–5652. doi: 10.1128/jb.177.19.5644-5652.1995.

Cole, S. T. *et al.* (1998) 'Deciphering the biology of mycobacterium tuberculosis from the complete genome sequence', *Nature*, 393, pp. 537–544. doi: 10.1038/31159.

Cotter, P. D., Gahan, C. G. M. and Hill, C. (2001) 'A glutamate decarboxylase system protects Listeria monocytogenes in gastric fluid', *Molecular Microbiology*, 40(2), pp. 465–475. doi: 10.1046/j.1365-2958.2001.02398.x.

Cowley, S. *et al.* (2004) 'The Mycobacterium tuberculosis protein serine/threonine kinase PknG is linked to cellular glutamate/glutamine levels and is important for growth in vivo', *Molecular Microbiology*, 52(6), pp. 1691–1702. doi: 10.1111/j.1365-2958.2004.04085.x.

Cunin, R. *et al.* (1986) 'Biosynthesis and metabolism of arginine in bacteria', *Microbiological Reviews*, 50(3), pp. 314–352.

Dadinova, L. A. *et al.* (2016) 'X-ray solution scattering study of four Escherichia coli enzymes involved in stationary-phase metabolism', *PLoS ONE*, 11(5), pp. 1–19. doi:

10.1371/journal.pone.0156105.

Damiano, M. A. *et al.* (2015) 'Glutamate decarboxylase-dependent acid resistance in Brucella spp.: Distribution and contribution to fitness under extremely acidic conditions', *Applied and Environmental Microbiology*, 81(2), pp. 578–586. doi: 10.1128/AEM.02928-14.

David, G. and Pérez, J. (2009) 'Combined sampler robot and high-performance liquid chromatography: A fully automated system for biological small-angle X-ray scattering experiments at the Synchrotron SOLEIL SWING beamline', *Journal of Applied Crystallography*, 42(5), pp. 892–900. doi: 10.1107/S0021889809029288.

De Biase, D. *et al.* (1996) 'Isolation, overexpression, and biochemical characterization of the two isoforms of glutamic acid decarboxylase from Escherichia coli', *Protein Expression and Purification*, 8(4), pp. 430–438. doi: 10.1006/prep.1996.0121.

De Biase, D. *et al.* (1999) 'The response to stationary-phase stress conditions in Escherichia coli: role and regulation of the glutamic acid decarboxylase system', *Molecular Microbiology*, 32(6), pp. 1198–1211. doi: 10.1046/j.1365-2958.1999.01430.x.

De Biase, D. and Lund, P. A. (2015) 'The Escherichia coli acid atress response and its significance for pathogenesis', in *Advances in Applied Microbiology*. Elsevier, pp. 49–88. doi: 10.1016/bs.aambs.2015.03.002.

De Biase, D., Maras, B. and John, R. A. (1991) 'A chromophore in glutamate decarboxylase has been wrongly identified as PQQ', *FEBS Letters*, 278(1), pp. 120–122. doi: 10.1016/0014-5793(91)80097-M.

De Biase, D. and Pennacchietti, E. (2012) 'Glutamate decarboxylase-dependent acid resistance in orally acquired bacteria: Function, distribution and biomedical implications of the gadBC operon', *Molecular Microbiology*, 86(4), pp. 770–786. doi: 10.1111/mmi.12020.

de Carvalho, L. P. S. *et al.* (2010) 'Activity-based metabolomic profiling of enzymatic function: identification of Rv1248c as a Mycobacterial 2-Hydroxy-3-oxoadipate synthase', *Chemistry and Biology*. Elsevier Ltd, 17(4), pp. 323–332. doi: 10.1016/j.chembiol.2010.03.009.

de Carvalho, L. P. S. *et al.* (2011) 'On the chemical mechanism of succinic semialdehyde dehydrogenase (GabD1) from Mycobacterium tuberculosis', *Archives of Biochemistry and Biophysics*, 509(1), pp. 90–99. doi: 10.1016/j.abb.2011.01.023.

DeJesus, M. A. *et al.* (2017) 'Comprehensive essentiality analysis of the Mycobacterium tuberculosis genome via aaturating transposon mutagenesis', 8(1), pp. e02133-16. doi: 10.1128/mBio.02133-16.

Dethlefsen, L. *et al.* (2006) 'Assembly of the human intestinal microbiota', *Trends in Ecology & Evolution*, 21(9), pp. 517–523. doi: 10.1016/j.tree.2006.06.013.

Dunathan, H. C. (1966) 'Conformation and reaction specificity in pyridoxal phosphate enzymes', *Proceedings of the National Academy of Sciences*, 55(4), pp. 712–716. doi: 10.1073/PNAS.55.4.712.

Duque-Correa, M. A. *et al.* (2014) 'Macrophage arginase-1 controls bacterial growth and pathology in hypoxic tuberculosis granulomas', *Proceedings of the National Academy of Sciences*, 111(38), pp. E4024–E4032. doi: 10.1073/pnas.1408839111.

Dutyshev, D. I. *et al.* (2005) 'Structure of Escherichia coli glutamate decarboxylase (GADα) in complex with glutarate at 2.05 Å resolution', *Acta Crystallographica Section D: Biological Crystallography*, 61(3), pp. 230–235. doi: 10.1107/S0907444904032147.

Eguchi, Y. *et al.* (2011) 'Regulation of acid resistance by connectors of two-component signal transduction systems in Escherichia coli', *Journal of bacteriology*. 2010/12/30. American Society for Microbiology (ASM), 193(5), pp. 1222–1228. doi: 10.1128/JB.01124-10.

Ehlers, S. and Schaible, U. E. (2012) 'The granuloma in tuberculosis: Dynamics of a host-pathogen collusion', *Frontiers in Immunology*, 3, pp. 1–9. doi: 10.3389/fimmu.2012.00411.

Ehrt, S. and Schnappinger, D. (2009) 'Mycobacterial survival strategies in the phagosome: defence against host stresses', *Cellular Microbiology*, 11(8), pp. 1170–1178. doi: 10.1111/j.1462-5822.2009.01335.x.

Eliot, A. C. and Kirsch, J. F. (2004) ‘Pyridoxal phosphate enzymes: mechanistic, structural, and evolutionary considerations’, *Annual Review of Biochemistry*, 73(1), pp. 383–415. doi: 10.1146/annurev.biochem.73.011303.074021.

Evans, D. F. *et al.* (1988) ‘Measurement of gastrointestinal pH profiles in normal ambulant human subjects’, *Gut*, 29(8), pp. 1035–1041. doi: 10.1136/gut.29.8.1035.

Feehily, C. and Karatzas, K. A. G. (2013) ‘Role of glutamate metabolism in bacterial responses towards acid and other stresses’, *Journal of Applied Microbiology*, 114(1), pp. 11–24. doi: 10.1111/j.1365-2672.2012.05434.x.

Feehily, C., O’Byrne, C. P. and Karatzas, K. A. G. (2013) ‘Functional γ-aminobutyrate shunt in listeria monocytogenes: role in acid tolerance and succinate biosynthesis’, *Applied and Environmental Microbiology*, 79(1), pp. 74–80. doi: 10.1128/AEM.02184-12.

Fenalti, G. *et al.* (2007) ‘GABA production by glutamic acid decarboxylase is regulated by a dynamic catalytic loop’, *Nature Structural &Amp; Molecular Biology*. Nature Publishing Group, 14, p. 280. Available at: http://dx.doi.org/10.1038/nsmb1228.

Feng, L., Chen, S. and Hu, Y. (2018) ‘PhoPR positively regulates whiB3 expression in response to low pH in pathogenic mycobacteria’, *Journal of Bacteriology*, 200(8). doi: 10.1128/JB.00766-17.

Fischer, H. *et al.* (2010) ‘Determination of the molecular weight of proteins in solution from a single small-angle X-ray scattering measurement on a relative scale’, *Journal of Applied Crystallography*, 43(1), pp. 101–109. doi: 10.1107/S0021889809043076.

Fishbein, S. *et al.* (2015) ‘Phylogeny to function: PE/PPE protein evolution and impact on Mycobacterium tuberculosis pathogenicity’, *Molecular Microbiology*, 96(5), pp. 901–916. doi: 10.1111/mmi.12981.

Fisher, M. a, Plikaytis, B. B. and Shinnick, T. M. (2002) ‘Microarray analysis of the Mycobacterium tuberculosis transcriptional response to the acidic conditions found in phagosomes’, *J Bacteriol*, 184(14), pp. 4025–32. doi: 10.1128/JB.184.14.4025.

Flint, H. J. *et al.* (2008) 'Polysaccharide utilization by gut bacteria: potential for new insights from genomic analysis', *Nature Reviews Microbiology*, 6(2), pp. 121–131. doi: 10.1038/nrmicro1817.

Fonda, M. L. (1972) 'Glutamate decarboxylase. Substrate specificity and inhibition by carboxylic acids', *Biochemistry*. American Chemical Society, 11(7), pp. 1304–1309. doi: 10.1021/bi00757a029.

Fontán, P. *et al.* (2008) 'Global transcriptional profile of Mycobacterium tuberculosis during THP-1 human macrophage infection', *Infection and Immunity*, 76(2), pp. 717–725. doi: 10.1128/IAI.00974-07.

Foster, J. W. (1999) 'When protons attack: microbial strategies of acid adaptation', *Current Opinion in Microbiology*, pp. 170–174. doi: 10.1016/S1369-5274(99)80030-7.

Foster, J. W. (2001) 'Acid stress responses of Salmonella and E. coli : survival mechanisms, regulation, and implications for pathogenesis', *The Journal of Microbiology*, 39(2), pp. 89–94.

Foster, J. W. (2004) 'Escherichia coli acid resistance: tales of an amateur acidophile', *Nature Reviews Microbiology*, pp. 898–907. doi: 10.1038/nrmicro1021.

Freddi, L. *et al.* (2017) 'The Glutaminase-dependent system confers extreme acid resistance to new species and atypical strains of Brucella', *Frontiers in microbiology*. Frontiers Media S.A., 8, p. 2236. doi: 10.3389/fmicb.2017.02236.

Galagan, J. E. *et al.* (2014) 'The Mycobacterium tuberculosis regulatory network and hypoxia', *Nature*, 499(7457), pp. 178–183. doi: 10.1038/nature12337.The.

Gale, E. F. (1946) *The Bacterial amino acid decarboxylases*, *Adv. Enzymol.* doi: 10.1002/9780470122518.ch1.

Gallant, J. L. *et al.* (2016) 'Glutamate dehydrogenase is required by Mycobacterium bovis BCG for resistance to cellular stress', *PLoS ONE*, 11(1), pp. 1–14. doi: 10.1371/journal.pone.0147706.

Gasteiger, E. *et al.* (2005) 'Protein identification and analysis tools on the ExPASy server', in *The Proteomics Protocols Handbook*. Humana Press, pp. 571–607. doi: 10.1385/1592598900.

Ghazaei, C. (2018) 'Mycobacterium tuberculosis and lipids: insights into molecular mechanisms from persistence to virulence', *Journal of Research in Medical Sciences*, pp. 23–63. doi: 10.4103/jrms.JRMS_904_17.

Giardina, G. *et al.* (2011) 'Open conformation of human DOPA decarboxylase reveals the mechanism of PLP addition to Group II decarboxylases', *Proceedings of the National Academy of Sciences*, 108(51), pp. 20514–20519. doi: 10.1073/pnas.1111456108.

Giardina, G. *et al.* (2015) 'How pyridoxal 5′-phosphate differentially regulates human cytosolic and mitochondrial serine hydroxymethyltransferase oligomeric state', *FEBS Journal*, 282(7), pp. 1225–1241. doi: 10.1111/febs.13211.

Giovannercole, F. *et al.* (2017a) 'On the effect of alkaline pH and cofactor availability in the conformational and oligomeric state of Escherichia coli glutamate decarboxylase', *Protein Engineering, Design and Selection*, 30(3), pp. 1–10. doi: 10.1093/protein/gzw076.

Giovannercole, F., Pennacchietti, E. and De Biase, D. (2017b) 'Glutamate decarboxylase in bacteria', in D'Mello, J. P. F. (ed.) *The handbook of microbial metabolism of amino acids*. CABI, p. 15. doi: 10.1079/9781780647234.0015.

Glatter, O. (1977) 'A new method for the evaluation of small-angle scattering data', *Journal of Applied Crystallography*, 10(5), pp. 415–421. doi: 10.1107/S0021889877013879.

Gobbetti, M., Di Cagno, R. and de Angelis, M. (2010) 'Functional microorganisms for functional food quality', *Critical Reviews in Food Science and Nutrition*, 50(8), pp. 716–727. doi: 10.1080/10408398.2010.499770.

Gong, S., Ma, Z. and Foster, J. W. (2004) 'The Era-like GTPase TrmE conditionally activates gadE and glutamate-dependent acid resistance in Escherichia coli', *Molecular Microbiology*, 54(4), pp. 948–961. doi: 10.1111/j.1365-2958.2004.04312.x.

Gordon, A. H., Hart, P. D. and Young, M. . (1980) ‘Ammonia inhibits phagosome-lysosome fusion in macrophages’, *Nature*, 286(5768), pp. 79–80.

Gouzy, A. *et al.* (2014a) ‘Mycobacterium tuberculosis exploits asparagine to assimilate nitrogen and resist acid stress during infection’, *PLoS Pathogens*. doi: 10.1371/journal.ppat.1003928.

Gouzy, A., Poquet, Y. and Neyrolles, O. (2014b) ‘Amino acid capture and utilization within the Mycobacterium tuberculosis phagosome’, *Future Microbiology*, 9(5), pp. 631–637. doi: 10.2217/fmb.14.28.

Gouzy, A., Poquet, Y. and Neyrolles, O. (2014c) ‘Nitrogen metabolism in Mycobacterium tuberculosis physiology and virulence’, *Nature Reviews Microbiology*, 12(11), pp. 729–737. doi: 10.1038/nrmicro3349.

Grant, P. L., Basford, J. M. and John, R. a (1987) ‘An investigation of transient intermediates in the reaction of 2-methylglutamate with glutamate decarboxylase from Escherichia coli.’, *The Biochemical journal*, 241(3), pp. 699–704. doi: 10.1042/bj2410699.

Grassini, G. *et al.* (2015) ‘Biochemical and spectroscopic properties of Brucella microti glutamate decarboxylase, a key component of the glutamate-dependent acid resistance system’, *FEBS Open Bio*, 5, pp. 209–2018. doi: 10.1016/j.fob.2015.03.006.

Griffin, J. E. *et al.* (2011) ‘High-resolution phenotypic profiling defines genes essential for mycobacterial growth and cholesterol catabolism’, *PLoS Pathogens*, 7(9), pp. 1–9. doi: 10.1371/journal.ppat.1002251.

Grishin, N. V., Phillips, M. A. and Goldsmith, E. J. (1995) ‘Modeling of the spatial structure of eukaryotic ornithine decarboxylases’, *Protein Science*, 4(7), pp. 1291–1304. doi: 10.1002/pro.5560040705.

Guinier, A. (1939) ‘La diffraction des rayons X aux très petits angles : application à l’étude de phénomènes ultramicroscopiques’, *Annales de Physique*, 11(12), pp. 161–237. doi: 10.1051/anphys/193911120161.

Guinier, A. and Fournet, G. (1955) *Small angle scattering of X-ray*. Ney York (USA): John Wiley & Sons, Inc.

Gut, H. *et al.* (2006) 'Escherichia coli acid resistance: pH-sensing, activation by chloride and autoinhibition in GadB', *EMBO Journal*, 25(11), pp. 2643–2651. doi: 10.1038/sj.emboj.7601107.

Gut, H. *et al.* (2009) 'A common structural basis for pH- and Calmodulin-mediated regulation in plant Glutamate decarboxylase', *Journal of Molecular Biology*, 392(2), pp. 334–351. doi: 10.1016/j.jmb.2009.06.080.

Harth, G. and Horwitz, M. A. (2003) 'Inhibition of Mycobacterium tuberculosis glutamine synthetase as a novel antibiotic strategy against tuberculosis: demonstration of efficacy in vivo', *Infection and Immunity*, 71(1), pp. 456–464. doi: 10.1128/IAI.71.1.456-464.2003.

Hazra, S. *et al.* (2015) 'Kinetic and structural characterization of the interaction of 6-Methylidene Penem 2 with the β-Lactamase from Mycobacterium tuberculosis', *Biochemistry*, 54(36), pp. 5657–5664. doi: 10.1016/j.trsl.2014.08.005.

Hinsinger, P. *et al.* (2003) 'Origins of root-mediated pH changes in the rhizosphere and their responses to environmental constraints: A review', *Plant and Soil*, 248, pp. 43–59. doi: 10.1023/A:1022371130939.

Hirshfield, I. N., Terzulli, S. and O'Byrne, C. (2003) 'Weak organic acids: a panoply of effects on bacteria.', *Science progress*, 86(Pt 4), pp. 245–269. doi: 10.3184/003685003783238626.

Ho, T. N. A. *et al.* (2013) 'Expanding the active pH range of Escherichia coli Glutamate decarboxylase by breaking the cooperativeness.', *Journal of bioscience and bioengineering*. Japan, 115(2), pp. 154–158. doi: 10.1016/j.jbiosc.2012.09.002.

Hommais, F. *et al.* (2004) 'GadE (YhiE): a novel activator involved in the response to acid environment in Escherichia coli', *Microbiology*, 150(1), pp. 61–72. doi: 10.1099/mic.0.26659-0.

Hong, W. *et al.* (2005) 'Periplasmic protein HdeA exhibits chaperone-like activity exclusively within stomach pH range by transforming into disordered conformation', *Journal of Biological Chemistry*, 280(29), pp. 27029–27034. doi: 10.1074/jbc.M503934200.

Hou, C. Y. *et al.* (2018) 'Selection of Escherichia coli Glutamate decarboxylase active at neutral pH from a focused library', *Biotechnology and Bioprocess Engineering*, 23(4), pp. 473–479. doi: 10.1007/s12257-018-0258-9.

Itou, J., Eguchi, Y. and Utsumi, R. (2009) 'Molecular mechanism of transcriptional cascade initiated by the EvgS/EvgA system in Escherichia coli K-12', *Bioscience, Biotechnology, and Biochemistry*, 73(4), pp. 870–878. doi: 10.1271/bbb.80795.

Jansonius, J. N. (1998) 'Structure, evolution and action of vitamin B6-dependent enzymes', *Current Opinion in Structural Biology*, 8(6), pp. 759–769. doi: 10.1016/S0959-440X(98)80096-1.

Johnson, D. B. and Hallberg, K. B. (2005) 'Acid mine drainage remediation options: a review', *Science of the Total Environment*, 338(1–2), pp. 3–14. doi: 10.1016/j.scitotenv.2004.09.002.

Kang, T. J., Ho, N. A. T. and Pack, S. P. (2013) 'Buffer-free production of gamma-aminobutyric acid using an engineered Glutamate decarboxylase from Escherichia coli', *Enzyme and Microbial Technology*. Elsevier, 53(3), pp. 200–205. doi: 10.1016/J.ENZMICTEC.2013.04.006.

Kanjee, U., Gutsche, I., Alexopoulos, E., *et al.* (2011a) 'Linkage between the bacterial acid stress and stringent responses: the structure of the inducible lysine decarboxylase', *EMBO Journal*. Nature Publishing Group, 30(5), pp. 931–944. doi: 10.1038/emboj.2011.5.

Kanjee, U., Gutsche, I., Ramachandran, S., *et al.* (2011b) 'The enzymatic activities of the Escherichia coli basic aliphatic amino acid decarboxylases exhibit a pH zone of inhibition', *Biochemistry*. American Chemical Society, 50(43), pp. 9388–9398. doi: 10.1021/bi201161k.

Kanjee, U. and Houry, W. a (2013) 'Mechanisms of acid resistance in Escherichia coli', *Annual review of microbiology*, 67, pp. 65–81. doi: 10.1146/annurev-micro-092412-155708.

Kass, I. *et al.* (2014) ‘Cofactor-dependent conformational heterogeneity of GAD65 and its role in autoimmunity and neurotransmitter homeostasis’, *Proceedings of the National Academy of Sciences*, pp. E2524–E2529. doi: 10.1002/ccd.26438.

Kern, R. *et al.* (2007) ‘Escherichia coli HdeB is an acid stress chaperone’, *Journal of Bacteriology*, 189(2), pp. 603–610. doi: 10.1128/JB.01522-06.

Kobayashi, A. *et al.* (2006) ‘Growth phase-dependent expression of drug exporters in Escherichia coli and its contribution to drug tolerance’, *Journal of Bacteriology*, 188(16), pp. 5693–5703. doi: 10.1128/JB.00217-06.

Konarev, P. V. *et al.* (2003) ‘PRIMUS: A Windows PC-based system for small-angle scattering data analysis’, *Journal of Applied Crystallography*, 36(5), pp. 1277–1282. doi: 10.1107/S0021889803012779.

Krulwich, T. A., Sachs, G. and Padan, E. (2011) ‘Molecular aspects of bacterial pH sensing and homeostasis’, *Nature reviews. Microbiology*, 9(5), pp. 330–343. doi: 10.1038/nrmicro2549.

Lammens, T. M. *et al.* (2009) ‘The application of glutamic acid α-decarboxylase for the valorization of glutamic acid’, *Green Chemistry*. The Royal Society of Chemistry, 11(10), pp. 1562–1567. doi: 10.1039/B913741F.

Lammens, T. M. (2011) *Biobased industrial chemicals from glutamic acid*. Wageningen University. Available at: http://edepot.wur.nl/186440.

Lin, J. *et al.* (1995) ‘Comparative analysis of extreme acid survival in Salmonella typhimurium, Shigella flexneri, and Escherichia coli’, *Journal of Bacteriology*, 177(14), pp. 4097–4104. doi: 10.1128/jb.177.14.4097-4104.1995.

Lin, J. *et al.* (1996) ‘Mechanisms of acid resistance in enterohemorrhagic Escherichia coli’, *Appl Environ Microbiol*, 62(9), pp. 3094–3100.

Lin, W. *et al.* (2012) ‘Urease activity represents an alternative pathway for Mycobacterium tuberculosis nitrogen metabolism’, *Infection and Immunity*, 80(8), pp. 2771–2779. doi: 10.1128/IAI.06195-11.

Lu, P. *et al.* (2013) 'L-glutamine provides acid resistance for Escherichia coli through enzymatic release of ammonia', *Cell Research*. Nature Publishing Group, 23(5), pp. 635–644. doi: 10.1038/cr.2013.13.

Lund, P., Tramonti, A. and De Biase, D. (2014) 'Coping with low pH: molecular strategies in neutralophilic bacteria', *FEMS Microbiology Reviews*, 38(6), pp. 1091–1125. doi: 10.1111/1574-6976.12076.

Ma, D. *et al.* (2012) 'Structure and mechanism of a glutamate-GABA antiporter', *Nature*, 483(7391), pp. 632–636. doi: 10.1038/nature10917.

Ma, D., Lu, P. and Shi, Y. (2013) 'Substrate selectivity of the acid-activated glutamate/γ-aminobutyric acid (GABA) antiporter GadC from Escherichia coli', *Journal of Biological Chemistry*, 288(21), pp. 15148–15153. doi: 10.1074/jbc.M113.474502.

Ma, Z. *et al.* (2003a) 'GadE (YhiE) activates glutamate decarboxylase-dependent acid resistance in Escherichia coli K-12', *Molecular Microbiology*, 49(5), pp. 1309–1320. doi: 10.1046/j.1365-2958.2003.03633.x.

Ma, Z., Masuda, N. and Foster, J. W. (2004) 'Characterization of EvgAS-YdeO-GadE branched regulatory circuit governing glutamate-dependent acid resistance in Escherichia coli', *J Bacteriol*, 186(21), pp. 7378–7389. doi: 10.1128/JB.186.21.7378-7389.2004.

Ma, Z., Richard, H. and Foster, J. W. (2003b) 'pH-Dependent modulation of cyclic AMP levels and gadW-dependent repression of RpoS affect synthesis of the GadX regulator and Escherichia coli acid resistance', *Journal of Bacteriology*, 185(23), pp. 6852–6859. doi: 10.1128/JB.185.23.6852-6859.2003.

Malashkevich, V. N., De Biase, D. and Bossa, F. (2009) *Crystal structure of apo glutamate decarboxylase beta from Escherichia coli*. doi: 10.2210/pdb3FZ7/pdb.

Maras, B. *et al.* (1992) 'The amino acid sequence of glutamate decarboxylase from Escherichia coli', *European Journal of Biochemistry*, 204(1), pp. 93–98.

Martinsen, T. C., Bergh, K. and Waldum, H. L. (2005) 'Gastric juice: a barrier against infectious diseases', *Basic and Clinical Pharmacology and Toxicology*, pp. 94–102. doi: 10.1111/j.1742-7843.2005.pto960202.x.

Masuda, N. and Church, G. M. (2003) 'Regulatory network of acid resistance genes in Escherichia coli', *Molecular Microbiology*, 48(3), pp. 699–712. doi: 10.1046/j.1365-2958.2003.03477.x.

Mates, A. K., Sayed, A. K. and Foster, J. W. (2007) 'Products of the Escherichia coli acid fitness island attenuate metabolite stress at extremely low pH and mediate a cell density-dependent acid resistance', *Journal of Bacteriology*, 189(7), pp. 2759–2768. doi: 10.1128/JB.01490-06.

McKinney, J. D. *et al.* (2000) 'Persistence of Mycobacterium tuberculosis in macrophages and mice requires the glyoxylate shunt enzyme isocitrate lyase', *Nature*, 406(6797), pp. 735–738. doi: 10.1038/35021074.

McLaggan, D. *et al.* (1994) 'Interdependence of K+ and glutamate accumulation during osmotic adaptation of Escherichia coli', *Journal of Biological Chemistry*, 269(3), pp. 1911–1917.

Mehta, M., Rajmani, R. S. and Singh, A. (2016) 'Mycobacterium tuberculosis WhiB3 responds to vacuolar pH-induced changes in mycothiol redox potential to modulate phagosomal maturation and virulence', *Journal of Biological Chemistry*, 291(6), pp. 2888–2903. doi: 10.1074/jbc.M115.684597.

Mertens, H. D. T. and Svergun, D. I. (2010) 'Structural characterization of proteins and complexes using small-angle X-ray solution scattering.', *J Struct Biol*. Elsevier Inc., 172(1), pp. 128–41. doi: 10.1016/j.jsb.2010.06.012.

Metzler, D. E. *et al.* (1973) 'Spectra of 3-Hydroxypyridines. Band-shape analysis and evaluation of tautomeric equilibria', *Biochemistry*, 12(26), pp. 5377–5392. doi: 10.1021/bi00750a022.

Migliori, G. B. *et al.* (2007) 'Extensively Drug-resistant Tuberculosis, Italy and Germany', *Emerging Infectious Diseases*, 13(5), pp. 780–782. doi: 10.3201/eid1305.070200.

Mishra, A. and Surolia, A. (2018) 'Mycobacterium tuberculosis: surviving and indulging in an unwelcoming host', *IUBMB LIFE*, 0(0), pp. 1–9. doi: 10.1002/iub.1882.

Momany, C. *et al.* (1995a) 'Crystallographic structure of a PLP-dependent ornithine decarboxylase from Lactobacillus 30a to 3.0 Å resolution', *Journal of Molecular Biology*, 252(5), pp. 643–655. doi: 10.1006/jmbi.1995.0526.

Momany, C., Ghosh, R. and Hackert, M. L. (1995b) 'Structural motifs for pyridoxal-5′-phosphate binding in decarboxylases: an analysis based on the crystal structure of the Lactobacillus 30a ornithine decarboxylase', *Protein Science*, 4(5), pp. 849–854. doi: 10.1002/pro.5560040504.

Mowbray, S. L. *et al.* (2014) 'Inhibition of glutamine synthetase: A potential drug target in Mycobacterium tuberculosis', *Molecules*, 19(9), pp. 13161–13176. doi: 10.3390/molecules190913161.

Mukhopadhyay, S., Nair, S. and Ghosh, S. (2012) 'Pathogenesis in tuberculosis: transcriptomic approaches to unraveling virulence mechanisms and finding new drug targets', *FEMS Microbiology Reviews*, 36(2), pp. 463–485. doi: 10.1111/j.1574-6976.2011.00302.x.

Murthy, P. S., Sirsi, M. and Ramakrishnan, T. (1962) 'Tricarboxylic acid cycle and related enzymes in cell-free extracts of Mycobacterium tuberculosis H37Rv.', *The Biochemical journal*, 84(1958), pp. 263–9.

Nishino, K., Senda, Y. and Yamaguchi, A. (2008) 'The AraC-family regulator GadX enhances multidrug resistance in Escherichia coli by activating expression of mdtEF multidrug efflux genes', *J Infect Chemother*, 14(1), pp. 23–29. doi: 10.1007/s10156-007-0575-y.

O'Leary, M. H. and Brummund, W. (1974) 'pH jump studies of glutamate decarboxylase. Evidence for a pH dependent conformation change', *Journal of Biological Chemistry*, 249(12), pp. 3737–3745.

O'Leary, M. H., Yamada, H. and Yapp, C. J. (1981) 'Multiple isotope effect probes of glutamate decarboxylase', *Biochemistry*. American Chemical Society, 20(6), pp. 1476–1481. doi: 10.1021/bi00509a011.

Occhialini, A. *et al.* (2012) 'The glutamic acid decarboxylase system of the new species Brucella microti contributes to its acid resistance and to oral infection of mice', *Journal of Infectious Diseases*, 206(9), pp. 1424–1432. doi: 10.1093/infdis/jis522.

Opdyke, J. A., Kang, J. G. and Storz, G. (2004) 'GadY, a small-RNA regulator of acid response genes in Escherichia coli', *Journal of Bacteriology*, 186(20), pp. 6698–6705. doi: 10.1128/JB.186.20.6698-6705.2004.

Pandey, A. K. and Sassetti, C. M. (2008) 'Mycobacterial persistence requires the utilization of host cholesterol', *Proceedings of the National Academy of Sciences*, 105(11), pp. 4376–4380. doi: 10.1073/pnas.0711159105.

Pennacchietti, E. *et al.* (2009) 'Mutation of His465 alters the pH-dependent spectroscopic properties of Escherichia coli glutamate decarboxylase and broadens the range of its activity toward more alkaline pH', *Journal of Biological Chemistry*, 284(46), pp. 31587–31596. doi: 10.1074/jbc.M109.049577.

Pennacchietti, E. *et al.* (2018) 'The Glutaminase-dependent acid resistance system: qualitative and quantitative assays and analysis of its distribution in enteric bacteria', *Frontiers in Microbiology*, 9, pp. 1–17. doi: 10.3389/fmicb.2018.02869.

Pennacchietti, E., Giovannercole, F. and De Biase, D. (2016) 'Acid survival mechanisms in neutralophilic bacteria', in Bruijn, F. J. De (ed.) *Stress and Environmental Regulation of Gene Expression and Adaptation in Bacteria, I&II*. WILEY, pp. 911–926.

Percudani, R. and Peracchi, A. (2003) 'A genomic overview of pyridoxal-phosphate-dependent enzymes', *EMBO Reports*, 4(9), pp. 850–854. doi: 10.1038/sj.embor.embor914.

Percudani, R. and Peracchi, A. (2009) 'The B6 database: a tool for the description and classification of vitamin B6-dependent enzymatic activities and of the corresponding protein families', *BMC Bioinformatics*, 10, p. 273. doi: 10.1186/1471-2105-10-273.

Perucho, J. *et al.* (2015) ‘Optimal excitation and emission wavelengths to analyze amino acids and optimize neurotransmitters quantification using precolumn OPA-derivatization by HPLC’, *Amino Acids*, 47(5), pp. 963–973. doi: 10.1007/s00726-015-1925-1.

Peterson, E. A. and Sober, H. A. (1954) ‘Preparation of Crystalline Phosphorylated Derivatives of Vitamin B6’, *Journal of the American Chemical Society*, 76(1), pp. 169–175. doi: 10.1021/ja01630a045.

Petoukhov, M. V. and Svergun, D. I. (2013) ‘Applications of small-angle X-ray scattering to biomacromolecular solutions’, *International Journal of Biochemistry and Cell Biology*. Elsevier Ltd, 45(2), pp. 429–437. doi: 10.1016/j.biocel.2012.10.017.

Pettersen, E. F. *et al.* (2004) ‘UCSF Chimera - A visualization system for exploratory research and analysis’, *Journal of Computational Chemistry*, 25(13), pp. 1605–1612. doi: 10.1002/jcc.20084.

Phelan, J. *et al.* (2016) ‘Mycobacterium tuberculosis whole genome sequencing and protein structure modelling provides insights into anti-tuberculosis drug resistance’, *BMC Medicine*, 14(31). doi: 10.1186/s12916-016-0575-9.

Porod, G. (1982) ‘General theory’, in Glatter, O. and Kratky, O. (eds) *Small angle X-ray scattering*. Academic Press: London, pp. 17–51.

Prabhakaran, K., Harris, E. B. and Kirchheimer, W. F. (1983) ‘Glutamic acid decarboxylase in Mycobacterium leprae.’, *Archives of microbiology*, 134, pp. 320–323.

Raviglione, M. C. (2015) ‘Tuberculosis’, in Kasper, D. L. et al. (eds) *Harrison’s Principles of Internal Medicine*. 19th edn. New York: Education, McGraw-Hill, pp. 1102–1121.

Rengarajan, J., Bloom, B. R. and Rubin, E. J. (2005) ‘Genome-wide requirements for Mycobacterium tuberculosis adaptation and survival in macrophages’, *Proceedings of the National Academy of Sciences*, 102(23), pp. 8327–8332. doi: 10.1073/pnas.0503272102.

Rhee, K. Y. *et al.* (2011) ‘Central carbon metabolism in Mycobacterium tuberculosis: an unexpected frontier’, *Trends in Microbiology*. Elsevier Ltd, 19(7), pp. 307–314. doi: 10.1016/j.tim.2011.03.008.

Rice, E. W. *et al.* (1993) 'Rapid glutamate decarboxylase assay for detection of Escherichia coli', *Applied and Environmental Microbiology*, 59(12), pp. 4347–4349.

Rieck, B. *et al.* (2017) 'PknG senses amino acid availability to control metabolism and virulence of Mycobacterium tuberculosis', *PLoS Pathogens*, 13(5), pp. 1–31. doi: 10.1371/journal.ppat.1006399.

Rohde, K. H. *et al.* (2012) 'Linking the transcriptional profiles and the physiological states of Mycobacterium tuberculosis during an extended intracellular infection', *PLoS Pathogens*, 8(6). doi: 10.1371/journal.ppat.1002769.

Rohde, K. H., Abramovitch, R. B. and Russell, D. G. (2007) 'Mycobacterium tuberculosis invasion of macrophages: linking bacterial gene expression to environmental cues', *Cell Host and Microbe*, 2(5), pp. 352–364. doi: 10.1016/j.chom.2007.09.006.

Sanders, J. W. *et al.* (1998) 'A chloride-inducible acid resistance mechanism in Lactococcus lactis and its regulation', *Molecular Microbiology*, 27(2), pp. 299–310. doi: 10.1046/j.1365-2958.1998.00676.x.

Sandmeier, E., Hale, T. I. and Christen, P. (1994) 'Multiple evolutionary origin of pyridoxal-5'-phosphate-dependent amino acid decarboxylases', *European Journal of Biochemistry*, 221(3), pp. 997–1002. doi: 10.1111/j.1432-1033.1994.tb18816.x.

Sassetti, C. M., Boyd, D. H. and Rubin, E. J. (2001) 'Comprehensive identification of conditionally essential genes in mycobacteria', *Proceedings of the National Academy of Sciences*, 98(22), pp. 12712–12717. doi: 10.1073/pnas.231275498.

Saviola, B., Woolwine, S. C. and Bishai, W. R. (2003) 'Isolation of acid-inducible genes of Mycobacterium tuberculosis with the use of recombinase-based in vivo expression technology', *Infection and Immunity*, 71(3), pp. 1379–1388. doi: 10.1128/IAI.71.3.1379-1388.2003.

Sayed, A. K., Odom, C. and Foster, J. W. (2007) 'The Escherichia coli AraC-family regulators GadX and GadW activate gadE, the central activator of glutamate-dependent acid resistance', *Microbiology*, 153(8), pp. 2584–2592. doi: 10.1099/mic.0.2007/007005-0.

Schaible, U. E. *et al.* (1998) 'Cytokine activation leads to acidification and increases maturation of Mycobacterium avium-containing phagosomes in murine macrophages', *The Journal of Immunology*, 160(3), p. 1290–1296. doi: 10.4049/jimmunol.172.7.4592.

Shepherd, M. *et al.* (2010) 'Compensations for diminished terminal oxidase activity in Escherichia coli: Cytochrome bd-II-mediated respiration and glutamate metabolism', *Journal of Biological Chemistry*, 285(24), pp. 18464–18472. doi: 10.1074/jbc.M110.118448.

Shin, J. H. *et al.* (2011) '1H NMR-based metabolomic profiling in mice infected with Mycobacterium tuberculosis', *Journal of Proteome Research*, 10(5), pp. 2238–2247. doi: 10.1021/pr101054m.

Shukuya, R. and Schwert, G. W. (1960) 'I. isolation procedures', *Journal of Biological Chemistry*, 235(6), pp. 6–9.

Sikora, A. L., Frankel, B. A. and Blanchard, J. S. (2010) 'Kinetic and chemical mechanism of arylamine acetyltransferase from Mycobacterium tuberculosis', *Reactions*, 47(40), pp. 10781–10789. doi: 10.1021/bi800398c.Kinetic.

Singh, A. K. *et al.* (2016) 'Investigating essential gene function in *Mycobacterium tuberculosis* using an efficient CRISPR interference system', *Nucleic Acids Research*, 44(18), pp. e143–e143. doi: 10.1093/nar/gkw625.

Slonczewski, J. L. *et al.* (2009) 'Cytoplasmic pH measurement and homeostasis in bacteria and archaea', *Advances in Microbial Physiology*, pp. 1–79. doi: 10.1016/S0065-2911(09)05501-5.

Somashekar, B. S. *et al.* (2011) 'Metabolic profiling of lung granuloma in Mycobacterium tuberculosis infected guinea pigs: ex vivo 1H magic angle spinning NMR studies.', *Journal of proteome research*, 10(9), pp. 4186–4195. doi: 10.1021/pr2003352.

Strausbauch, P. H. and Fischer, E. H. (1970) 'Chemical and physical properties of Escherichia coli glutamate decarboxylase', *Biochemistry*. American Chemical Society, 9(2), pp. 226–233. doi: 10.1021/bi00804a006.

Struzycka, I. (2014) ‘The oral microbiome in dental caries’, *Polish Journal of Microbiology*, 63(2), pp. 127–135.

Studier, F. W. *et al.* (1990) ‘Use of T7 RNA polymerase to direct expression of cloned genes’, *Methods in Enzymology*, 185, pp. 60–89.

Sukhareva, B. S. (1986) ‘Amino acid decarboxylases. Pyridoxal phosphate: chemical, biochemical and medical aspects’, in Dolphin, D., Poulson, R., and Avramovic, O. (eds) *Vitamine B6*. Wiley,NY, pp. 325–353.

Svergun, D., Barberato, C. and Koch, M. H. J. (1995) ‘CRYSOL – a program to evaluate X-ray solution scattering of biological aacromolecules from atomic coordinates’, *Journal of Applied Crystallography*, 28, pp. 768–773. Available at: http://linkinghub.elsevier.com/retrieve/pii/S0167811615000506.

Svergun, D. I. (1992) ‘Determination of the regularization parameter in indirect-transform methods using perceptual criteria’, *Journal of Applied Crystallography*, 25, pp. 495–503. doi: 10.1107/S0021889892001663.

Teixeira, J. S. *et al.* (2014) ‘Glutamine, glutamate, and arginine-based acid resistance in Lactobacillus reuteri.’, *Food microbiology*. England, 42, pp. 172–180. doi: 10.1016/j.fm.2014.03.015.

Tian, J. *et al.* (2005a) ‘Mycobacterium tuberculosis appears to lack α-ketoglutarate dehydrogenase and encodes pyruvate dehydrogenase in widely separated genes’, *Molecular Microbiology*, 57(3), pp. 859–868. doi: 10.1111/j.1365-2958.2005.04741.x.

Tian, J. *et al.* (2005b) ‘Variant tricarboxylic acid cycle in Mycobacterium tuberculosis: identification of α-ketoglutarate decarboxylase’, *Proceedings of the National Academy of Sciences*, 102(30), pp. 10670–10675. doi: 10.1073/pnas.0501605102.

Tikhonenko, A. S., Sukhareva, B. S. and Braunstein, A. E. (1968) ‘Electron-microscopic investigation of Escherichia coli glutamate decarboxylase’, *Biochimica et Biophysica Acta (BBA)*, 167(2), pp. 476–479.

Tiwari, S. *et al.* (2018) 'Arginine-deprivation–induced oxidative damage sterilizes Mycobacterium tuberculosis', *Proceedings of the National Academy of Sciences*, p. 201808874. doi: 10.1073/pnas.1808874115.

To, C. M. (1971) 'Quaternary structure of glutamate decarboxylase of Escherichia coli as revealed by electron microscopy', *Journal of Molecular Biology*, 59(1), pp. 215–217. doi: 10.1016/0022-2836(71)90424-4.

Toney, M. D. (2005) 'Reaction specificity in pyridoxal phosphate enzymes', *Archives of Biochemistry and Biophysics*, 433(1), pp. 279–287. doi: 10.1016/j.abb.2004.09.037.

Tramonti, A. *et al.* (1998) 'The roles of His-167 and His-275 in the reaction catalyzed by glutamate decarboxylase from Escherichia coli', *Journal of Biological Chemistry*, 273(4), pp. 1939–1945. doi: 10.1074/jbc.273.4.1939.

Tramonti, A., John, R. A., *et al.* (2002a) 'Contribution of Lys276 to the conformational flexibility of the active site of glutamate decarboxylase from Escherichia coli', *European Journal of Biochemistry*, 269(20), pp. 4913–4920. doi: 10.1046/j.1432-1033.2002.03149.x.

Tramonti, A., Visca, P., *et al.* (2002b) 'Functional characterization and regulation of gadX, a gene encoding an AraC/XylS-like transcriptional activator of the Escherichia coli glutamic acid decarboxylase system?', *Journal of Bacteriology*, 184(10), pp. 2603–2613. doi: 10.1128/JB.184.10.2603-2613.2002.

Tramonti, A. *et al.* (2006) 'Mechanisms of transcription activation exerted by GadX and GadW at the gadA and gadBC gene promoters of the glutamate-based acid resistance system in Escherichia coli', *Journal of Bacteriology*, 188(23), pp. 8118–8127. doi: 10.1128/JB.01044-06.

Tramonti, A., De Canio, M. and De Biase, D. (2008) 'GadX/GadW-dependent regulation of the Escherichia coli acid fitness island: transcriptional control at the gadY-gadW divergent promoters and identification of four novel 42 bp GadX/GadW-specific binding sites', *Molecular Microbiology*, 70(4), pp. 965–982. doi: 10.1111/j.1365-2958.2008.06458.x.

Tsai, M.-F., McCarthy, P. and Miller, C. (2013) 'Substrate selectivity in glutamate-dependent acid resistance in enteric bacteria', *Proceedings of the National Academy of Sciences*, 110(15), pp. 5898–5902. doi: 10.1073/pnas.1301444110.

Tucker, D. L. *et al.* (2003) 'Genes of the GadX-GadW regulon in Escherichia coli', *Journal of Bacteriology*, 185(10), pp. 3190–3201. doi: 10.1128/JB.185.10.3190-3201.2003.

Umbarger, H. E. (1978) 'Amino acid biosynthesis and its regulation.', *Annual review of biochemistry*, 47(1), pp. 532–606. doi: 10.1146/annurev.bi.47.070178.002533.

Vandal, O. H. *et al.* (2008) 'A membrane protein preserves intrabacterial pH in intraphagosomal Mycobacterium tuberculosis', *Nature Medicine*, 14(8), pp. 849–854. doi: 10.1038/nm.1795.

Vandal, O. H. *et al.* (2009b) 'Acid-susceptible mutants of mycobacterium tuberculosis share hypersusceptibility to cell wall and oxidative stress and to the host environment', *Journal of Bacteriology*, 191(2), pp. 625–631. doi: 10.1128/JB.00932-08.

Vandal, O. H., Nathan, C. F. and Ehrt, S. (2009a) 'Acid resistance in Mycobacterium tuberculosis', *Journal of Bacteriology*, 191(15), pp. 4714–4721. doi: 10.1128/JB.00305-09.

Venkatasubban, K. S. and Schowen, R. L. (1984) 'The proton inventory technique', *CRC critical reviews in biochemistry*. United States, 17(1), pp. 1–44.

Vergne, I. *et al.* (2004) 'Cell biology of Mycobacterium tuberculosis phagosome', *Annual Review of Cell and Developmental Biology*, 20(1), pp. 367–394. doi: 10.1146/annurev.cellbio.20.010403.114015.

Viljoen, A. J. *et al.* (2013) 'The role of glutamine oxoglutarate aminotransferase and glutamate dehydrogenase in nitrogen metabolism in Mycobacterium bovis BCG', *PLoS ONE*, 8(12), p. e84452. doi: 10.1371/journal.pone.0084452.

Walker, M. C. and van der Donk, W. A. (2016) 'The many roles of glutamate in metabolism', *Journal of Industrial Microbiology and Biotechnology*, 43(0), pp. 419–430. doi: 10.1007/s10295-015-1665-y.

Weber, H. *et al.* (2005) 'Genome-wide analysis of the general stress response network in Escherichia coli: σS-dependent genes, promoters, and sigma factor selectivity', *Journal of Bacteriology*, 187(5), pp. 1591–1603. doi: 10.1128/JB.187.5.1591-1603.2005.

White-Ziegler, C. A. *et al.* (2008) 'Low temperature (23 °C) increases expression of biofilm-, cold-shock- and RpoS-dependent genes in Escherichia coli K-12', *Microbiology*, 154(1), pp. 148–166. doi: 10.1099/mic.0.2007/012021-0.

World Health Organization (2017) *TUBERCULOSIS*. Available at: http://www.who.int/tb/publications/global_report/gtbr2017_main_text.pdf.

World Health Organization (2018) *WHO Preferred Product Characteristics for New Tuberculosis Vaccines DEPARTMENT OF IMMUNIZATION, VACCINES AND BIOLOGICALS*. Available at: http://apps.who.int/bookorders.

Xu, H., Hegde, S. S. and Blanchard, J. S. (2011) 'The reversible acetylation and inactivation of Mycobacterium tuberculosis acetyl-CoA synthetase is dependent on cAMP', *Biochemistry*, 50(26), pp. 5883–5892. doi: 10.1021/bi200156t.

Yang, B. I.-Y. and Metzler, D. E. (1979) 'Pyridoxal 5'-phosphate and analogs as probes of coenzyme-protein interaction 1', *Methods in Enzymology*.

Yu, K. *et al.* (2012) 'C-terminal truncation of glutamate decarboxylase from Lactobacillus brevis CGMCC 1306 extends its activity toward near-neutral pH.', *Enzyme and microbial technology*. United States, 50(4–5), pp. 263–269. doi: 10.1016/j.enzmictec.2012.01.010.

RINGRAZIAMENTI

Questo lavoro di tesi è stato svolto presso il Dipartimento di Scienze e Biotecnologie Medico-Chirurgiche di Latina sotto la guida della Prof.ssa Daniela De Biase. Alla professoressa mando i miei più sinceri ringraziamenti per avermi coinvolto attivamente nei progetti di questa tesi e per i numerosi insegnamenti scientifici da lei ricevuti. Desidero ringraziarla in particolare per la precisione, l'impegno, la costanza, la passione e la curiosità che ha saputo trasmettermi nel corso di questi anni.

In qualità di studente di dottorato, ringrazio il Coordinatore della scuola di dottorato, Prof. Marco Tripodi, e tutto il Collegio Docenti.

Un ringraziamento speciale va alla Dott.ssa Eugenia Pennacchietti per essere stata una figura essenziale durante la mia formazione scientifica in laboratorio. A lei devo tantissimo per gli insegnamenti ricevuti, per la sua preziosa amicizia e per tutto il tempo trascorso serenamente insieme tra un esperimento e l'altro.

Ringrazio anche tutti i membri, passati e presenti, del laboratorio DDB; in particolare la Dott. Chiara D'Alonzo per tutte le belle esperienze condivise, dentro e fuori il lab, e per i numerosi pranzi che ha preparato per me, assecondando la mia presuntuosa pigrizia.

Sentiti ringraziamenti vanno alla mia famiglia per essermi sempre stata vicino, per aver condiviso le mie scelte e per costituire da sempre un costante e fondamentale punto di riferimento per me.

Desidero ringraziare anche tutti i miei amici (troppi da poter elencare) per tutte le meravigliose esperienze condivise e per tutte quelle che verranno. In particolare, sentiti ringraziamenti vanno a Simone Ciolfi per tutto il bello del bello che ha saputo darmi e trasmettermi in questi anni senza mai pretendere nulla in cambio.